ORNL/TM-2000/302

TANK WASTE TRANSPORT STABILITY: SUMMARIES OF HANFORD SLURRY AND SALT-SOLUTION STUDIES FOR FY 2000

June 2002

ORNL/TM-2000/302

TANK WASTE TRANSPORT STABILITY: SUMMARIES OF HANFORD SLURRY AND SALT-SOLUTION STUDIES FOR FY 2000

Compiled by

Timothy D. Welch
Nuclear Science and Technology Division
Oak Ridge National Laboratory

Published: June 2002

Prepared by the
OAK RIDGE NATIONAL LABORATORY
Oak Ridge, Tennessee 37831-6221
Managed by
UT-Battelle, LLC
For the
U. S. DEPARTMENT OF ENERGY
Under contract DE-AC05-00OR22725

CONTRIBUTORS

Hani Alhabbash, Diagnostic Instrumentation and Analysis Laboratory, Mississippi State University, Starkville, Mississippi
Anthony Francis, AEA Technology, Oxfordshire, UK
Jim Henshaw, AEA Technology, Oxfordshire, UK
Rodney D. Hunt, Nuclear Science and Technology Division, Oak Ridge National Laboratory, Oak Ridge, Tennessee
Christopher Kemp, AEA Technology, Oxfordshire, UK
Jeff S. Lindner, Diagnostic Instrumentation and Analysis Laboratory, Mississippi State University, Starkville, Mississippi
Ruben D. Lopez, Hemispheric Center for Environmental Technology, Florida International University, Miami, Florida
Machelle Manning, AEA Technology, Oxfordshire, UK
Nicholas Pilkington, AEA Technology, Oxfordshire, UK
Rajiv Srivastiva, Hemispheric Center for Environmental Technology, Florida International University, Miami, Florida
Rebeca K. Toghiani, Department of Chemical Engineering, Mississippi State University, Starkville, Mississippi
Timothy D. Welch, Nuclear Science and Technology Division, Oak Ridge National Laboratory, Oak Ridge, Tennessee

CONTENTS

ACKNOWLEDGMENTS

This work was sponsored by the U.S. Department of Energy through the Office of Science and Technology's Tank Focus Area. The authors would like to thank Jim Jewett of Numatec Hanford Corporation for providing valuable information and guidance and Dan Reynolds of CH2MHILL for his insights on Hanford operations. We would also like to thank Phil McGinnis, the Tanks Focus Area Technical Integration Manager, for his support and direction.

PREFACE

This report provides, in one convenient document summary, articles on studies of tank waste slurry transport and salt-well pumping at the U.S. Department of Energy's Hanford site in southeastern Washington state. These studies were performed in FY 2000 by five different organizations. The studies are concerned with the chemistry and stability (steady, uninterrupted flow) of tank waste transfers as a collaboration among AEA Technology, the Diagnostic Instrumentation and Analysis Laboratory at Mississippi State University, the Hemispheric Center for Environmental Technology at Florida International University, the Numatec Hanford Corporation, and the Oak Ridge National Laboratory.

The document has been lightly edited for a consistent format, but much of the original flavor (technical content and style) of each institution's contribution has been retained. Readers are encouraged to consult the individual detailed reports published by each of the contributors or to contact the authors for more detailed information.

During the course of the work, researchers provided current results to site engineering organizations, and the latter provided real-time feedback through regular biweekly conference calls and annual on-site workshops.

1. INTRODUCTION

This report is a collection of summary articles on FY 2000 studies of slurry transport and salt-well pumping related to Hanford tank waste transfers. These studies are concerned with the stability (steady, uninterrupted flow) of tank waste transfers, a subset of the Department of Energy (DOE) Tanks Focus Area Tank (TFA) Waste Chemistry effort. This work is a collaborative effort of AEA Technology plc, the Diagnostic Instrumentation and Analysis Laboratory at Mississippi State University (DIAL-MSU), the Hemispheric Center for Environmental Technology at Florida International University (HCET-FIU), Numatec Hanford Corporation (NHC), and the Oak Ridge National Laboratory (ORNL). The purpose of this report is to provide, in a single document, an overview of these studies to help the reader identify contacts and resources for obtaining more detailed information and to help promote useful interchanges between researchers and users.

Despite over 50 years of experience in transporting radioactive tank wastes to and from equipment and tanks at the Department of Energy's Hanford, Savannah River, and Oak Ridge sites, waste slurry transfer pipelines and process piping become plugged on occasion. At Hanford, several tank farm pipelines are no longer in service because of plugs. At Savannah River, solid deposits in the outlet line of the 2H evaporator have resulted in an unplanned extended downtime. Although waste transfer criteria and guidelines intended to prevent pipeline plugging are in place, they are not always adequate. To avoid pipeline plugging in the future, other factors that are not currently embodied in the transfer criteria may need to be considered. The work summarized here is being conducted to develop a better understanding of the chemical and waste flow dynamics during waste transfer. The goal is to eliminate pipeline plugs by improving analysis and engineering tools in the field that incorporate this understanding.

The first article (Sect. 2) outlines some of the factors that affect the stability of tank waste transport and provides an overview of how the studies included in this report address these factors through testing, modeling, and development of technologies for stable waste transfer. Simulated tank wastes, both sludge-supernatant slurry and saltcake solutions, were used in these tests. Section 3 describes the development of these simulated tank wastes (AN-103, AZ-101, SX-104, and U-103) for use by collaborators at AEA Technology, DIAL-MSU, and HCET-FIU. Precipitation rates, solids volume fraction, and particle density have been identified as factors that influence pipeline plugging. In the third article (Sect. 4), collaborators from AEA Technology describe results from their work to measure particle sizes, number densities, and crystal densities. They performed tests with fluoride/phosphate solutions, tank simulant SX-104, tank simulant AN-103, and Savannah River waste simulant. HCET-FIU researchers studied fluid flow rates, pipeline diameter, waste composition, temperature reduction, and waste solid volume fraction in 3/8-in. and 1-in.-diam pipe loops. The fourth article (Sect. 5) describes FIU studies related to cross-site slurry transfers with phosphate/fluoride solutions and simulated tank AN-103 wastes to measure pressure drops, plugging dynamics, slurry rheology, and particle characteristics. Cross-site transfers are carried out in the turbulent flow regime. The pumping of salt solution from salt wells, on the other hand, occurs in the laminar flow regime. The salt solutions may be saturated and may become supersaturated if the solution is cooled during the transfer. Salt-well pumping lines have plugged occasionally as a result. In Sect. 6, researchers at DIAL-MSU describe tests with simulated SX-104 waste in a salt-well-pumping flow loop and related Environmental Simulation Program (ESP) equilibrium calculations. The final article (Sect. 7) describes initial work at MSU to explore computational fluid dynamics (CFD) modeling of tank waste transfers.

The emphasis of the work reported here is on tank waste dynamics during transport. The static and equilibrium aspects of tank waste chemistry, including solubility studies, chemical phase equilibrium, solids identification and waste viscosity, are described by Hunt et al. (2000).

1.1 References

Hunt, R. D, T. A. Dillow, J. R. Parrot, Jr., J. C. Schryver, C. F. Weber, and T. D. Welch, 2000. *Waste Preparation and Transport Chemistry: Results of the FY 2000 Studies*, ORNL/TM-2000/298, Oak Ridge National Laboratory, Oak Ridge, Tenn. (December).

2. FACTORS AFFECTING WASTE TRANSPORT STABILITY

Timothy D. Welch
Nuclear Science and Technology Division
Oak Ridge National Laboratory

Abstract

Attempts to avoid pipeline plugging have focused on fluid flow factors for slurries and chemistry factors for salt solutions. For slurries, the solids volume fraction is restricted to keep the pressure within pipeline design limits and the flow velocity is kept high enough to keep solid particles suspended. For salt solutions, the salt concentration and temperature are controlled to avoid excessive precipitation. Process perturbations and upsets such as fluctuation in the flow rate, temperatures changes, composition variations, and pump failure can result in unstable conditions and lead to a pipeline plug. The work described in this report is designed to address the following questions: What operating conditions will guarantee that the pipeline will not plug? How far can operations deviate from these conditions before the pipeline becomes unstable and plugs? How much time do operators have to respond to avoid a plugged line?

The waste transport stability tasks help to determine the operating conditions for tank waste transfers that avoid plugging. These tasks all address some aspect of chemical dynamics in a flowing waste stream—by laboratory-, bench-, and pilot-scale tests with simulated wastes and by predictions of flow and chemical behavior.

2.1 Introduction

An important challenge at Hanford is to reduce the risk of pipeline plugging. Pipeline plugs have been attributed to a variety of causes. Some of these are discussed by Shekarriz et al. (1997), while others are documented in unpublished letter reports at Hanford. Among the identified causes are the following:

- solids precipitation and accumulation on the pipe walls due to waste cooling during transfer,
- inadequate dilution and formation of interlocking, needle-like crystals of Na_3PO_4,
- gel formation,
- precipitation of $Al(OH)_3$,
- precipitation of Na_2CO_3,
- precipitation leading to increased viscosity, and
- solids settling.

Reynolds (2000) observed that recent plugs during saltwell pumping have occurred at sharp turns like those of Hanford PUREX connectors on pipe jumpers found in valve pits. However, plugs in cross-site transfer lines have also occurred in pipelines well away from the valve pits.

Laboratory tests are being conducted (Herting et al. 1999; Herting 2000a, 2000b, 2000c), and chemical equilibrium calculations are being performed (Toghiani et al. 2000, Toghiani and Dial 2001) to identify the solid phases formed and to predict the quantity of these solids that can precipitate from Hanford salt solutions.

To keep particles suspended, the velocity must be above the critical velocity. A number of empirical and semiempirical correlations have been developed to calculate the critical velocity. Shekarriz et al. (1977) recommend the correlations of Oroskar and Turian (1980) and Wani et al. (1982) for Newtonian flow and Hanks (1986) for non-Newtonian flow. Estey and Hu (1998) investigated eight critical velocity correlations. They concluded that the Oroskar and Turian correlation generally provided the most conservative estimate of critical velocity. Liquid density, particulate solids density, flow rate, particle size, and liquid viscosity are important parameters needed to apply these correlations. Julyk et al. (2000) analyzed slurry waste transfers using the empirical correlation of Oroskar and Turian to calculate the critical velocity and the approach of Wasp et al. (1979) to calculate the pressure drop.

In the case of tank wastes, chemical dynamics and fluid-particle interactions in the flowing slurry can result in dynamic changes to the particle-size distribution and the solution chemical composition, as well as dramatic changes in slurry properties.

2.2 Waste Transfer Dynamics

Waste transfer dynamics may need to be considered if the properties of the waste deviate significantly from the desired operating conditions during transport. As illustrated in Fig. 1, chemical changes influence the properties and the quantity of solids in the waste stream, which, in term, influence the slurry viscosity. The slurry viscosity and the solids properties both influence the flow velocity patterns and pressure. Some of the factors involved in waste dynamics and efforts to obtain relevant data are discussed below.

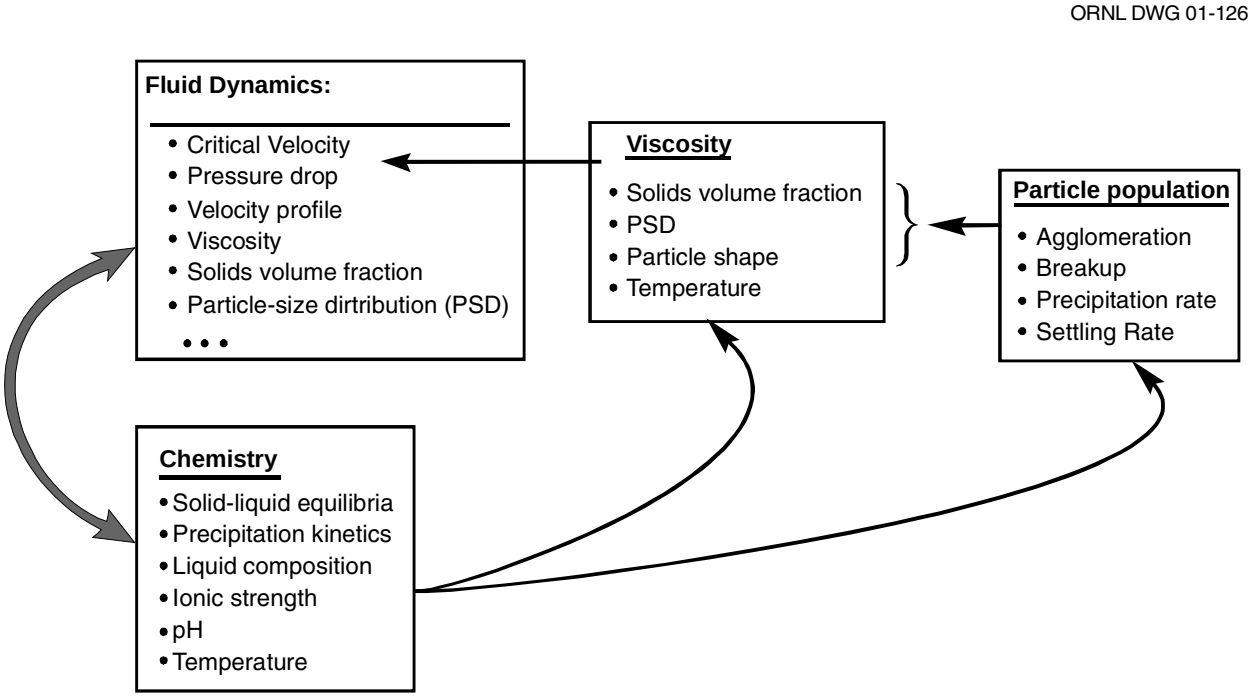

Fig. 1. Coupling of waste flow to waste chemistry. Properties such as viscosity that determine flow behavior depend on the slurry particle characteristics.

Viscosity. Slurry viscosity depends on the solids volume fraction, the particle-size distribution, and the particle shape. Hunt et al. (2000) have measured viscosity data for simulated Hanford tank waste. Theoretical predictions of the viscosity for stable colloidal dispersions are given by Lionberger and

Russel (2000), who predict macroscopic transport properties from the nonequilibrium distribution characterizing the microstructure in an applied field starting from thermodynamic and hydrodynamic approximations. Results are presented for bimodal and polydispersed colloidal dispersions. Lionberger and Russel discuss the reduction of viscosity caused by polydispersity and the dependence of viscosity on volume fraction and particle-size distribution. [Refer also to Macosko (1994) for applications of suspension rheology.] Adler et al. (1990) also provide a good review of rheological models of suspensions. Practical and theoretically sound viscosity correlations useful for waste flow analysis can be obtained based on reduction of the simulated waste data using the appropriate viscosity model.

Fluid particle-particle interactions. The approach required for modeling solid suspensions in turbulent flow depends on the solids volume fraction (Elgobashi 1991). For very dilute suspensions [volume fraction (ϕ) < 10^{-6}], the fluid motion affects the particles. However, the particles have no significant effect on the turbulent structure. This "one-way coupling" would apply to pumping of supernatants containing very few solids. For dilute suspensions with solids volume fractions in the 10^{-6} to 10^{-3} range, "two-way coupling" must be considered. In this regime, the fluid motion affects the particles and the particles affect the turbulent structure of the continuous phase. For "dense" suspensions [volume fraction (ϕ) > 10^{-3}], particle-particle interactions must also be considered. This "four-way coupling" would apply to slurry transfer. A Hanford supernatant transfer could transition from the one-way coupling to the two-way coupling regime, or even to the four-way coupling regime, if the precipitation rate and the concentration of the precipitating species are sufficiently high. Accounting for four-way coupling drives up the cost of doing the simulation. Thus, for practical estimates, predictions initially will use approximate techniques to simulate these interactions

Particle growth, agglomeration, and disruption. Since slurry viscosity depends on particle size, changes in particle-size distribution during transport are an important consideration. Francis et al. (2000) has performed experimental tests to measure particle growth rates for several Hanford tanks using simulated wastes. Preliminary results from tests on the disruption of sludge particles under shear were obtained by Herting (2000c). Until more data are available for high-level waste tank solutions, the results from industrial crystallizers may be instructive. Serra and Casamitjana (1998) studied the aggregation and breakup of 2-μm latex particles in Couette flow and propose a population balance model describing the simultaneous agglomeration and fragmentation during shear. They found that the probability of agglomeration from particle collisions depends on the chemical interactions between particles and their physical properties but not on the flow characteristics. The fragmentation parameter, however, depended on both the shear rate and the volume fraction of particles. Melis et al. (1999) studied the effect of fluid motion on aggregation of small particles subject to van der Waals forces and electrostatic repulsive forces. They found that the aggregation rate constant increases with particle size in the case of a thick double layer. Systems with a thin double layer are almost unaffected by shear. Chin et al. (1998) have investigated the effects of pH, ionic strength, particle size, and particle concentration on the flocculation rate in a stirred tank under turbulent shear flow. Particles flocculate into larger agglomerates more rapidly at high ionic strength.

Nonspherical particles. The motion of cylindrical (rod-shaped) and other nonspherical particles is much more complex than the motion of spherical particles. This behavior may account in part for the observations of mats of rod-shaped particles in the plugs that have been analyzed. The particle shape affects the pressure drop, critical velocity, and settling velocity. In *Bubbles, Drops, and Particles*, Clift and Weber (1978) present drag coefficients; describe the regimes of motions for a variety of shapes including spheroids, disks, and cylinders; and discuss heat and mass transfer correlations.

Slurry flow with reaction and precipitation. For heterogeneous reactions, the reaction rate expression involves a reaction rate constant and a geometric factor (e.g., surface area per phase volume). Chemical systems of interest in waste slurry transport exhibit a wide range in both intrinsic reaction rate and size.

For example, the formation of small gibbsite crystals is slow, while the formation of long needle-shaped phosphate crystals is rapid.

For complex systems, it is often useful to show relationships in terms of dimensionless groups. A Damköhler number (Da), representing the ratio of the chemical-reaction velocity to mass-transport velocity, is useful for correlating and understanding the behavior of heterogeneous systems (see, e.g., Carberry 1976). For surface reactions, when the reaction rate is slow relative to diffusion, the value of Da approaches 0 and the system behaves like a homogeneous one. When the surface reaction is rapid relative to the diffusion of reactant, the value of Da is large and the observed rate depends on the surface area per unit of solid-phase volume.

The observed kinetics of formation and the structure of aggregates particles are influenced by the fluid flow patterns. The aggregate morphology will depend on the value of Da and the Reynolds number (Re). The Damköhler number, Lewis number, Weber number, and Reynolds number, among others, will be useful for reducing and analyzing waste slurry system data.

Table 1 lists TFA activities to develop data and predictive tools.

Table 1. TFA tank waste transport stability activities

Task	Performer
Precipitation rates and solid properties	AEA Technology
Waste slurry transport tests	Florida International University
Salt-well pumping tests	Mississippi State University (DIAL)
Waste transport modeling	Mississippi State University (DIAL)
Waste transport chemistry simulant development	Oak Ridge National Laboratory
Waste transport analysis and modeling support	Oak Ridge National Laboratory

The work involves investigators from five organizations: AEA Technology plc, the Diagnostic Instrumentation and Analysis Laboratory at Mississippi State University (DIAL-MSU), the Hemispheric Center for Environmental Technology at Florida International University (HCET-FIU), the River Protection Project at Numatec Hanford Corporation (NHC-RPP), and the Oak Ridge National Laboratory (ORNL). ORNL is developing simulated waste for use in the experimental tests at the other sites. AEA Technology is measuring precipitation rates and particle properties for simulated tank wastes, and viscosity data for simulated tank wastes are being obtained by ORNL and FIU. DIAL-MSU is performing tests on salt-well solution transfers, while FIU is conducting tests of tank slurry transport in a 1-in.-diam pipe loop. Viscosity models are being developed at ORNL, and the application of computational fluid dynamics (CFD) to tank waste transport is being investigated at DIAL-MSU.

Data and models from this effort support both immediate site design and operations needs and longer-term site risk-reduction objectives. As an example of the application of results to a near-term issue, data from the slurry flow test at HCET-FIU are being used to validate and extend the empirical correlations currently used to predict the critical velocity and pressure drop for slurry transfers.

2.3 References

Adler, P. M,, A. Nadim, and H. Brenner. 1990. “Rheological Models of Suspensions,” pp. 1–72 in *Advances in Chemical Engineering*, Vol. 15, ed. J. Wei, Academic Press, New York.

Carberry, J. J. 1976. *Chemical and Catalytic Reaction Engineering*, McGraw-Hill, New York.

Chin, C.-J., S. Yiacoumi, and C. Tsouris. 1998. "Shear-Induced Flocculation of Colloidal Particles in Stirred Tanks," *J. Colloid Interface Sci.* **206**, 532–545.

Clift, R., J. R. Grace, and M. E. Weber. 1978. *Bubbles, Drops, and Particles*, Academic Press, New York.

Collier, A. P., and M. J. Hounslow. 1999. "Growth and Aggregation Rates for Calcite and Calcium Oxalate Monohydrate," *AIChE J.* **45**(11), 2298–2305 (November).

Elgobashi, S. 1991. "Particle-Laden Turbulent Flows: Direct Numerical Simulations and Closure Models," *Appl. Sci. Res.* **48**, 301.

Estey, S. D., and T. A. Hu. 1998. *Flow Velocity Analysis for Avoidance of Solids Deposition During Transport of Hanford Tank Waste Slurries*, HNF-2728, Lockheed Martin Hanford Corporation, Richland, Wash.

Francis, A., J. Henshaw, M. Manning, N. Pilkington, and C. Kemp. 2000. *Summary Report on Precipitation Studies of Tank Simulant Mixtures*, AEAT/R/NT/0284, AEA Technology, Harwell, Oxfordshire, U.K. (November).

Hanks, R. W. 1986. "Principles of Slurry Pipeline Hydraulics," Chap. 6 in *Encyclopedia of Fluid Mechanics, Vol. 5: Slurry Flow Technology*, ed. N. P. Cheremisinoff, Gulf Publishing Company, Houston.

Herting, D. L. 2000a. *Results of Dilution Studies with Waste from Tank 241-AN-103*, HNF-7153, Fluor Hanford, Richland, Wash. (September).

Herting, D. L. 2000b. *Saltcake Dissolution FY 2000 Status Report*, HNF-7031, Fluor Hanford, Richland, Wash. (September).

Herting, D. L. 2000c. *Results of Shear Studies with 241-AZ-102 Sludge*, HNF-6585, Fluor Hanford, Richland, Wash. (July).

Herting, D. L., D. W. Edmonson, J. R. Smith, T. A. Hill, and C. H. Delegard. 1999. *Saltcake Dissolution FY 1999 Status Report*, HNF-5193, Fluor Daniel Hanford, Inc., Richland, Wash. (September).

Hunt, R. D., T. A. Dillow, J. R. Parrott, Jr., J. C. Schryver, C. F. Weber, and T. D. Welch. 2000. *Waste Preparation and Transport Chemistry: Results of the FY 2000 Studies*, ORNL/TM-2000/298, Oak Ridge National Laboratory, Oak Ridge, Tenn. (December).

Julyk, L. J., T. C. Oten, and W. L. Willis. 2000. *Waste Feed Delivery Transfer Analysis*, RPP-5356, Rev. 0, CH2M Hill Hanford Group, Inc., Richland, Wash. (May).

Lionberger, R. A., and W. B. Russel. 2000. "Microscopic Theories of the Rheology of Stable Colloidal Dispersions," pp. 399–474 in *Advances in Chemical Physics*, Vol. 111, ed. I. Prigogine and S. A. Rice, Wiley, New York.

Macosko, C. W. 1994. *Rheology: Principles, Measurements, and Applications*, VCH, New York.

Melis, S., M. Verduyn, G. Storti, and M. Morbidelli. 1999. “Effect of Fluid Motion on the Aggregation of Small Particles Subject to Interaction Forces,” *AIChE J.* **45**(7), 1383–1393.

Oroskar, A. R., and R. M. Turian. 1980. “The Critical Velocity in Pipeline Flow of Slurries,” *AIChE J.* **26**, 550–558.

Reynolds, D. 2000. Presentation at the TFA Saltcake and Stability Workshop, May 16–17, 2000, Richland, Wash.

Serra, T., and X. Casamitjana. 1998. “Effect of the Shear and Volume Fraction on the Aggregation and Breakup of Particles,” *AIChE J.* **44**(8), 1724–1730.

Shekarriz, A., Y. Onichi, P. A. Smith, M. Sterner, D. R. Rector, and J. Virden. 1997. *Cross-Site Transfer System at Hanford: Long-Term Strategy for Waste Acceptance*, PNNL-11497, Pacific Northwest National Laboratory, Richland, Wash.

Toghiani, B., J. S. Lindner, C. F. Weber, and R. D. Hunt. 2000. *Modeling of Sulfate Double-Salt in Nuclear Wastes*, ORNL/TM-2000/317, Oak Ridge National laboratory, Oak Ridge, Tenn. (October).

Toghiani, B., and J. S. Lindner. 2001. *DIAL/MSU Saltcake Dissolution: Fiscal Year 2000 Status Report*, TR 00-1, Tanks Focus Area, Mississippi State University, Starkville, Miss.

Wani, G. A., M. K. Sarkar, and B. P. Mani, 1982. “Velocity in Multi Particle Transportation Through Horizontal Pipes,” *J. Pipelines* **2**, 57–62.

Wasp, E. J., J. P. Kenny, and R. L. Gandhi. 1979. *Solid-Liquid Flow Slurry Pipeline Transportation*, Gulf Publishing Company, Houston.

3. SIMULANTS FOR THE TRANSFER TESTS AT AEA, FIU, AND MSU

Rodney D. Hunt
Nuclear Science and Technology Division
Oak Ridge National Laboratory

3.1 Introduction

The Tanks Focus Area (TFA) and the River Protection Project (RPP) requested that research staff members at AEA Technology, Florida International University (FIU), and Mississippi State University (MSU) study the waste transfers during salt-well pumping and retrieval operations. The waste in the salt-well pumping will contain high salts and no solids initially, and the flow rate for the waste will be between 0.5 and 3 gal/min. In contrast, the waste in the retrieval operations can contain a maximum of 20 wt % solids, and the flow of the waste should remain turbulent during the transfer. The researchers at FIU focused on the waste in Hanford tanks AN-103 and AZ-101, which will be retrieved by the RPP in the near future. The staff members at MSU examined the saltcake liquid from Hanford tanks SX-104 and U-103, which had led to plugged pipelines during salt-well pumping. In order to support the activities at the university, AEA Technology examined the key precipitation properties of the waste in tanks AN-103 and SX-104.

The test conditions such as flow rates and temperature ranges were provided by personnel at Oak Ridge and Hanford. The best-basis inventories in the Tank Waste Information Network System were used to develop simulants of tanks AN-103, AZ-101, and U-103, while the development of the SX-104 simulant was described earlier (Hunt et al. 2000). For tank AN-103, the retrieval of the waste will be conducted in two stages. The supernatant in tank AN-103 will be transferred to tank AN-103 with a moderate amount of dilution water if needed to ensure transportability. The remaining solids will then be dissolved or slurried with 500,000 gal of water and delivered directly to the plant for pretreatment and vitrification. This effort focused on the second transfer of waste. For tank AZ-101, the entire contents of the tank will be slurried with no additional water and transported to the pretreatment and vitrification facility. For the simulants of wastes in tanks AN-103 and AZ-101, the primary objectives were to closely mimic the chemical composition of the selected waste and to minimize the probability of potentially hazardous reactions, such as the formation of poisonous nitrogen oxide. The chemical components in the AN-103 and AZ-101 simulants are listed in Table 1. In addition, the percentages of solids in the simulants of tanks AN-103 and AZ-101 were required to be below the limits that were set by the RPP. Small samples of the AN-103 and AZ-101 simulants were prepared, and the volume percent of solids was determined. The AN-103 and AZ-101 simulants contained 10 and 5% solids, respectively. Calculations using the Environmental Simulation Program (ESP) were performed by MSU researchers to confirm the suitability of the simulants. This evaluation indicated that the AZ-101 simulant would not present a sufficient challenge. Therefore, the RPP recommended that tank AZ-101 be replaced with tank C-104.

3.2 Formulation of Tank C-104 Simulant

Because tank C-104 contains primarily sludge, dilution water must added to the tank so the volume of solids will be less than 30%. The initial formulation of the tank C-104 simulant was based on the best-basis inventory prior to any water additions. As shown in Table 2, various amounts of deionized water were added to the initial formulation. Each sample was placed in a water bath shaker and mixed at 30°C for 1 week. The volume of solids was then determined. The formulation of the tank C-104 simulant, which contains 30% solids, is presented in Table 1.

Table 1. Formulations and concentrations of the AN-103, AZ-101, and C-104 simulants

Compound	Tank AN-103		Tank AZ-101		Tank C-104	
	(g)	(*m*)	(g)	(*m*)	(g)	(*m*)
$NaAlO_2$	162.49	1.982	9.68	0.118	367.73	4.486
$Al(NO_3)_3 \cdot 9H_2O$	413.82	1.103	113.54	0.303	0.00	0.000
NaCl	8.62	0.148	0.00	0.000	0.00	0.000
Na_2CO_3	73.30	0.692	44.19	0.417	115.21	1.087
NaF	2.55	0.061	3.12	0.074	0.00	0.000
$Fe(NO_3)_3 \cdot 9H_2O$	0.00	0.000	0.00	0.000	153.80	0.381
Fe_2O_3	0.00	0.000	0.00	0.000	22.78	0.143
$Mn(NO_3)_2$	0.00	0.000	0.00	0.000	30.78	0.172
$NaNO_3$	170.16	2.002	89.92	1.058	0.00	0.000
NaOH	269.75	6.744	49.36	1.777	81.52	2.038
$Na_2C_2O_4$	0.00	0.000	0.00	0.000	28.94	0.216
$Na_3PO_4 \cdot 12H_2O \cdot ¼NaOH$	12.18	0.031	4.52	0.012	28.48	0.073
$Na_2SiO_3 \cdot 5H_2O$	6.04	0.028	2.40	0.011	103.95	0.490
Na_2SO_4	6.40	0.045	20.01	0.141	8.95	0.063
ZrF_4	0.00	0.000	0.00	0.000	102.17	0.611
ZrO_2	0.00	0.000	0.00	0.000	42.51	0.345
H_2O	884.78	49.113	952.27	52.859	1086.60	60.316

Table 2. Effects of water dilution on the viscosity for the tank C-104 simulant

Temperature (°C)	Dilution water (wt % of initial sample)	Viscosity (cP)	Shear rate (s^{-1})
50	0	19	37
40	0	4400	0.1
40	25	3300	0.1
40	50	420	1
40	75	13	55
15	75	17	43

While the potential for pipeline plugs during the proposed retrieval transfers was not known at the time the simulants were formulated, the transfers of liquid in tanks SX-104 and U-103 have led to plugged pipelines. Therefore, suitable simulants of tanks SX-104 and U-103 should form high-viscosity solids as they are permitted to cool to ambient conditions. Three simulants of the SX-104 waste were prepared based on the analytical results provided by the RPP, and the simulant samples were tested extensively in the Brookfield rheometer. The compositions of two of these simulants, which were labeled B7 and B11, are reported in Table 2 of ORNL/TM-2000/298 (Hunt et al. 2000). The composition of the third simulant was based on the composition of the B7 sample with the addition of 0.4 *M* sodium carbonate. While the three formulations are very similar, their abilities to form a pipeline plug were considerably different. The viscosity of the B11 sample always remained low. An intermediate viscosity of 31 cP was observed after the B7 sample was cooled from 50°C to room temperature during a simulated pump failure. In sharp contrast, the viscosity of the B7 + 0.4 *M* sodium carbonate sample exceeded 6000 cP during the simulated pump failure at 50°C. The requirement to form a plug as the simulant is cooled led to the recommendation of the B7 + 0.4 *M* sodium carbonate formulation as the SX-104 simulant for AEA Technology and MSU. It is important to remember that the flow conditions of the tests at AEA Technology, MSU, and ORNL

were considerably different. Therefore, the other sites were permitted to make small modifications in the formulation so that their simulants could more closely mimic the conditions that led to the actual pipeline plug at Hanford.

3.3 Formulation of Tank U-103 Simulant

The initial formulation of the simulant for tank U-103 was based on the liquid associated with the saltcake in the best-basis inventory. This initial formulation of the U-103 solution did not form high-viscosity solids as it was cooled from 30°C to room temperature. Viscosity results at 30 and 20°C, which are shown in Table 3, confirmed that the initial formulation could not adequately simulate the pipeline plug due to filtered liquid from tank U-103. The presence of a considerable amount of solids in the simulant of a liquid was also a concern. Therefore, a modification to the formulation was required. This modified formulation contained 1.2 *M* sodium aluminate, 1.5 *M* sodium hydroxide, and 6.2 *M* sodium nitrate. The only variable in this new formulation was the phosphate concentration, which is 0.04 *M* in the best-basis inventory. The concentration of sodium phosphate (i.e., the molarity) was increased from 0.04 to 0.06 to 0.08 to 0.10 *M* in an effort to the increase the probability of plug formation. The viscosity results clearly show that small increases in the phosphate concentrations can lead to dramatic increases in the viscosity of the samples. This modified formulation with a phosphate concentration between 0.06 and 0.08 *M* was provided to MSU for their initial tests on tank U-103 even though the simulant contained solids at 30°C.

Table 3. Viscosity results for Tank U-103 simulants

Sample ID	Viscosity at 30°C (cP)	Volume percent of solids at 30°C	Types of solids at 30°C	Viscosity at 20°C (cP)
Best-basis inventory	3.6	15	Fine powder	4.2
Modified formula + 0.10 *M* PO_4	>6000[a]	20	Fine powder, large crystals, and long-needle crystals	>6000[a]
Modified formula + 0.08 *M* PO_4	6.8	10	Fine powder	>6000[a]
Modified formula + 0.06 *M* PO_4	6.6	15	Fine powder and large crystals	455[b]
Modified formula + 0.04 *M* PO_4	5.1	10	Fine powder	7.2

[a]Shear rate of 0.1 s^{-1}.
[b]Shear rate of 1 s^{-1}.

Previously, the RPP has stated its concern about the uncertainties in the best-basis inventory and in analytical results. This study of the tank U-103 simulants clearly demonstrates that the uncertainties in the best-basis inventory can lead to erroneous assumptions about the potential for plug formation. Potential problems due to uncertainties in the analytical results can be easily seen in the chemical analysis of an actual liquid sample from tank U-103 (Herting 1999). The phosphate concentration was more than 2.4 times greater with the inductively coupled plasma spectroscopy than with the ion chromatography. Our study has demonstrated that a much smaller difference in phosphate concentration can lead to pipeline plugs.

3.4 References

Herting, D. L., D. W. Edmonson, J. R. Smith, T. A. Hill, and C. H. Delegard. 1999. *Saltcake Dissolution FY 1999 Status Report*, HNF-5193, Fluor Daniel Hanford, Inc., Richland, Wash. (September).

Hunt, R. D., T. A. Dillow, J. R. Parrott, Jr., J. C. Schryver, C. F. Weber, and T. D. Welch. 2000. *Waste Preparation and Transport Chemistry: Results of the FY 2000 Studies*, ORNL/TM-2000/298, Oak Ridge National Laboratory, Oak Ridge, Tenn. (December).

4. SUMMARY OF AEA PRECIPITATION STUDIES OF TANK SIMULANT MIXTURES

Anthony Francis, Jim Henshaw, Michelle Manning, Nicholas Pilkington, and Christopher Kemp
AEA Technology
B220 Harwell, Didcot
Oxfordshire
OX11 0RA
UK
Telephone 44 (0)1235 435843
Facsimile 44 (0)1235 436314

Abstract

It is intended that nuclear waste currently stored at a number of sites in the United States be vitrified before long-term storage. The waste, currently stored in single- and double-shell tanks, will be transferred to intermediate tanks before processing. At Hanford alone, there are 177 such storage tanks. Although many have undergone some degree of chemical analysis, the exact contents of these tanks are unknown. During waste transfer, control of solids formation will be needed to deliver waste feed for treatment within specified solids-content limits; to avoid adversely affecting pretreatment operations such as ion exchange and sludge washing; and to optimize retrieval, pretreatment, and immobilization processes.

This research has attempted to measure particle sizes, number densities, and crystal densities for a range of mixtures of interest to the Tanks Focus Area (TFA) and the storage tank facilities in the United States. In particular the following have been studied:

1. fluoride/phosphate solutions,
2. tank simulant SX-104,
3. tank simulant AN-103, and
4. Savannah River simulant.

Precipitates have been generated and studied using either an optical microscope or laser light scattering. Experiments have been carried out under highly turbulent conditions (beaker experiments) or under flow conditions more akin to the pipe transfer lines (pipe flow experiments).

The following conclusions have been derived from this work:

1. At appropriate concentrations, precipitation from fluoride/phosphate mixtures gives rise to the mixed salt $Na_7F(PO_4)_2 \cdot 19H_2O$, as identified by X-ray diffraction (XRD).
2. Precipitation of the mixed salt under flow conditions similar to those in pipe transfer lines can result in large particles (>1000 μm). At very high Reynolds numbers, large particles are still formed.
3. In the case of the simulant SX-104, long, needle-like crystals are precipitated out of solution at approximately 30°C. Cubic/octahedral-type crystals are

precipitated out of solution in the presence of a large surface area for nucleation.

4. XRD on the precipitate from SX-104 identified the salts and $Na_3PO_4 \cdot 12H_2O$, Na_3PO_4, $AlPO_4$, and $NaNO_3$. Density measurements confirmed that the salt is primarily $Na_3PO_4 \cdot 12H_2O$.
5. Particle sizing on the SX-104 precipitate indicates that large particles (>1000 μm) are easily formed.
6. It was impossible to get all the solids into solution for the simulant AN-103.
7. The hot filtrate from attempts to dissolve all the salts for AN-103 turned orange on cooling, yielding a very fine precipitate. XRD identified this material as $NaNO_3$, the density of which was measured as 2.23 g/cm^3, which is close to the literature value of 2.26 g/cm^3.
8. Attempts to produce an alternative AN-103 simulant failed.
9. Addition of 0.0036 *M* silicate to the Savannah River simulant led to precipitation in small-scale laboratory tests but did not produce a precipitate in the flow equipment.
10. In preparing 0.0048 *M* silicate Savannah River simulant, a reaction took place at 80°C that led to a change in the color of the solution and to the formation of a precipitate. This precipitate remained on cooling.
11. Particle sizing on the Savannah River simulant precipitate indicated that it initially forms small particles, <20 μm, which can grow to greater than 1000 μm within a week.

Further work is required on the simulants used in this study to understand the observed behavior. AEA Technology is currently investigating other experiments and possible equipment that may be used in future work.

4.1 Introduction

It is intended that nuclear waste currently stored at a number of sites in the United States be vitrified before long-term storage. The waste, currently stored in single- and double-shell tanks, will be transferred to intermediate tanks before processing. At Hanford alone, there are 177 such storage tanks. Although many have undergone some degree of chemical analysis, the exact contents of these tanks are unknown. During waste transfer, control of solids formation will be needed to deliver waste feed for treatment within specified solids content limits; to avoid adversely affecting pretreatment operations such as ion exchange and sludge washing; and to optimize retrieval, pretreatment, and immobilization processes. For example, the formation of unwanted solids has interrupted waste transfers at Hanford and waste processing at Savannah River. The Hanford effort has focused on the formation of pipeline plugs, while the formation of aluminosilicates in the evaporator system is the immediate concern at Savannah River.

Understanding the kinetics of solids formation and the physical properties of precipitates is important for controlling solids formation and for material processing and transport. The work that has been undertaken this year by AEA Technology as part of the International Agreement DE-GI01-96EW56054 has focused on measuring many of the physical properties of a number of precipitates likely to form during waste retrieval. The work is part of the coordinated effort of the Tanks Focus Area (TFA) to understand the chemistry and mechanisms leading to precipitation and its possible detrimental effects. This program also involves studies at Oak Ridge National Laboratory, Florida International University, Mississippi State University, and the Hanford site laboratory.

Many of the tanks contain fluoride and phosphate salts; therefore, the general precipitation properties of these ions are of interest. Some initial studies by AEA Technology on fluoride and phosphate salt mixtures, undertaken last year, focused primarily on induction times for precipitation. This work is reported in Henshaw et al. (1999), where it was shown that a number of supersaturated solutions could remain stable for significant periods before precipitating. The work this year has focused largely on the properties of the precipitates, particularly the particle size, shape, number density, and particle density. In addition to investigating the relatively simple F^-/PO_4^{3-} system, we have also conducted work on the tank simulant mixtures SX-104, AN-103, and the Savannah River simulant. These are relatively complex salt mixtures at relatively high pH and ionic strength.

In the next section, we will briefly describe the experimental procedures that have been adopted in this year's work, in particular, the use of optical microscopes and laser light scattering techniques to measure particle sizes and shapes. Some of the results from this work are then presented. These results have already been discussed in detail in a number of separate reports (Francis et al. 2000a, 2000b, 2000c). A general discussion is then provided and conclusions from the work summarized.

4.2 Experimental Methods

4.2.1 Methods for Studying Particle Formation in Precipitation Processes

Method 1: Stirred Beaker Experiments

This is a simple setup in which supersaturated solutions are prepared in a stirred beaker and solids are then allowed to form, usually by cooling from an elevated temperature. The beaker is approximately 1 L in volume and 10 cm in diameter. In some cases, the supersaturated solution may be stable at room temperature for a significant length of time so that heating to elevated temperatures is unnecessary. Once precipitation has taken place and the system no longer appears to be changing with time, the solutions are filtered. The crystals are washed on the filter paper before examination. Once precipitation has started, particle formation and growth are relatively rapid; nevertheless, the solutions are often left for several hours before filtering. The filtered particles are examined using an optical microscope to determine the shape and size of the particles. The total amount of precipitate is also measured by drying and weighing, and this information, along with the average particle size and particle density, is used to calculate the particle number density.

Prior to using this setup, an experiment was performed to determine the flow velocity and Reynolds number for the flow in the beaker. This consisted of dropping a visible dye into the beaker while it was being stirred and videotaping the movement of the dye. The mean linear flow velocity was estimated as 50 cm/s, and a Reynolds number for the flow between 10^4 and 10^5 was estimated. These numbers are high compared with typical transfer line velocities and Reynolds numbers at the waste storage sites.

Method 2: Laser Diffraction Method

This method uses laser light scattering by small particles to determine their size and number density. Figure 1 is a diagram of the apparatus that is used, and Fig. 2 is a photograph of the actual equipment (Malvern Laser Diffractometer Longbed 2600e). A solution, which either contains particles or is supersaturated, is placed in a stirred bath (far right, Fig. 2), from which it is pumped along tubes of approximately 8-mm ID. The bath is either mechanically or ultrasonically stirred. The solution is pumped along approximately 1 m of pipe to a sample cell through which the laser beam is passed. Particles present in the solution will scatter the laser beam, and the scattered light is detected by a diode ring detection system (far left, Fig. 2). From the analysis of the scattered light, the size distribution by volume

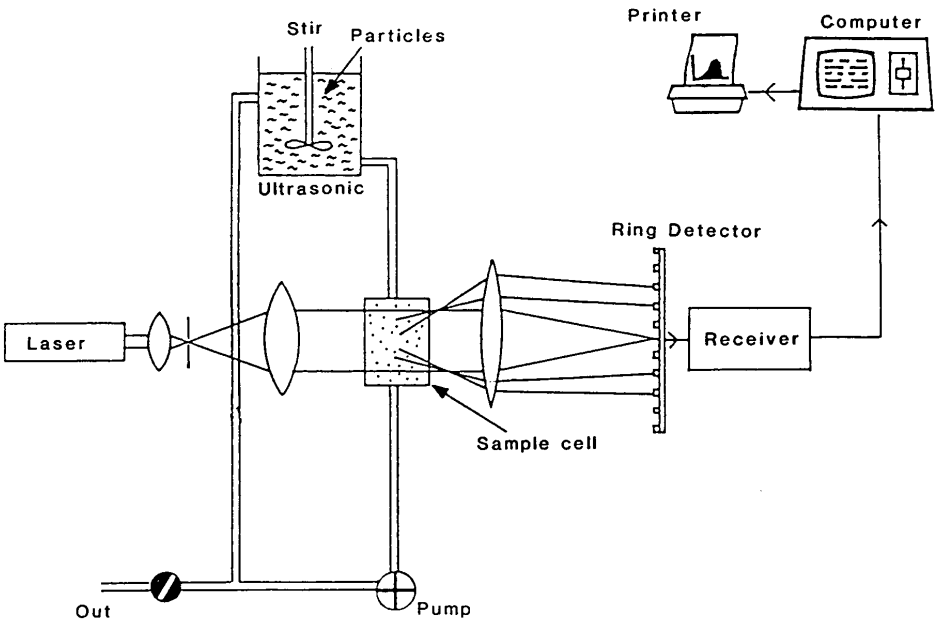

Fig. 1. Diagram of laser light scattering equipment for flow precipitation studies.

Fig. 2. Photograph of laser light scattering equipment for flow precipitation studies.

(weight) is calculated along with the particle number density. From the sample cell, the solution passes back to the bath along 1 m of piping and then begins the circuit over again.

Potentially this particular experimental setup can be used in these ways:

1. by adding preprecipitated solids in solution to the bath and then investigating the particles with the equipment,
2. by adding supersaturated solutions to the bath and then allowing them to cool in situ and studying the particle formation with time, or
3. by using the laser to interrogate a small sample cell (15 cm^3) with a magnetic stirrer.

All these approaches have been adopted in this study.

4.2.3 Crystal Density Measurements

In addition to measuring the size and shape of the crystals formed in these studies, the densities of the crystal were also measured. This was done using Sartorius Master Series balance and density measurement equipment. A sample of the crystals is weighed in air and then subsequently weighed suspended in a suitable liquid. The difference in weights (i.e., the buoyancy) is then used to calculate the density. Various correction factors are used, for example, for the volume of the sample holder and the changes in volume with temperatures.

4.3 Experimental Results

Experiments have been carried out on the following four systems:

1. fluoride/phosphate solutions,
2. tank simulant SX-104,
3. tank simulant AN-103, and
4. Savannah River simulant.

Precipitates have been generated and studied using either an optical microscope or laser light scattering. The results of these experiments are discussed below.

4.3.1 Precipitation of F^-/PO_4^{3-} Mixtures

Fluoride/Phosphate Beaker Experiments

This work has already been reported in more detail in Francis et al. (2000a). Two mixtures were examined in this study, 0.1 *M* F^-/0.4 *M* PO_4^{3-} and 0.2 *M* F^-/0.2 *M* PO_4^{3-}, both in 1 *M* NaOH. The precipitate was identified by X-ray diffraction (XRD) as $Na_7F(PO_4)_2 \cdot 19H_2O$ (see Fig. 3). Experiments in the beaker arrangement were initially carried out under static conditions. Precipitation took place primarily on the surface of the beaker, with crystals as large as a few millimeters being observed. The size of these crystals was largely independent of the beaker material. In the stirred system, experiments were carried out under three cooling regimes: (1) fast cooling in an ice bath, (2) slow cooling, and (3) mixing of supersaturated solutions at room temperature. Using the optical microscope, crystal sizes were measured. Results for the 0.2 *M* F^-/0.2 *M* PO_4^{3-} mixture are given in Table 1.

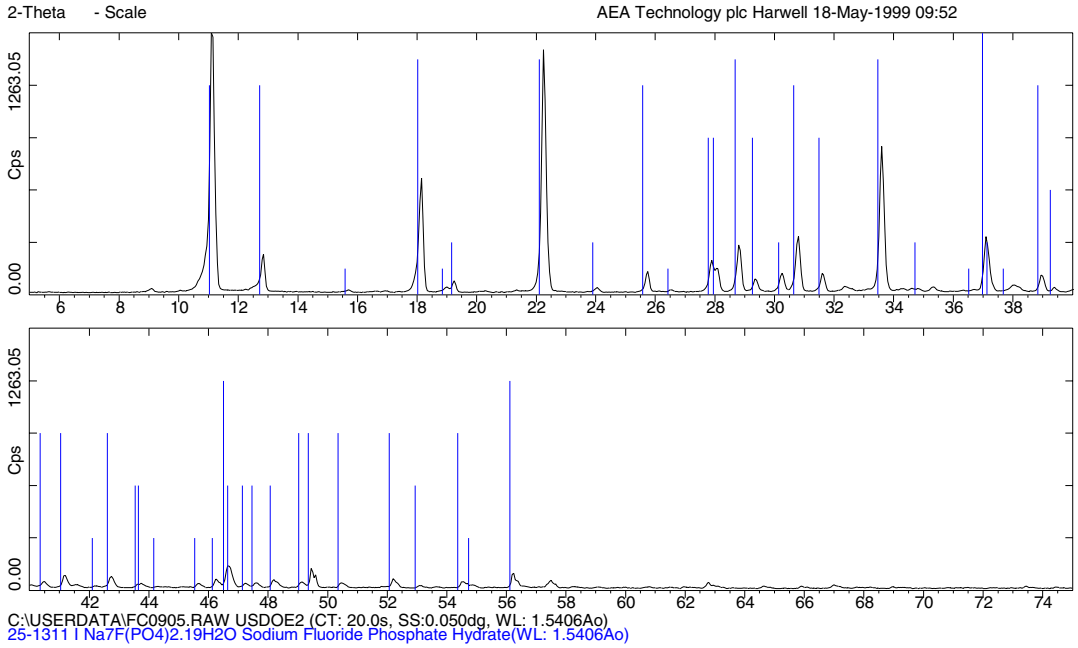

Fig. 3. XRD spectra of crystals precipitated from 0.2 *M* F^-/0.2 *M* PO_4^{3-} in 1 *M* NaOH solution.

Table 1. Summary of results for the 0.2 *M* F^-/0.2 *M* PO_4^{3-} beaker experiment

Experiment	Size (μm)	Average number density (cm^3)	Comment
Fast cooling	98 ± 62	3.5×10^3	Some large crystals observed (>1000 μm)
Slow cooling	94 ± 51	3.5×10^3	No large crystals observed
Mixing at room temperature	150 ± 72	10^3	No large crystals observed

A microphotograph of one of the larger crystals is shown in Fig. 4. Samples from each of the beaker experiments were analyzed in the small-cell laser diffraction equipment, and the particle size distributions (by weight) are shown in Fig. 5. The distributions from all three experiments show peaks between 100 and 200 μm, and the fast-cooled experiment shows an additional large peak at 1200 to 1400 μm. The laser diffraction results, therefore, largely confirm the results from the optical microscope measurements.

The total amount of precipitate was also measured in these experiments and was generally in the range of 3 to 3.5% solids by weight. The average number densities presented in Table 1 are based on 3% solids.

Fluoride/Phosphate Pipe Flow Experiments

The light scattering equipment was used to analyze particle sizes during precipitation as the mixture flowed along the experimental pipe work. Experiments were again performed on 0.1 *M* F^-/0.4 *M* PO_4^{3-} and 0.2 *M* F^-/0.2 *M* PO_4^{3-} in 1 *M* NaOH mixtures. Experiments were carried out for four sets of conditions: (1) fast flow (Re = 5.2×10^3) and fast cooling (ice bath), (2) medium flow (Re = 3×10^3) and fast cooling, (3) slow flow (Re = 7×10^2) and fast cooling, and (4) medium flow and natural cooling.

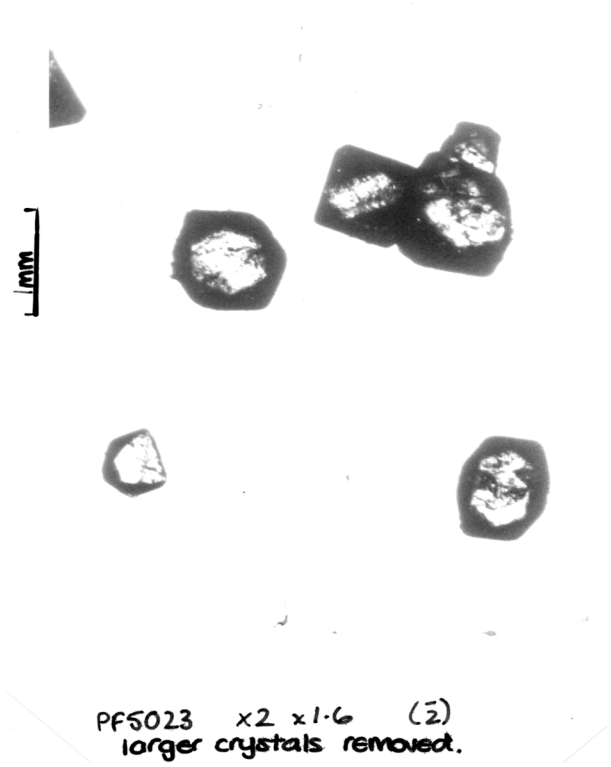

Fig. 4. Microphotograph of crystals precipitated from the stirred beaker solution (0.2 *M* PO_4^{3-}/0.2 *M* F^-/1 *M* NaOH).

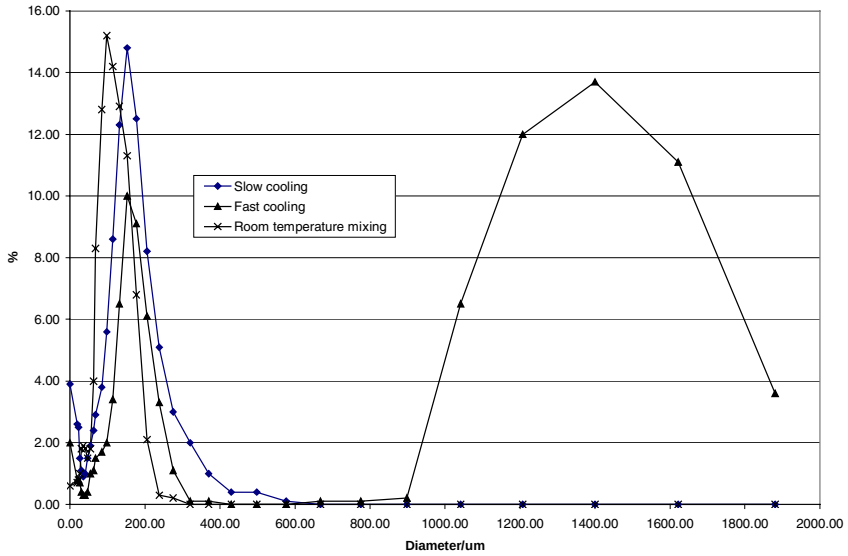

Fig. 5. Particle size distributions from beaker experiments with 0.2 *M* PO_4^{3-}/0.2 *M* F^-/1 *M* NaOH solution measured using the small-cell laser diffractometer equipment.

After heating the solution to 60°C, precipitate was observed at temperatures in the range of 22 to 30°C (depending on the experiment). Once precipitation occurred in the fast-cooled experiment, the cooling rate on average was 0.15°C/min. For natural cooling, the rate was 0.1°C/min.

Figures 6–16 present the results for the 0.2 *M* F^-/0.2 *M* PO_4^{3-} mixture. Plotted are the particle size and number density distributions for the four sets of conditions discussed above. The temperatures in the legend are those at which the measurements were made. The following points should be noted from these plots:

1. In all the fast-cooling experiments, large particles (on the order of 1000 μm) were observed.
2. In the natural-cooling experiments, particles above 600 μm were not observed.
3. The number of large particles is small. However, such particles make a significant contribution, at least early in the precipitation process, to the mass of particles in solution.

4.3.2 Precipitation from the Tank Simulant Mixture SX-104

This work has been reported in Francis et al. (2000b). The recipe used for this simulant mixture is given in Table 2.

Both stirred beaker experiments using the optical microscope and the pipe flow arrangement using laser scattering were used to study this mixture.

SX-104 Stirred Beaker Experiments

The simulant mixture was heated to 70°C and allowed to cool to room temperature, during which time precipitate was observed between 28 and 29°C. The precipitate was filtered and examined using the microscope. Figure 17 shows the precipitate as fine, matted, needle-like crystals. It proved impossible to

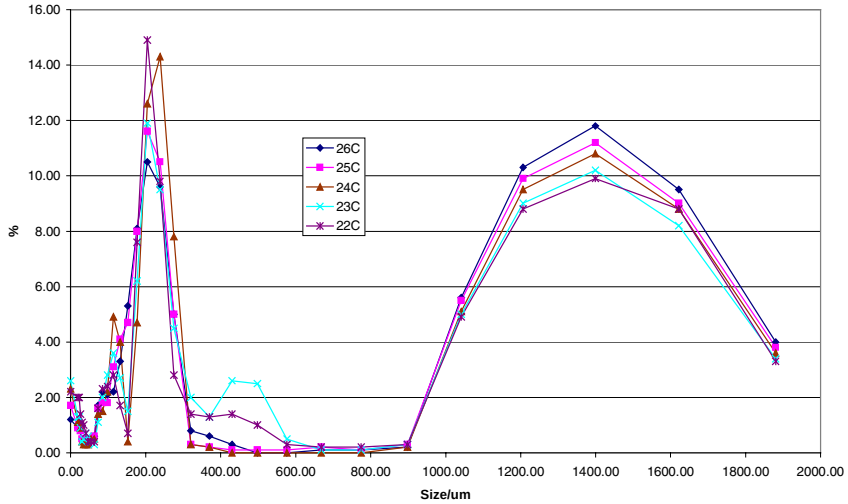

Fig. 6. Particle size distributions from 26 to 22°C, for precipitate from the 0.2 *M* PO_4^{3-}/0.2 *M* F^-/1 *M* NaOH solution (fast flow, fast cooling).

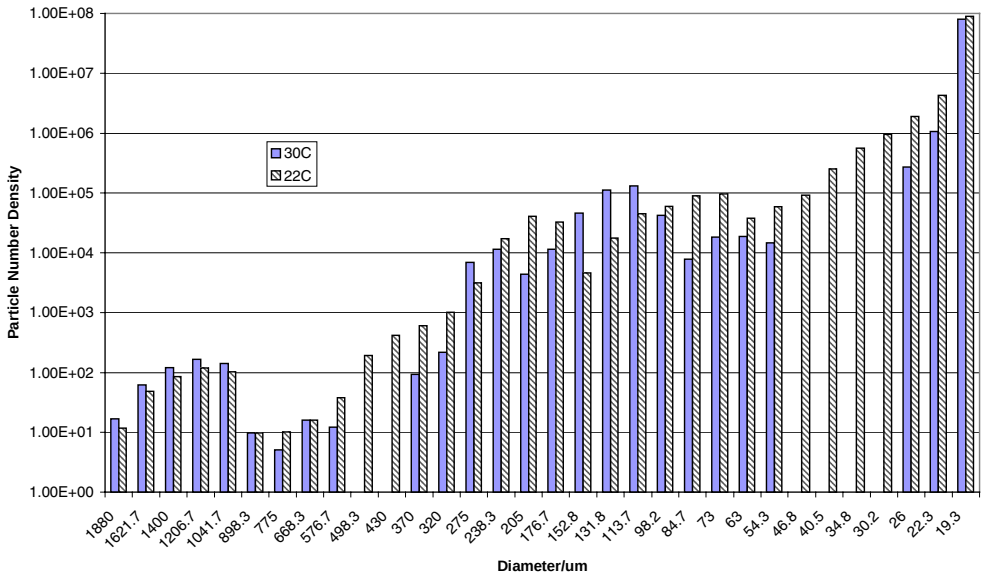

Fig. 7. Particle number densities at 30 to 22°C, for precipitate from the 0.2 *M* PO_4^{3-}/0.2 *M* F^-/1 *M* NaOH solution (fast flow, fast cooling).

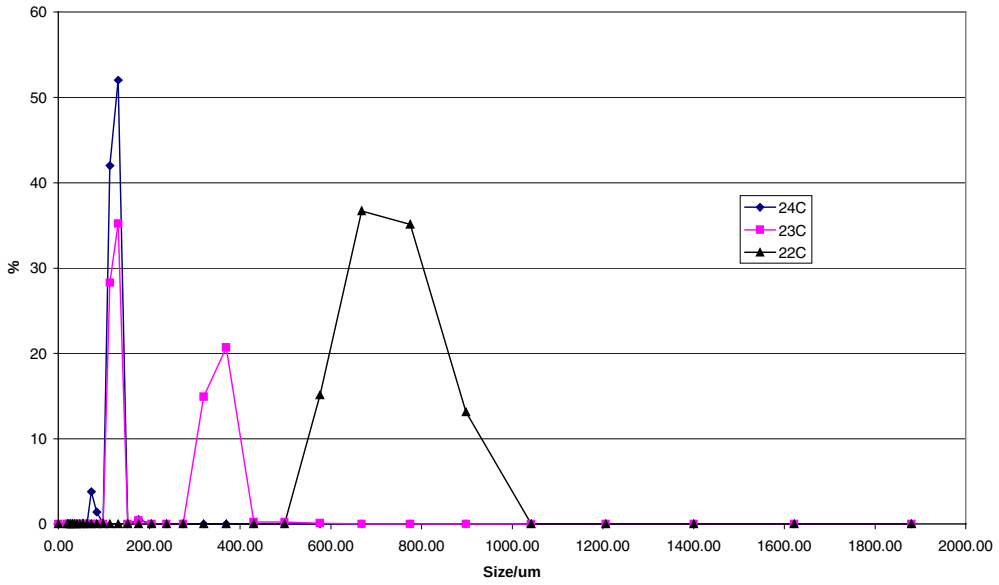

Fig. 8. Particle size distributions from 24 to 22°C, for precipitate from the 0.2 *M* PO_4^{3-}/0.2 *M* F^-/1 *M* NaOH solution (medium flow, fast cooling).

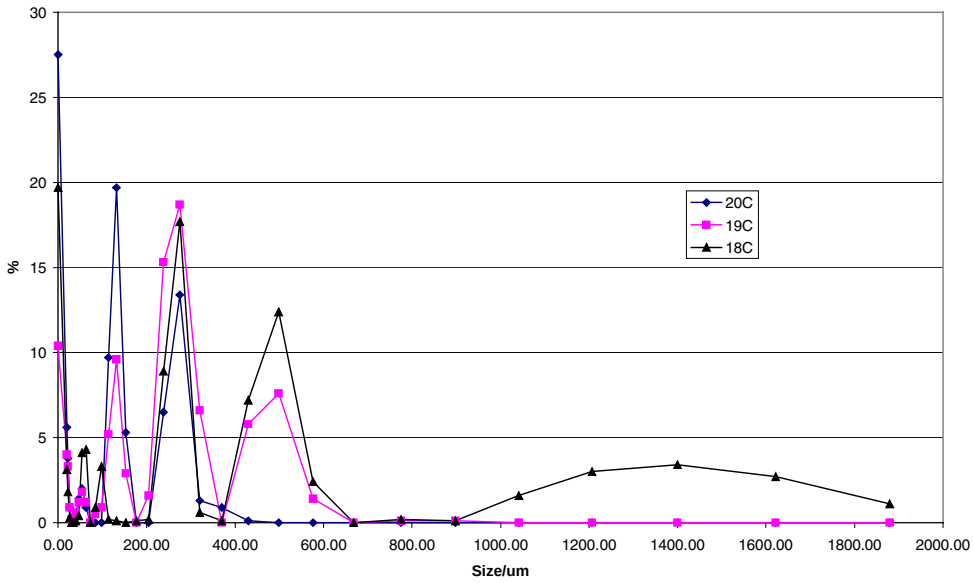

Fig. 9. Particle size distributions from 20 to 18°C, for precipitate from the 0.2 *M* PO_4^{3-}/0.2 *M* F^-/1 *M* NaOH solution (medium flow, fast cooling).

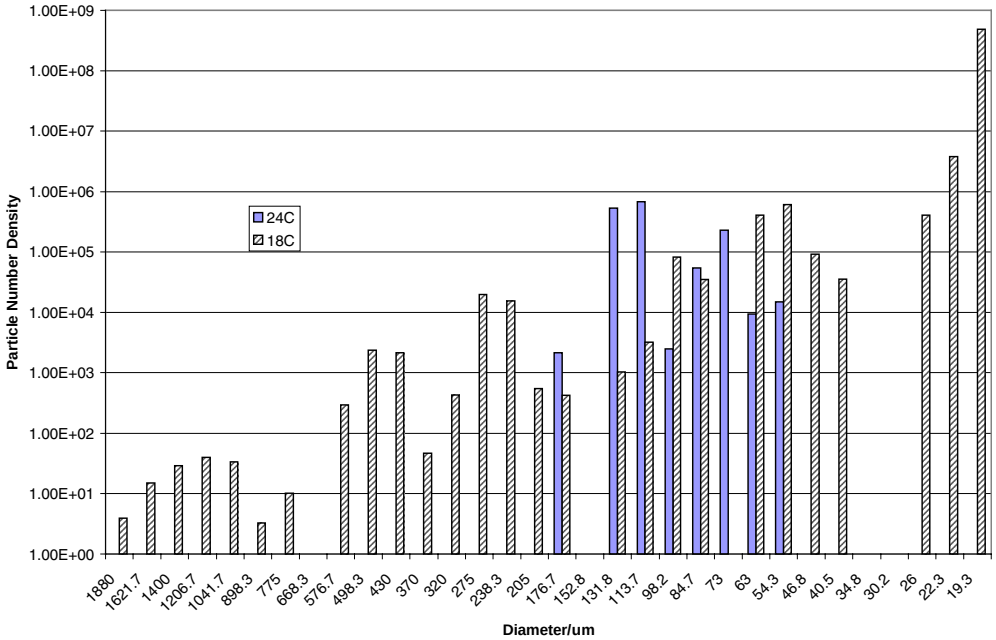

Fig. 10. Particle number densities at 24 to 18°C, for precipitate from the 0.2 *M* PO_4^{3-}/0.2 *M* F^-/1 *M* NaOH solution (medium flow, fast cooling).

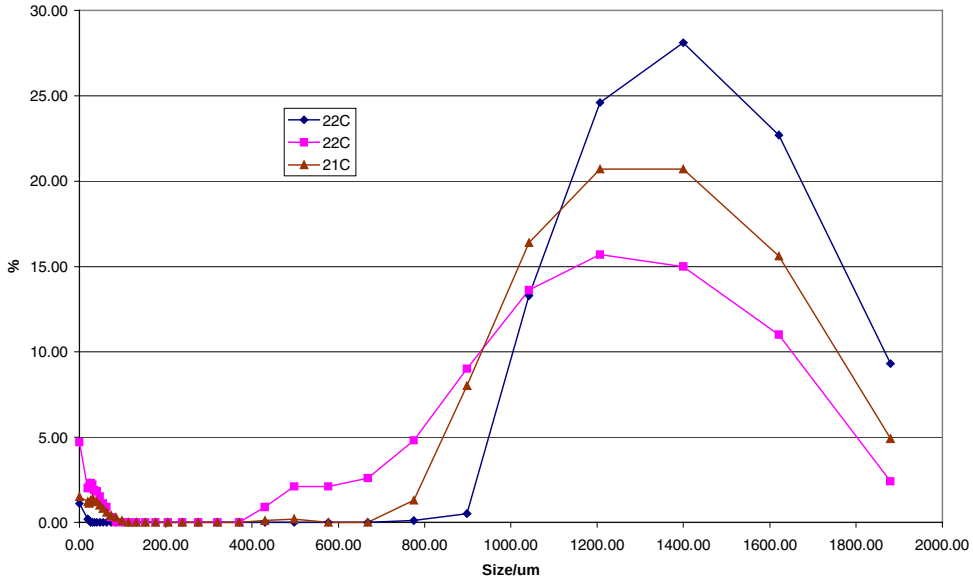

Fig. 11. Particle size distributions from 22 to 21°C, for precipitate from the 0.2 *M* PO_4^{3-}/0.2 *M* F^-/1 *M* NaOH solution (slow flow, fast cooling).

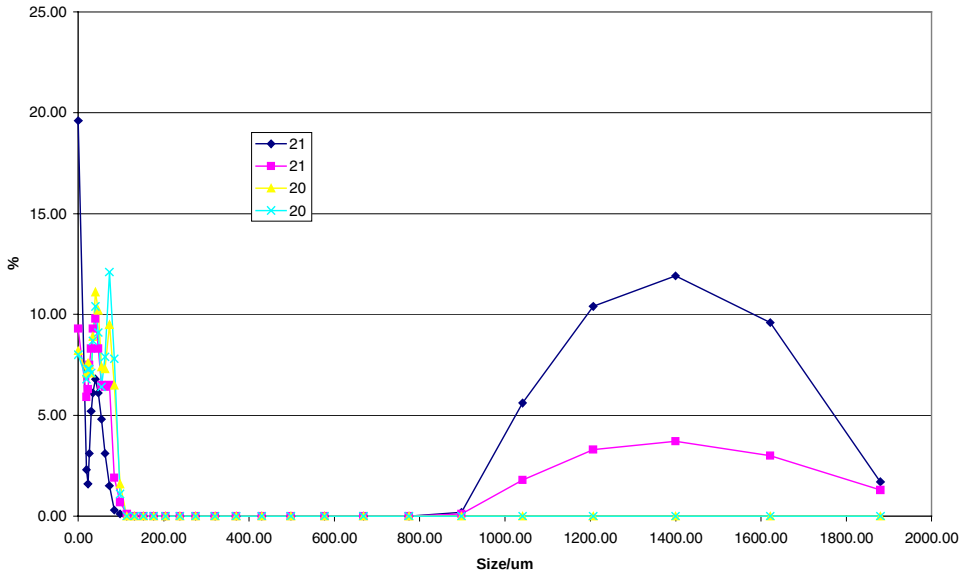

Fig. 12. Particle size distributions from 21 to 20°C, for precipitate from the 0.2 *M* PO_4^{3-}/0.2 *M* F^-/1 *M* NaOH solution (slow flow, fast cooling).

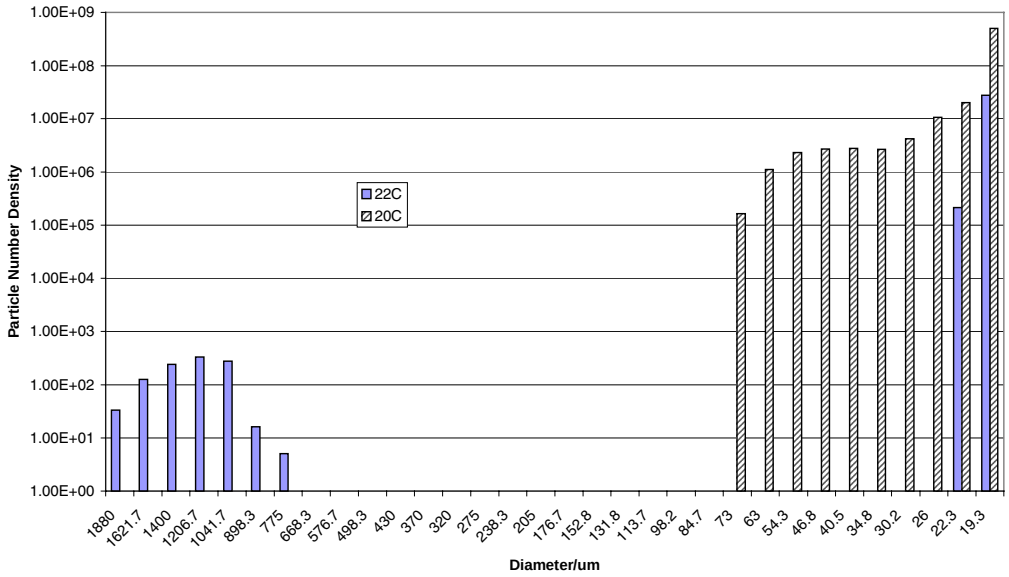

Fig. 13. Particle number densities at 22 and 18°C, for precipitate from the 0.2 *M* PO_4^{3-}/0.2 *M* F^-/1 *M* NaOH solution (slow flow, fast cooling).

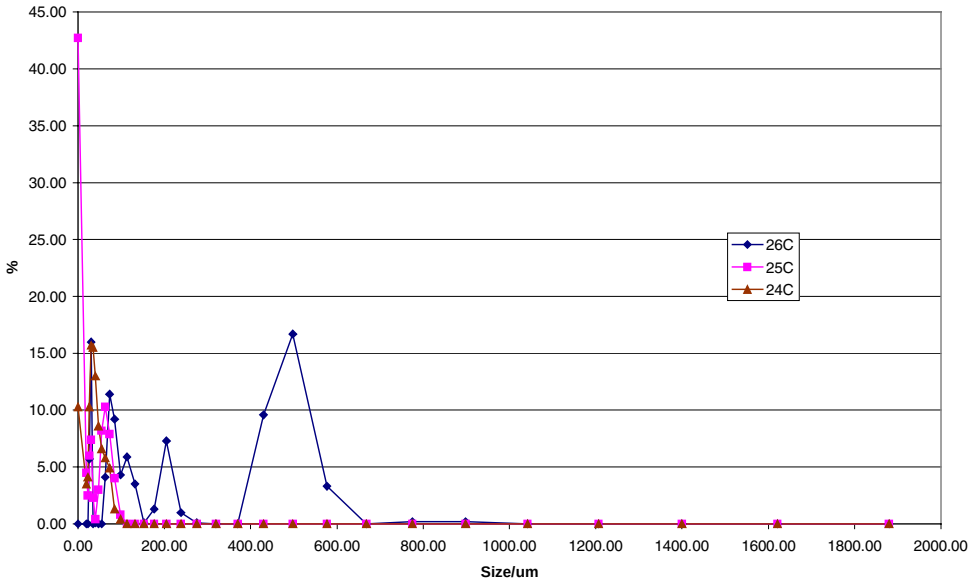

Fig. 14. Particle size distributions from 26 to 24°C, for precipitate from the 0.2 *M* PO_4^{3-}/0.2 *M* F^-/1 *M* NaOH solution (medium flow, natural cooling).

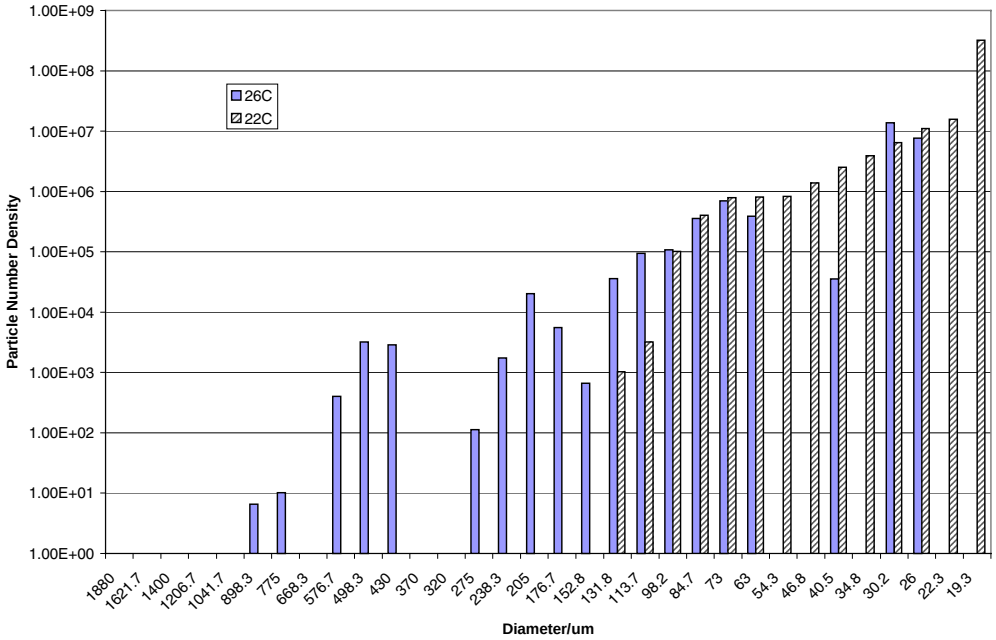

Fig. 15. Particle size distributions from 24 to 22°C, for precipitate from the 0.2 *M* PO_4^{3-}/0.2 *M* F^-/1 *M* NaOH solution (medium flow, natural cooling).

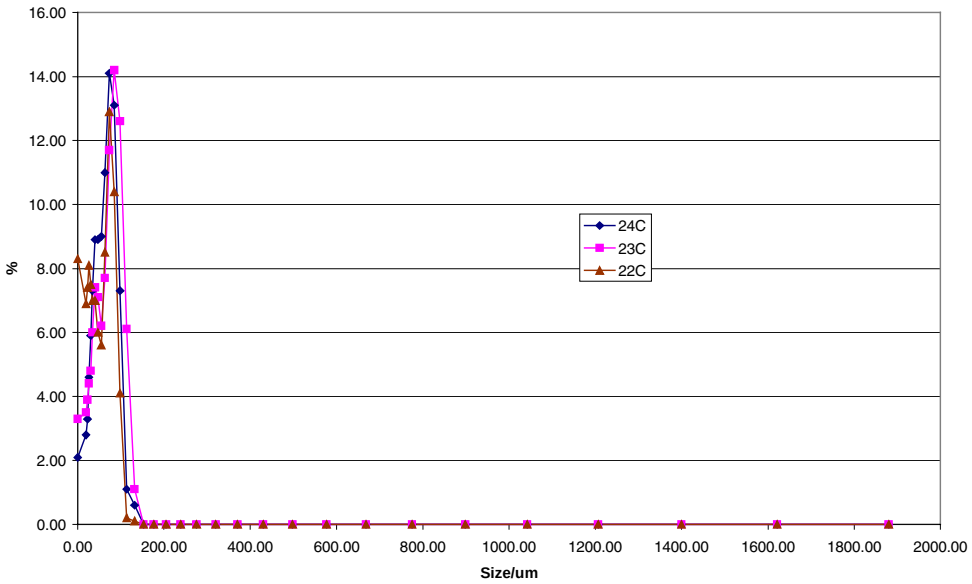

Fig. 16. Particle number densities at 26 and 22°C, for precipitate from the 0.2 *M* PO_4^{3-}/0.2 *M* F^-/1 *M* NaOH solution (medium flow, natural cooling).

Table 2. Simulant mixture used for SX-104

Species	Chemical	Weight (g)	Molarity
CO_3^{2-}	Na_2CO_3	42.4	0.35
SO_4^{2-}	Na_2SO_4	9.94	0.06
PO_4^{3-}	$Na_3PO_4 \cdot 12H_2O$	76.03	0.18
NO_3^-	$NaNO_3$	340	3.52
$Al(OH)_4^-$	$Al(NO_3)_3 \cdot 9H_2O$	375.15	0.88
OH^-	NaOH	240	1.78
	Water	1000	

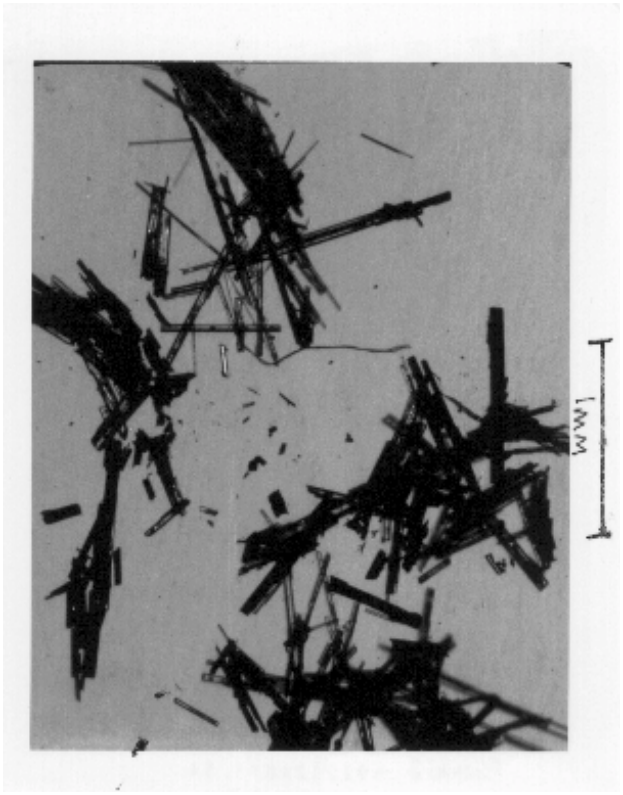

Fig. 17. Microphotograph of sample of crystals from the filtered SX-104 precipitate.

separate well-defined crystals from this filtrate by washing with solvents. Several solvents were used, including water, isopropyl alcohol, methanol, acetone, and hexane. Therefore, in order to examine well-defined individual crystals, a sample of the solution and suspended precipitate was retrieved using a syringe. A drop of this mixture was then placed on a microscope slide. Figure 18 shows such a drop at high magnification, and the fine, needle-like structure of the crystals can be clearly seen. A collection of crystals was measured, and the average length of a crystal was determined to be 205 μm (with a standard deviation of 117 μm). After several minutes of observation of the sample drop, a second cubic/octahedral crystalline form appeared, as shown in Fig. 19. (The nucleation sites on the microscope slide enabled a second salt to precipitate out of solution, a process that does not occur while the solution is being stirred in the beaker.)

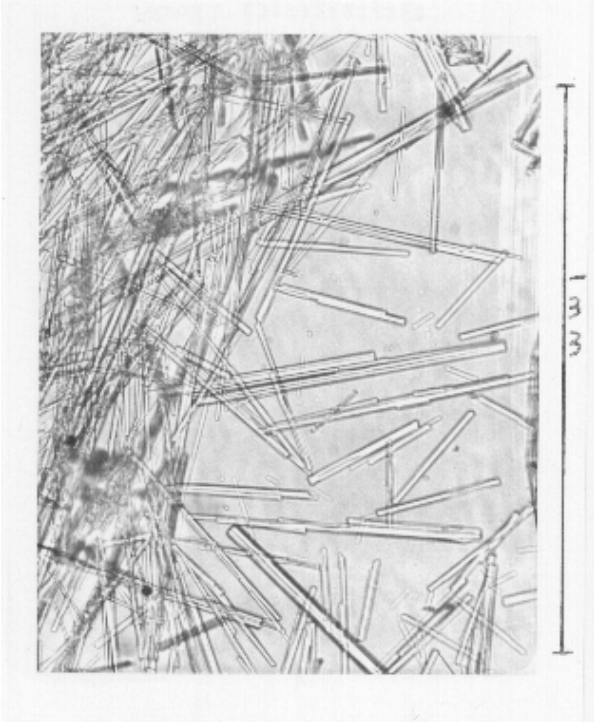

Fig. 18. Microphotograph of solution/ precipitate sample at high magnification.

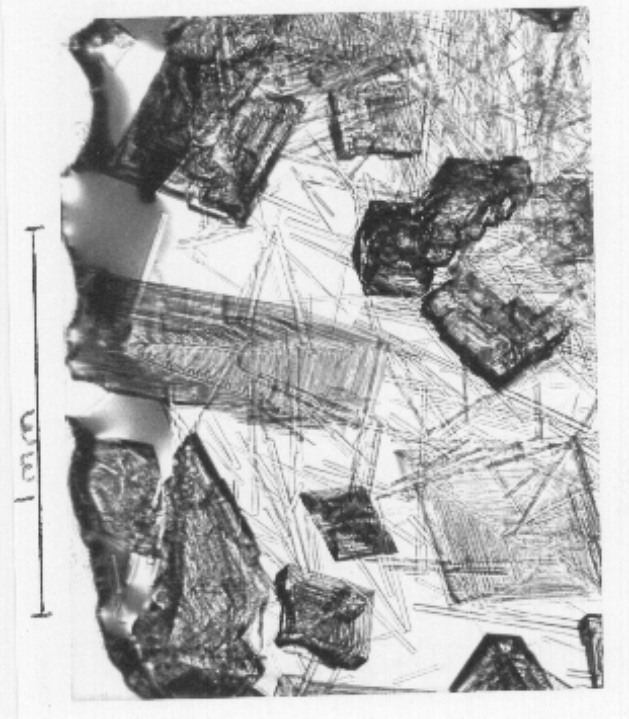

Fig. 19. Microphotograph of solution/ precipitate sample at high magnification several minutes after being placed on the slide.

A sample of the precipitate from these experiments was sent for examination by XRD, and the X-ray pattern is shown in Fig. 20. Four salts—Na_3PO_4, $Na_3PO_4 \cdot 12H_2O$, $AlPO_4$, and $NaNO_3$—were identified by comparing this pattern with those in the XRD database. It is difficult to quantify the amounts of the various salts present in the precipitate except to conclude that the major salt is probably $Na_3PO_4 \cdot 12H_2O$, followed by $NaNO_3$. It is likely that these are the two salts shown on the microscope slide in Fig. 19.

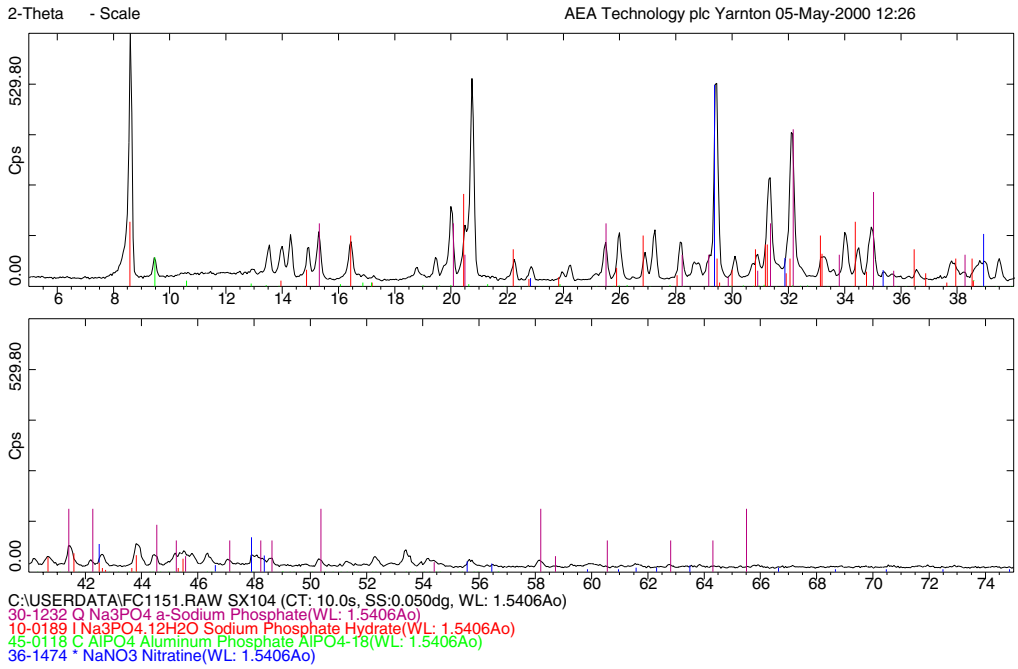

Fig. 20. X-ray pattern from SX-104 sample taken from filtered precipitate in the beaker experiments.

SX-104 Pipe Flow Experiments

Three sets of conditions were used in the pipe flow experiments:

1. fast cooling and fast flow,
2. fast cooling and slow flow, and
3. natural cooling and fast flow.

Figure 21 shows the particle size distribution for the fast-cooling, fast-flow conditions. Precipitation was observed at 30°C, and only two spectra at this temperature were obtained before the number of particles in solution became too large to obtain further readings. The corresponding particle number density plot is shown in Fig. 22. It takes approximately 15 min to reach 30°C under fast-cooling conditions. The cooling rate at this point is approximately 1 to 2°C/min, and the number in brackets in the legend indicates the time after the first detection of particles that subsequent spectra were recorded. Figures 21 and 22 indicate a broad band of particle sizes from 1800 to 20 μm, with the majority of particles smaller than 50 μm.

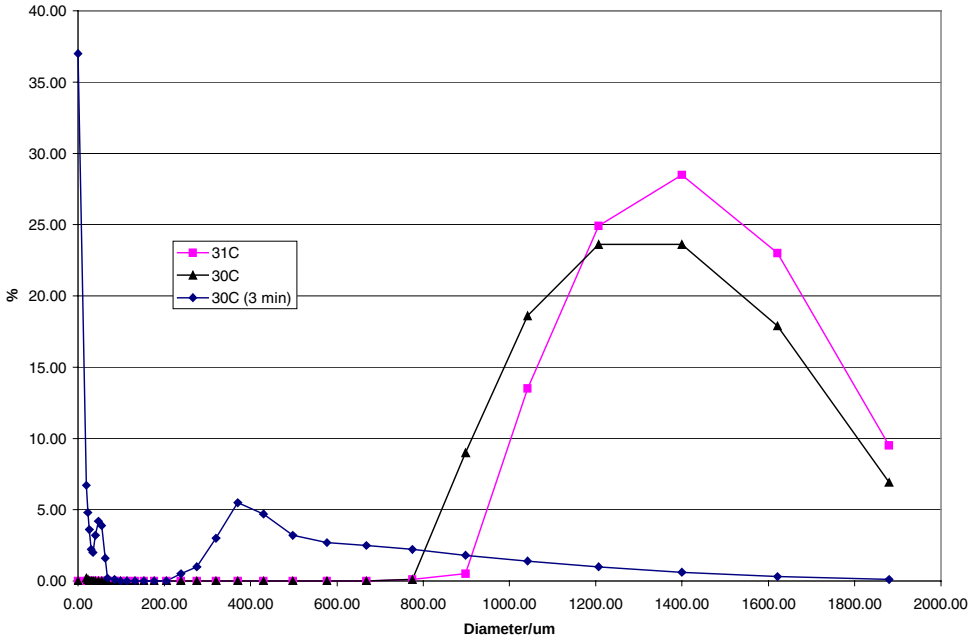

Fig. 21. Particle size distribution from repeat experiment carried out under fast-flowing, fast-cooling conditions for SX-104 simulant.

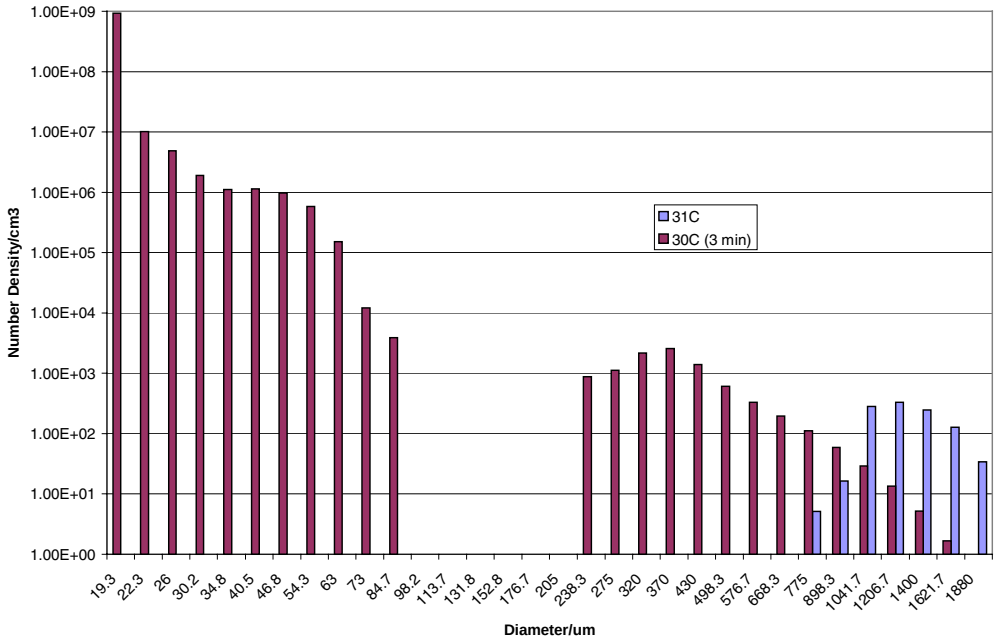

Fig. 22. Particle number density distribution from repeat experiment carried out under fast-flowing, fast-cooling conditions for SX-104 simulant.

Figure 23 is plot of the particle size distribution for the fast-flow, natural cooling conditions, and Fig. 24 shows the corresponding number density plot. The cooling rate here was approximately 1°C every 2 to 3 min. Precipitation was first observed at 32°C, and the largest observed particle size was approximately 500 µm. As time progresses, the large particles are rapidly obscured by the large number of small particles (i.e., those <50 µm).

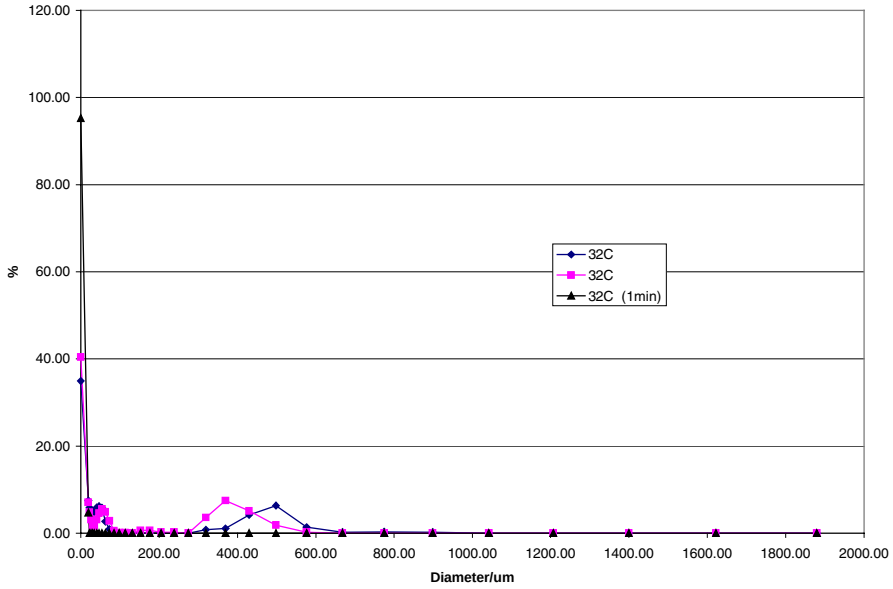

Fig. 23. Particle size distribution from experiment carried out under fast-flowing, natural-cooling conditions for SX-104 simulant.

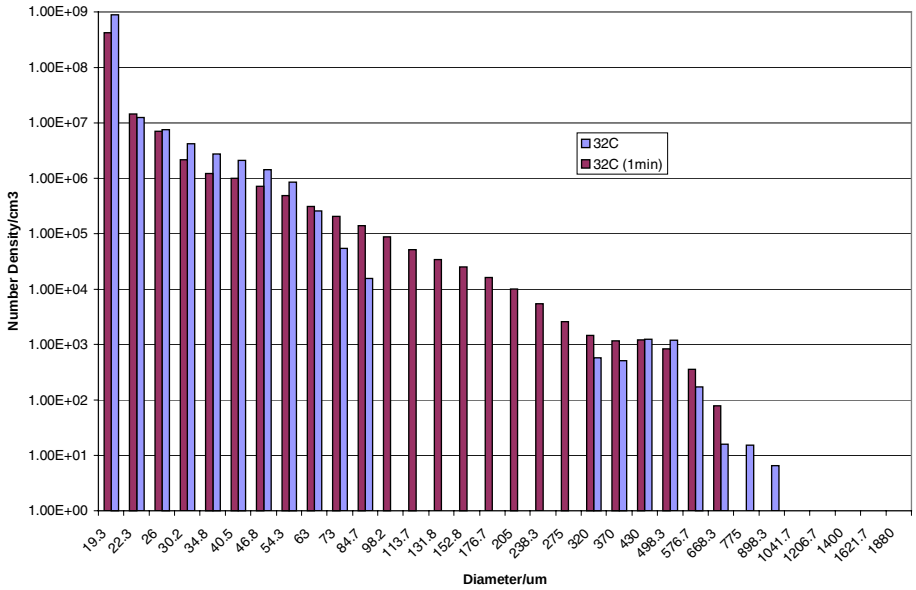

Fig. 24. Particle number density distribution from experiment carried out under fast-flowing, natural-cooling conditions for SX-104 simulant.

4.3.3 Precipitation from the Tank Simulant Mixture An-103

The goal of the experiments being carried out by AEA Technology is to examine the properties of the precipitates generated by tank simulant mixtures. A prerequisite therefore is that the material is first soluble at elevated temperature. If some of the material is not soluble at elevated temperature, then the meaning of any particle sizing becomes obscure and results may simply reflect the size and shape of the crystals used to form the simulant. In addition, if the material is not completely soluble and the initial solids content is high, then laser light scattering may not work. In the case of AN-103, it proved impossible to get all the material into solution using the initial formulation provided by Hunt (2000). Modifications to this formulation were then attempted. The results of these experiments are outlined below. None of the formulations used provided particle-sizing data.

The initial recipe used by AEA is shown in Table 3.

Table 3. Initial AN-103 recipe, as provided by Hunt

Chemical	Weight (g)
$NaAlO_2$	162.49
$Al(NO)_3 \cdot 9H_2O$	413.82
NaCl	8.62
Na_2CO_3	73.3
NaF	2.55
$NaNO_3$	170.16
NaOH	269.75
$Na_3PO_4 \cdot 12H_2O \cdot ¼NaOH$	12.18
$Na_2SiO_3 \cdot 5H_2O$	3.03
Na_2SO_4	6.4
H_2O	884.78

The fluorophosphate mixed salt was expected to precipitate. However, attempts to dissolve this mixture proved impossible, and eventually two solids remained: a brown solid (15.9 g) and the other white (97.5 g). After storage for 1 week, the solution turned orange and precipitated large well-formed octahedral colorless crystals (~5 mm in length). These crystals were sent for XRD analysis and identified as $NaNO_3$.

Various experiments were performed to reformulate the AN-103 simulant mixture in order to improve the dissolution. The final modified recipe is presented in Table 4.

Further dissolution of aluminate in this mixture was impossible; on cooling, this recipe produced no precipitate after standing at room temperature for over a week. The modified recipe given in Table 4 is very different from the initial recipe in Table 3 and thus is not really a good representation of AN-103. Discussions with TFA concerning how to proceed with AN-103 are ongoing.

Table 4. Modified recipe and addition sequence for AN-103 containing aluminate

Chemical	Weight (g)
NaF	0.288
Water	100
NaOH	13.56
$Na_2SiO_3 \cdot 5H_2O$	0.34
$NaAlO_2$	7
$Na_3PO_4 \cdot 12H_2O$	1.33
Na_2SO_4	0.723
Na_2CO_3	8.28
NaCl	0.974
$NaNO_3$	19.22
NaOH	16.94
$Al(NO_3)_3 \cdot 9H_2O$	46.74

4.3.4 Precipitation from the Savannah River Tank Simulant Mixture

The recipe for the Savannah River simulant is given in Table 5 and was provided by Hobbs (2000).

Table 5. Mixture used for Savannah River simulant

Chemical	Weight (g)	Species molarity	Species molarity
Na_2CO_3	21.198	0.4 Na	0.2 carbonate
$NaNO_2$	55.89	0.81 Na	0.81 nitrite
Na_2SO_4	1.0795	0.0152 Na	0.0076 sulphate
$(COONa)_2$	0.9246	0.0138 Na	0.0069 oxalate
$Na_3PO_4 \cdot 12H_2O$	3.8012	0.03 Na	0.01 phosphate
NaF	0.2225	0.0053 Na	0.0053 fluoride
NaCl	0.3273	0.0056 Na	0.0056 chloride
$Al(NO_3)_3 \cdot 9H_2O$	90.0312	0.24 aluminate	0.72 nitrate
$NaNO_3$	5.9493	0.07 Na	0.07 nitrate
KOH	1.1783	0.021 K	0.021 hydroxide
NaOH	122.36	3.059 Na	3.059 hydroxide
Water	958.96		

The following factors should be noted:

1. All aluminate was added as aluminum nitrate: $Al^{3+} + 2OH^- \rightarrow AlO_2^- + 2H^+$.
2. Total sodium = 4.409 *M*, not 4.9 *M* as stated by Hobbs (2000).
3. Total nitrate = 0.79 *M*.
4. Net hydroxide = 2.6 *M*.

The solution was made up in a beaker, and small amounts of silicate were then added to this basic recipe. First, a concentration of 0.0036 *M* silicate was used. After a 3-h dissolving period and allowing the solution to cool down naturally to room temperature, particles could be seen with the naked eye. This

recipe was therefore used in the flow light scattering equipment; however, under these conditions, no particles were observed. The concentration of silicate was therefore increased further, and a small bench-scale trial was carried out at 0.0048 *M* silicate. At this concentration, the silicate did not readily dissolve at 80°C. After 4 h, the silicate appeared to have dissolved but immediately began to change in color and to form a light-brown/grey particulate. This did not dissolve even with an increase of the temperature to 90°C. This sample was then left to stand at room temperature for a period of 1 week with no apparent change.

A sample of the precipitate from the 0.0048 *M* silicate mixture was taken 24 h after precipitation and particle sizes analyzed using the small-cell light scattering device and isopropyl alcohol as the medium. The results of these measurements are shown in Figs. 25 and 26. Figure 25 is a plot of the weight percent in each size category, and Fig. 26 is a plot of particle number density against particle size. After 24 h, the particles are mainly very small, with 30% (by weight) less than 19 μm. A sample of this solution was then analyzed 1 week later. The results of this analysis are shown in Figs. 27 and 28. The particles had grown in size, with 35% (by weight) between 1041.7 and 1400 μm.

4.3.5 Crystal Density Measurements

Crystals generated and identified in the work reported in Sect. 4.2.1 were used to obtain crystal densities. In order to measure the crystal densities, a Sartorius Master Series balance and density measurement equipment were used. A sample of the crystals was weighed in air and then subsequently weighed suspended in a suitable liquid. The difference in weights (i.e., the buoyancy) is then used to calculate the density. The crystal sample is contained on a wire-framed holder, and corrections for the volume of this structure are applied. Corrections are also applied for density changes with temperature, and various thermal expansion coefficients are used for air, the solvent, and the wire holder. This device incorporates software for performing all these calculations.

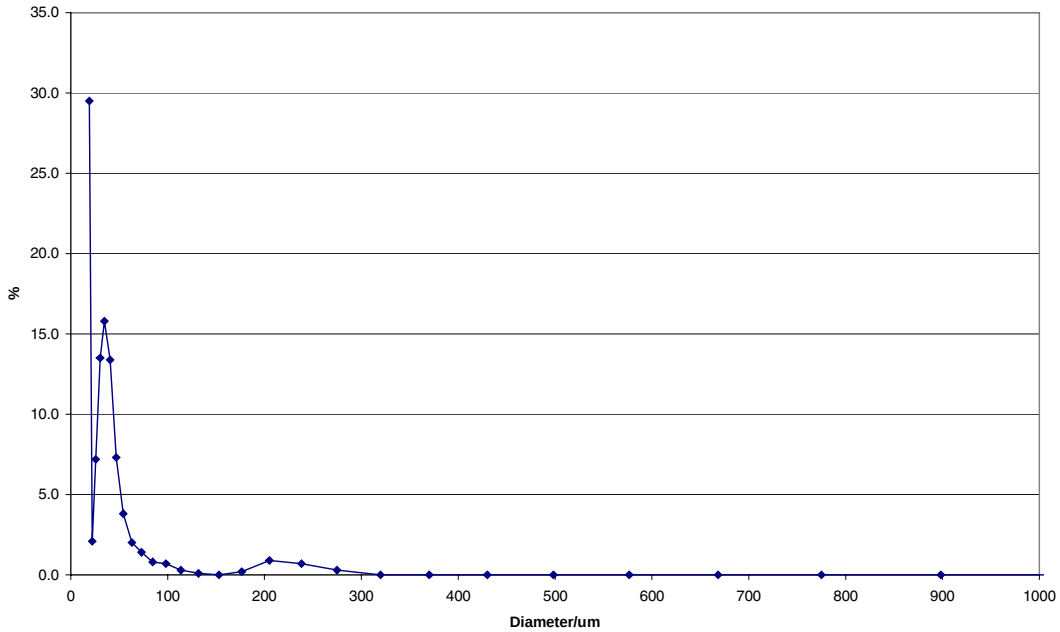

Fig. 25. Particle size distribution for precipitate from Savannah River simulant mixture. Distribution for 0.0048 *M* silicate solution shows results 24 h after precipitation.

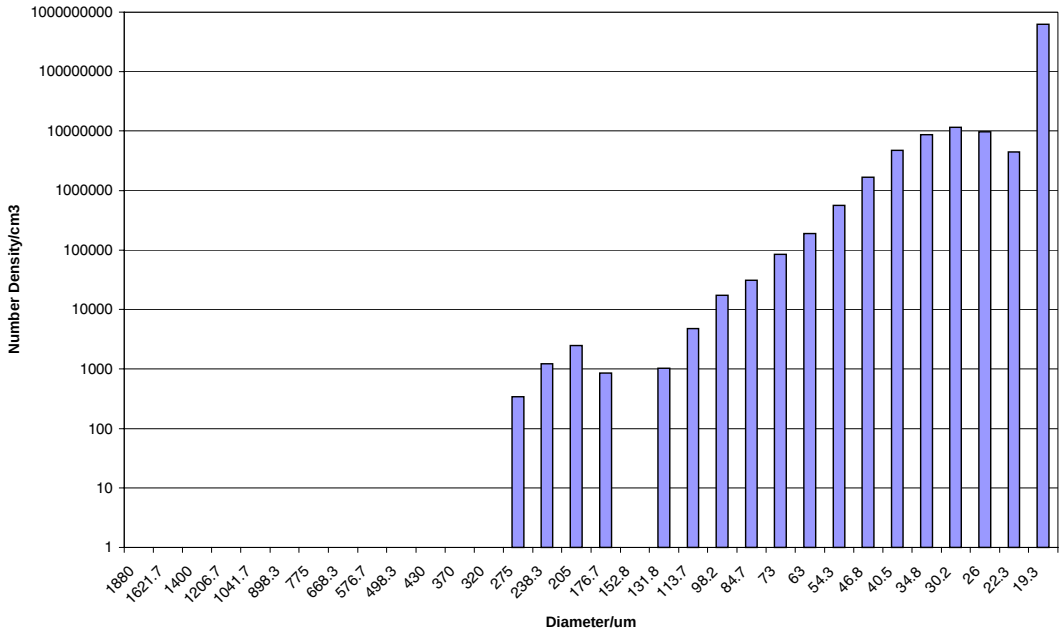

Fig. 26. Particle number density distribution for precipitate from Savannah River simulant mixture. Distribution for 0.0048 *M* silicate solution shows results 24 h after precipitation.

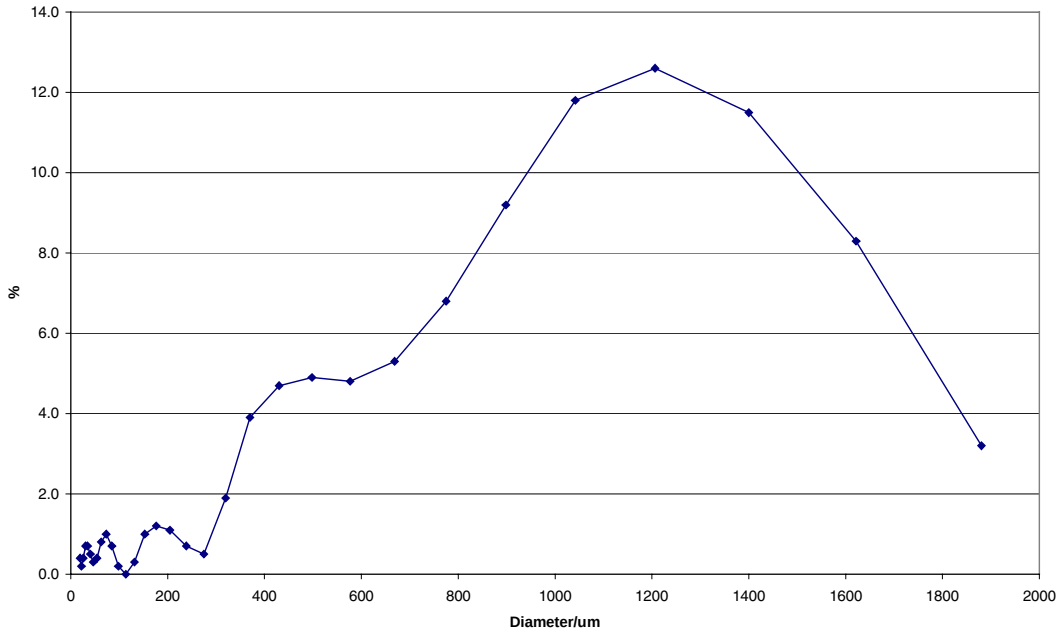

Fig. 27. Particle size distribution for precipitate from Savannah River simulant mixture. Distribution for 0.0048 *M* silicate solution shows results 1 week after precipitation.

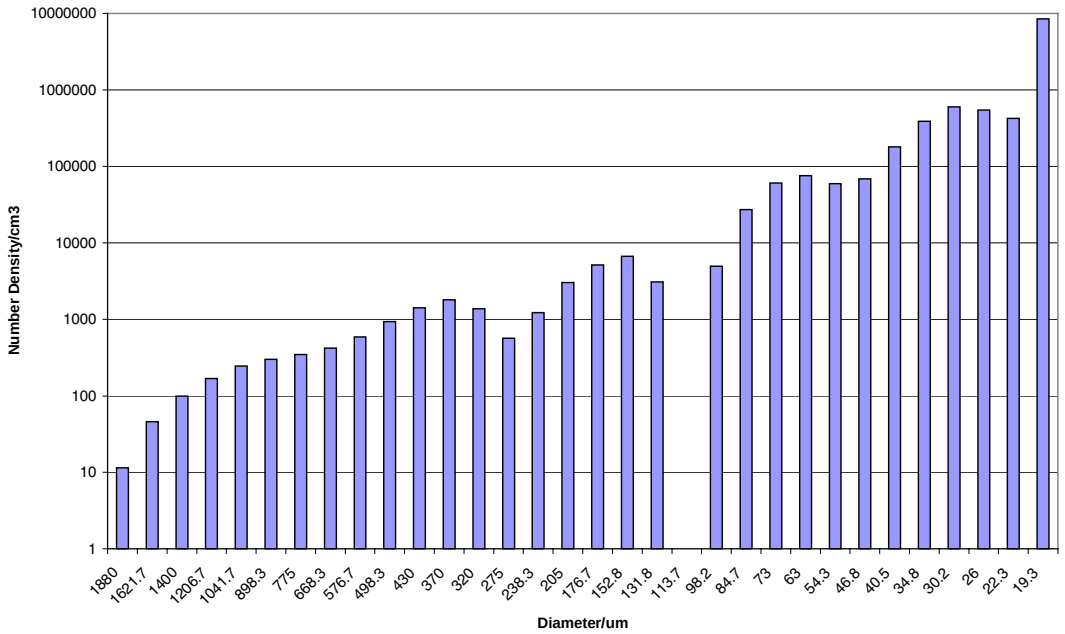

Fig. 28. Particle number density distribution for precipitate from Savannah River simulant mixture. Distribution for 0.0048 *M* silicate solution shows results 1 week after precipitation.

The results from the measurement are given in Table 6. As indicated, where literature data are available, they compare well with tabulated values (Weast 1987).

Table 6. Results from crystal density measurements

Experiment	Crystal	Density (g/cm^3)	Literature value (g/cm^3)
0.2 *M* F^-/0.2 *M* PO_4^{3-} in 1 *M* NaOH (fast cooled from 50°C)	$Na_7F(PO_4)_2 \cdot 19H_2O$	1.75 ± 0.05	
AN-103 precipitate that arose from decanted liquid (initially at 90°C)	$NaNO_3$	2.23 ± 0.05	2.26
SX-104 precipitate from 1-L trial experiments heated to 80°C and then natural or fast cooled	$Na_3PO_4 \cdot 12H_2O$	1.66 ± 0.05	1.62

4.4 Discussion

This report summarizes the main results reported previously in Francis et al. (2000a, 2000b, 2000c). This work has attempted to measure particle sizes, number densities, and crystal densities of precipitates formed from solution for a range of mixtures of interest to TFA and the storage tank facilities in the United States. In particular, the following solutions have been studied:

1. fluoride/phosphate solutions,
2. tank simulant SX-104,

3. tank simulant AN-103, and
4. Savannah River simulant.

Precipitates have been generated and studied using either an optical microscope or a laser light scattering technique. Experiments have been carried out under highly turbulent conditions (beaker experiments) or under flow conditions that more clearly simulate the behavior in the pipe transfer lines (pipe flow experiments).

Two main problems have been encountered in performing all these measurements:

1. dissolving all the solids into solution at the appropriate concentrations and
2. performing light scattering experiments on solutions with a high solid fraction.

The light scattering measurements of particle size on the fluoride/phosphate system indicated the presence of large (>1000-μm) particles. Although the number of such particles could be small, because they represent a significant weight fraction of the precipitate, they still make a significant contribution to the particle distribution. Studying the behavior of such large particles over a long duration was impossible with the current experimental arrangement because the particles were soon obscured after the onset of precipitation. Experiments with the beaker arrangement yielded similar large particles. Contrary to expectation, there is some indication that fast cooling of the solutions may enhance the formation of these large particles, but further work is required to confirm this. All the crystals generated in the fluoride/phosphate study were identified by XRD as the mixed salt $Na_7F(PO_4)2{\cdot}19H_2O$, which has an octahedral crystalline form with a measured density of 1.75 g/cm^3.

In the case of the SX-104 simulant, two major crystalline forms precipitated out of solution. These were identified by XRD as $Na_3PO_4{\cdot}12H_2O$ and $NaNO_3$, the densities of which have been reported. The beaker experiments indicated that the phosphate salts precipitated readily out of solution while the nitrate seemed to require a large surface-to-volume ratio to provide nucleation sites. The phosphate salts rapidly form long needle-like crystals, which can lead to matted structures. Optical microscope analyses indicate that these crystals can become quite large (~1000 μm) upon precipitation. Laser light scattering experiments in the flowing system also indicated the presence of such large crystals, in addition to a high concentration of small crystals (<20 μm). The precipitation process, which occurred at about 30°C after cooling from 60°C, could not be followed for a very long period of time, because the large quantity of solids being formed obscured the laser beam.

It proved impossible to get all the salts in the simulant mixture for AN-103 into solution. Attempts were made to improve the dissolution process by modifying the simulant recipe, but no sensible mixture could be derived. Consequently, no particle-sizing experiments were carried out on AN-103.

In the case of the Savannah River simulant mixture, precipitation was observed on addition of 0.0036 *M* silicate to the basic recipe. This was initially done in small-scale beaker experiments. A hot solution of the same mixture, however, did not produce particles in the flowing light scattering equipment upon cooling. Attempts to increase the silicate concentration to 0.0048 *M* failed, in that a reaction took place at 80 to 90°C that produced a brown solution containing precipitate at the elevated temperature. After cooling, particle sizing on this precipitate was carried out by light scattering and subsequently reported.

Several issues associated with the current work may need to be resolved. Some of these, such as how to progress with the simulant AN-103, need to be discussed within the TFA. The experimental plan for next year's work is intended to resolve some of these issues. The work reported has demonstrated that the monitoring of some of the relevant systems (phosphate/fluoride, SX-104) can be successfully achieved

using light scattering techniques. Currently under investigation is the use of alternative equipment (based on the same approach) that may deal with higher solid fractions in solution. The systems could then be monitored for significantly longer periods of time after the onset of precipitate formation.

4.5 Conclusions

The following conclusions have arisen from this work:

1. At appropriate concentrations, precipitation from fluoride/phosphate mixtures gives rise to the mixed salt $Na_7F(PO_4)2{\cdot}19H2O$, as identified by XRD.
2. Precipitation of the mixed salt under flow conditions similar to those in pipe transfer lines can result in the formation of large particles (>1000 μm). At very high Reynolds numbers, large particles are still formed.
3. Fast cooling may enhance the formation of such large particles, but further experiments are needed to confirm this supposition.
4. In the case of the simulant SX-104, long needle-like crystals precipitate out of solution at approximately 30°C.
5. In the case of SX-104, cubic/octahedral-type crystals precipitate out of solution in the presence of a large surface area for nucleation.
6. The salts $Na_3PO_4{\cdot}12H_2O$, Na_3PO_4, $AlPO_4$, and $NaNO_3$ were identified by XRD from the SX-104 precipitate.
7. The density of the SX-104 precipitate was measured as 1.66 g/cm^3, close to the literature value of 1.62 g/cm^3 for $Na_3PO_4{\cdot}12H_2O$; the literature values for the other salts (Na_3PO_4, $AlPO_4$, and $NaNO_3$) are 2.1, 2.57 and 2.26 g/cm^3, respectively, indicating that the predominant needle crystals are $Na_3PO_4{\cdot}12H_2O$. This also confirms earlier observations (Henshaw et al. 1999).
8. The octahedral crystals from SX-104 are probably $NaNO_3$.
9. Particle sizing on the SX-104 precipitate indicates that large particles (>1000 μm) are easily formed and make a significant contribution to the particle size distribution. Such large crystals were also observed with the optical microscope.
10. It was impossible to get all the solids into solution for the simulant AN-103.
11. The hot filtrate from attempts to dissolve all the salts for AN-103 turned orange on cooling, yielding a very fine precipitate. XRD identified this material as $NaNO_3$, the density of which was measured as 2.23 g/cm^3, which is close to the literature value of 2.26 g/cm^3.
12. Attempts to produce an alternative AN-103 simulant failed. The only mixture containing all the relevant salts that could be prepared at elevated temperature failed to result in a precipitate on cooling.
13. Addition of 0.0036 *M* silicate to the Savannah River simulant led to precipitation in small-scale laboratory tests but did not produce a precipitate in the flow equipment.
14. In preparing a 0.0048 *M* silicate Savannah River simulant, a reaction took place at 80°C that led to a change in color of the solution and to the formation of a precipitate. This precipitate remained on cooling.
15. Particle sizing on the Savannah River simulant precipitate indicated it initially forms small particles, <20 μm, which can grow to greater than 1000 μm within a week.

A number of issues need to be resolved to understand some of the results obtained. The first issue is the nature of the precipitate produced in the 0.0048 and 0.0036 *M* silicate Savannah River simulants; these should be identified using XRD. In the case of the 0.0036 *M* silicate, researchers need to determine why precipitation was not observed under flowing conditions and whether this is simply a result of fewer nucleation sites in the flowing system. Several simple experiments could be done to investigate this behavior. The situation with AN-103 needs to be discussed further with TFA, and a possible path forward

should be identified. Relatively successful results were obtained for the SX-104 simulant and the F^-/PO_4^{3-} mixtures; however, it would be very useful to follow the particle growth for much longer periods during the precipitation process. This effort would require light scattering particle-sizing equipment that can deal with higher solid fractions than can be accommodated in the current arrangement. Alternative equipment also needs to deal with the quite large particle size range observed in these studies. This is currently being investigated by AEA Technology.

4.6 References

Francis, A., J. Henshaw, M. Manning, N. Pilkington, and S. Swanton. 2000a. *Progress Report on Precipitation Studies of $Na^+/PO_4^{3-}/F^-$ Solutions*, AEAT/R/NS/0069, Harwell, Oxfordshire, U.K.

Francis, A., J. Henshaw, M. Manning, N. Pilkington, and C. Kemp. 2000b. *Progress Report on Precipitation Studies of Hanford Tank Simulant Mixtures*, AEAT/R/NS/0164, Harwell, Oxfordshire, U.K.

Francis, A. J. Henshaw, M. Manning, N. Pilkington, and C. Kemp. 2000c. *Progress Report on Precipitation Studies of Tank Simulant Mixtures (AN-103, SRS*), AEAT/R/NT/0285, Harwell, Oxfordshire, U.K.

Henshaw, J., N. Pilkington, M. Manning, and S. Swanton. 1999. *Precipitation Studies on $Na/PO_4^{3-}/SO_4^{2-}$ Solutions*, AEAT-6256, Harwell, Oxfordshire, U.K.

Hobbs, D. (Westinghouse Savannah River Company). 2000. E-mail communication (October 8).

Hunt, R. D. (Oak Ridge National Laboratory). 2000. E-mail communication, "Recipe for the Simulant of AN-103" (May 5).

Weast, R. C. (ed.). 1987. *CRC Handbook of Chemistry and Physics*, 67th ed., CRC Press, Boca Raton, Fla.

5. SOLIDS FORMATION AND FEED STABILITY: WASTE SLURRY TRANSFER TESTS WITH SIMULATED HANFORD WASTES

Rubén Darío López and Rajiv Srivastava
Hemispheric Center for Environmental Technology
Florida International University
10555 West Flagler Street, CEAS 2100
Miami, Florida 33174

Abstract

This section summarizes the research carried out at Florida International University's Hemispheric Center for Environmental Technology (FIU-HCET) for FY 2000 under the Tanks Focus Area (TFA) project "Solids Formation and Feed Stability During Waste Slurry Transfer." During FY 2000, bench- and pilot-scale flow loop studies were performed using waste slurry simulants based on DOE's Hanford tank materials specifications. The objective was to identify operating conditions that will lead to solids formation and, ultimately to plugs, in a slurry flow as a result of phase change.

The following conclusions were drawn based on the experimental observations from both the scoping tests and the pilot-scale study.

- A feed temperature of 50°C or higher was critical, because a considerable quantity of solids precipitated when the temperature was just below this number.
- Most plugging and solids formation occurred at a low temperature (15 to 20°C) and at flow velocities lower than 3 ft/s.
- The Hanford simulant AN-103 showed a plugging behavior similar to the X1 and X2 simulants (hydroxide-phosphate-fluoride and nitrate systems).
- Increasing the flow rate and raising the temperature of the system succeeded in unplugging the AN-103 and X2 simulants. The plugs in the X1 simulant had to be removed manually.
- Plug analysis showed needle-like phosphate crystals as well as aluminate, carbonate, and fluoride crystals in most samples.
- Rheology measurements of the slurry simulants tested showed a Bingham plastic behavior. Tests performed indicate that the yield stress and the apparent viscosity of the simulants decrease as the temperature is increased.

5.1 Introduction

During FY 2000, bench- and pilot-scale flow loop studies were carried out using waste slurry simulants based on Hanford tank wastes. The objective was to identify conditions that define the boundary between stable waste flow and particle formation and, ultimately, pipeline plugging. The data will be needed to specify and validate waste transfer criteria and to validate and develop engineering tools for slurry transport.

Plugging has hampered waste-slurry transport operations at the Department of Energy (DOE) Hanford site and the Savannah River Site. The pipelines can become plugged when solids settle, adhere to the wall, or form rapidly under certain operating conditions. This project addresses the effects of temperature reduction, flow regime, slurry composition, and chemical and physical processes on slurry transfer behavior by experimental tests with simulated waste in bench- and pilot-scale pipe loops. The main objectives are as follows:

- to identify the operating parameters and feed conditions that cause solids formation and pipeline plugging,
- to obtain correlation of the observed data that will enable the prediction of slurry transport characteristics, and
- to provide engineering data and technical recommendations to support the Hanford Tank Waste Remediation System (TWRS) operation.

Flow experiments were conducted in a bench-scale unit and a pilot-scale flow loop, designed to represent some aspects of a Hanford transfer line. Waste simulants recommended by the River Protection Project (RPP), representing the actual waste slurries present in the Hanford tanks, were prepared based on simulant recipes (Table 1) developed by Oak Ridge National Laboratory (ORNL). The simulants were tested in our pipe loops under both normal operating conditions and off-normal conditions to evaluate their plugging potential. Independent variables being investigated included the composition of the simulant, flow rates, initial temperature, and temperature drops (see Table 2); dependent variables included pressure drops, plug characteristics, and time required to plug. By understanding the operating conditions that can be used to avoid pipeline plugging, the risk and cost of the slurry transfer operation can be reduced and the process capacity can be increased.

Experiments were conducted in accordance with the test plan and technical plan prepared for the project (López and Srivastava 1999a, 1999b). Project findings will be used to support tank closure activities, waste pretreatment, and tank waste feed transport operations at the DOE sites.

Table 1. Formulations and concentrations of the X1, X2, and AN-103 simulants

Compound	X1 molality	X2 molality	AN-103 molality
$NaAlO_2$	0	0	1.982
Na_2CO_3	0	0	0.692
$Al(NO_3)_3 \cdot 9H_2O$	0	0	1.103
$Fe(NO_3)_3 \cdot 9H_2O$	0	0	0
NaCl	0	0	0.148
NaF	0.2	0.2	0.061
$NaNO_3$	0	7	2.016
Fe_2O_3	0	0	0
$Mn(NO_3)_2$	0	0	0
NaOH	3	3	6.744
$Na_2C_2O_4$	0	0	0
$Na_3PO_4 \cdot 12H_2O$	0.6	0.6	0.031
$Na_2SiO_3 \cdot 5H_2O$	0	0	0.028
Na_2SO_4	0	0	0.045
ZrF_4	0	0	0
ZrO_2	0	0	0
H_2O	0	0	49.113

Table 2. Test matrix for scooping tests of X1, X2, and AN-103

Feed tank temperature (°C)	Tubing temperature (°C)	Flow velocity[a] (ft/s)
50	15	0.26 (0.72) Laminar flow
	40	
50	15	0.57 (1.80) Transition flow
	40	
50	15	(0.72) 2.10 Transition flow
	40	
50	15	0.91 (2.66) Turbulent flow
	40	
50	15	1.05 (3.05) Turbulent flow
	40	
50	15	1.24 (3.50) Turbulent flow
	40	
50	15	1.54 (3.90) Turbulent flow
	40	

[a]The following assumptions were made to calculate the flow rate: pipe diameter = 3/8-in. ID, viscosity = 1 cP, and density = 1 g/cm^3.

5.2 Bench-Scale Study

5.2.1 Experimental

A bench-scale unit was set up for the scoping experiments, as shown in Fig. 1. The system design included the following features:

- Simulated waste transfer using a rotary progressive cavity pump.
- A simulant feed tank. The temperature in the feed tank is controlled (50°C is the Hanford criterion for the minimum temperature of slurry feed) by a heating system mounted on the side of the tank. It includes two 1.5-kW electrical heaters. A mixer is also attached to the lid of the tank.

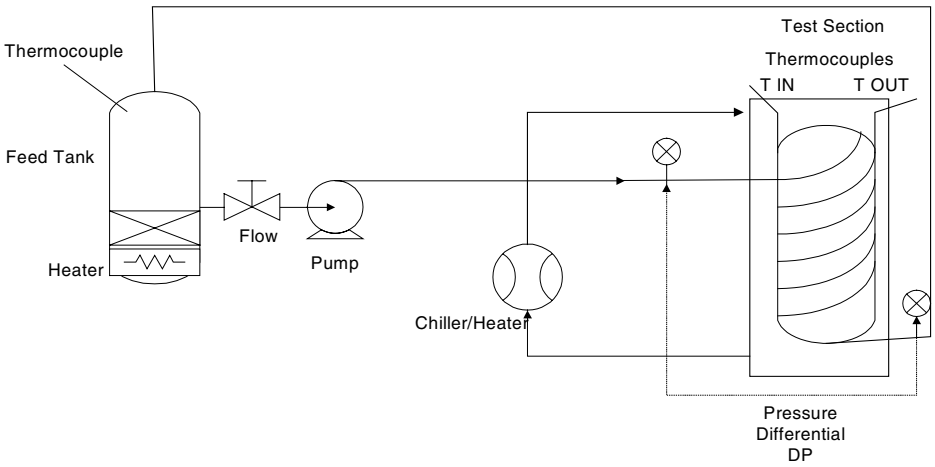

Fig. 1. Schematic of the bench-scale unit.

- A test section containing a 3/8-in. ID, 30-ft-long clear polyethylene tubing inside a transparent cooling/heating bath (see Fig. 2). This section is placed inside the water bath so the temperature of the test section can be controlled. Test temperatures are 15, 40, and 50°C.
- Pressure transducers to measure the pressure differential across the test section.
- Thermocouples for temperature monitoring, one in the feed tank and two at the test section (inlet and outlet).
- A flowmeter to measure the simulant flow rate.
- A time-lapse video recorder system for plug monitoring (formation and location).
- An automated data acquisition system (LabVIEW), by which temperature (feed tank and test section), flow rate, and pressure drop (across test section) are monitored.

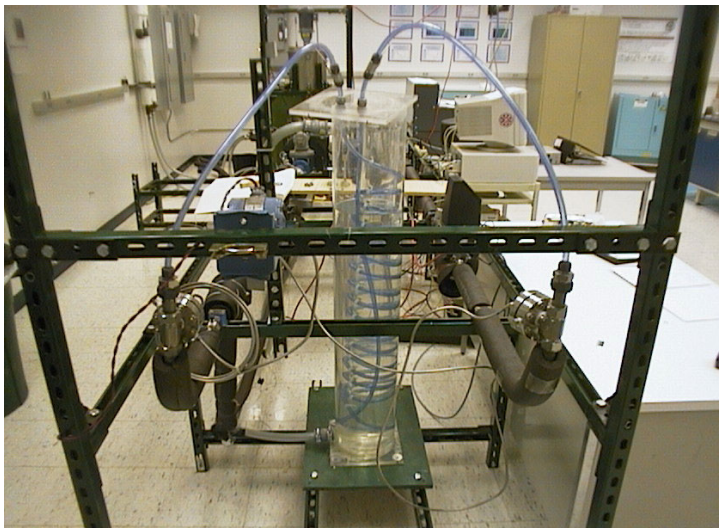

Fig. 2. Test section inside the cooling/heating bath.

5.2.2 Results

This section summarizes results from the scoping tests. Tables 3 through 5 show the experimental observations from the scoping tests for simulants X1, X2, and AN-103, respectively. Figures 3 through 6 show some of the plugs that were formed during these tests.

Table 3. X1 simulant scoping tests experimental observations
(3 *M* NaOH + 0.2 *M* NaF + 0.6 *M* Na_3PO_4)

Feed tank temperature (°C)	Flow velocity (ft/s)	Comments	
		Temperature at test section (15°C)	**Temperature at test section (40°C)**
50	0.72 Laminar flow	• Complete plugging. • No flow after plugging. • The pump speed was increased to maximum power to try to unplug the system. However, this procedure was unsuccessful since the system did not unplug after several tries. • Plugs were manually removed after pump shutdown.	• Partial plugging. • Crystal formation after cooling samples obtained from loop. • Abnormal flow conditions.
50	1.80 Transition flow	• Abnormal flow (flow reading fluctuations due to increase in solids formation). • Partial plugging. Solids formation.	• No plugging. • Solids formation. • Normal flow conditions.
50	2.10 Transition flow	• No plugging. Some solids formation. • Normal flow conditions.	• No plugging. • Normal flow conditions.
50	2.66 Turbulent flow	• No plugging. Solids observed. • Normal flow.	• Normal flow conditions. • Some solids.
50	3.05 Turbulent flow	• No plugging. Very little solids formation observed. • Normal flow.	• Normal flow conditions. • No solids observed.
50	3.5 Turbulent flow	• No plugging. • Normal flow conditions.	• Normal flow conditions. • No solids observed.
50	3.9 Turbulent flow	• No solids formation observed. • Flow normal.	• Normal flow conditions. • No solids observed.

Table 4. X2 simulant scoping tests experimental observations
(3 *M* NaOH + 0.6 *M* Na_3PO_4 + 0.2 *M* NaF + 7 *M* $NaNO_3$)

Feed tank temperature (°C)	Flow rate (ft/s) (Re)[a]	Comments	
		Temperature at test section (15°C)	Temperature at test section (40°C)
50	0.72 (2201) Laminar flow	• Plugging observed with significant solids formation. • Unplugging of the system was attained when pump power and temperature were increased. • System was successfully flushed after unplugging. • Any remaining solids were manually removed after pump shutdown.	• Partial plugging. • Solids formation. • Needle-like crystals observed in samples. • Abnormal flow conditions (flow reading fluctuations due to crystals formation).
50	1.80 (4826) Transition flow	• Abnormal flow. • Partial plugging. • Solids formation increased.	• No plugging. • Some solids formation. • Normal flow conditions.
50	2.10 (6096) Transition flow	• No plugging. • Some solids formation. • Normal flow conditions.	• No plugging. • Normal flow conditions. • Few solids observed.
50	2.66 (7705) Turbulent flow	• No plugging. Solids observed. • Normal flow.	• Normal flow conditions. • Very few solids.
50	3.05 (8890) Turbulent flow	• No plugging. • Solids observed. • Normal flow.	• Normal flow conditions. • No solids observed.
50	3.5 (10498) Turbulent flow	• No plugging. • Some solids observed. • Normal flow conditions.	• Normal flow conditions. • No solids observed.
50	3.9 Turbulent flow	• No plugging. • Little solids formation observed. • Flow normal.	• Normal flow conditions. • No solids observed.

[a]Reynolds number indicated parenthetically.

Table 5. AN-103 simulant scoping tests experimental observations
(1.982 *M* $NaAlO_2$ + 1.103 *M* $Al(NO_3)_3 \cdot 9H_2O$ + 0.148 *M* NaCl + 0.692 *M* Na_2CO_3 + 0.061 *M* NaF + 2.016 *M* $NaNO_3$ + 6.744 *M* NaOH + 0.031 *M* Na_3PO_4 + 0.028 *M* $Na_2SiO_3 \cdot 5H_2O$ + 0.045 *M* Na_2SO_4 + 49.113 *M* H_2O)

Feed tank temperature (°C)	Flow velocity (ft/s)	Comments	
		Temperature at test section (15°C)	Temperature at test section (40°C)
50	0.72 Laminar flow	• Plugging observed with significant solids formation. • Moving bed observed. • Unplugging attained when temperature and flow rate were increased.	• Partial plugging. • Solids formation.
50	1.80 Transition flow	• Partial plugging. • Solids formation increased.	• No plugging. • Solids formation.
50	2.10 Transition flow	• No plugging. • Solids formation.	• No plugging. • Solids observed.
50	2.66 Turbulent flow	• Solids observed. • Normal flow.	• Normal flow conditions. • Few solids.
50	3.05 Turbulent flow	• No plugging. • Solids observed. • Normal flow.	• Normal flow conditions. • No solids observed.
50	3.5 Turbulent flow	• No plugging. • Some solids observed. • Normal flow conditions.	• Normal flow conditions. • No solids observed.
50	3.9 Turbulent flow	• No plugging. • Little solids formation observed.	• Normal flow conditions. • No solids observed.

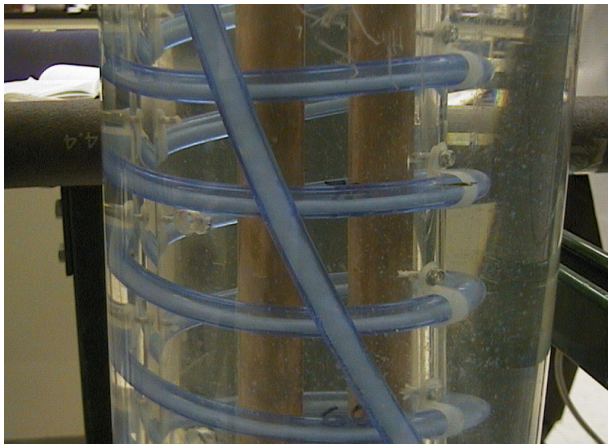

Fig. 3. System plugging in test section (X2 simulant).

Fig. 4. Clear tubing partially plugged at test section (AN-103 simulant).

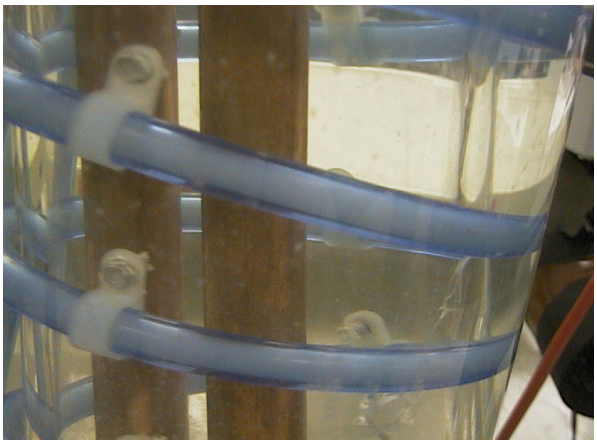

Fig. 5. Clear tubing fully plugged at test section (X1 simulant).

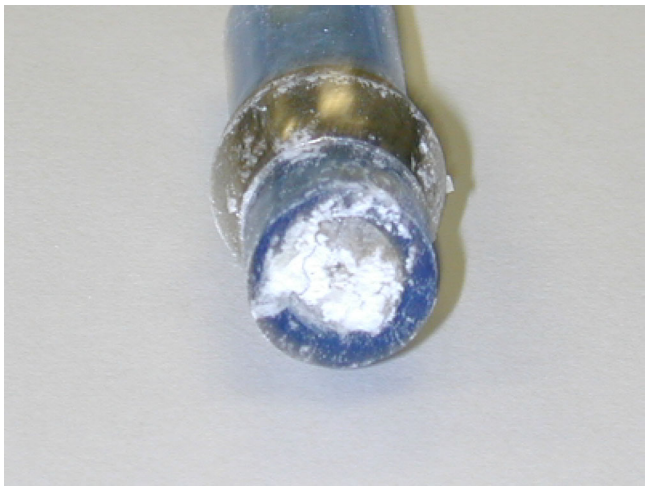

Fig. 6. Cross-sectional view of a typical plug.

Pressure Drop Data

Validation control tests were performed with water prior to testing the simulants in the flow loop. This information was needed to test the accuracy of the different pressure transducers present in the loop. Figure 7 shows that an excellent correlation exists between theoretical and measured values.

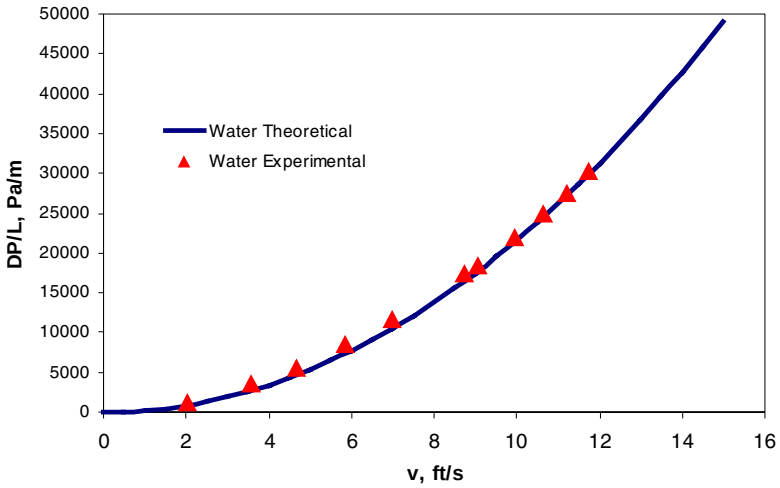

Fig. 7. Pressure drop versus flow velocity data for AN-103 simulant.

Figures 8–13 show the pressure differential versus flow velocity correlation for the three simulants tested at two different test section temperatures (15 and 40°C). Experimental and theoretical water pressure drops (control tests) are included in each figure for comparison. As can be observed, the simulants behave as Bingham plastic, non-Newtonian fluids. Also note that the pressure gradient increases with the percentage solids (X2 simulant had the greater solids concentration, about 28% by weight).

Plug Analyses

Several samples were prepared and obtained from the different scoping tests. The samples were mounted on a carbon tape and placed on the stage of a Phillips XL30/DX4i scanning electron microscopy (SEM) with X-ray dispersive analysis. The samples were imaged with an accelerating voltage of 20.0 kV, and the detector was a secondary electron.

X1 plug samples. SEM images for simulant X1 after first plugging are presented in Figs. 14 through 18. The particles from this X1 simulant contain carbon, oxygen, fluorine, sodium, and phosphorus, as shown in Table 6.

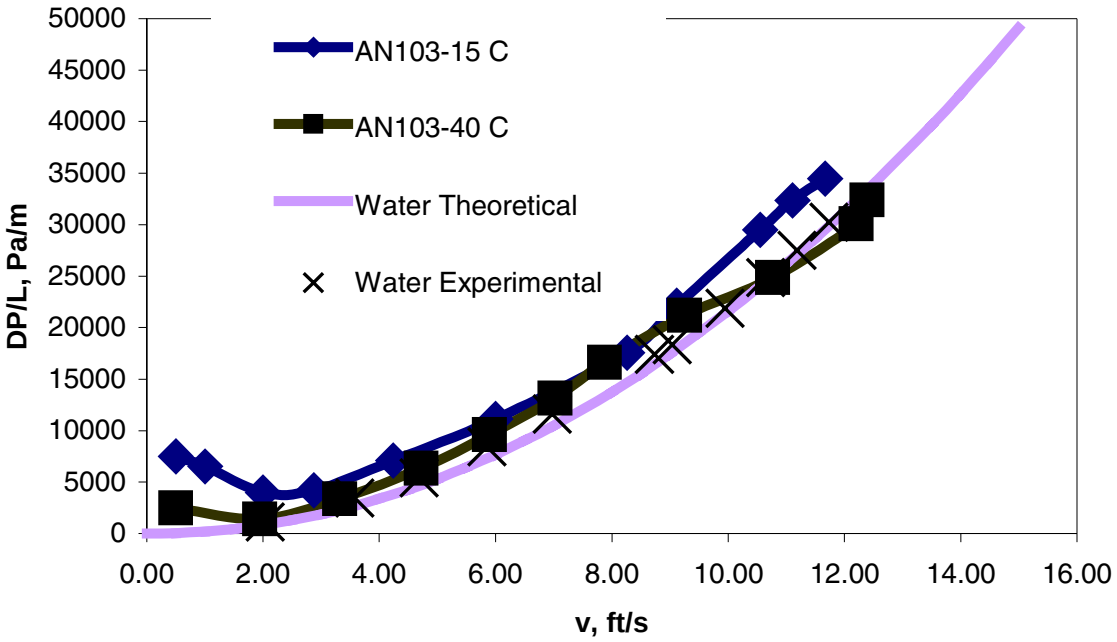

Fig. 8. Pressure drop versus flow velocity data for AN-103 simulant.

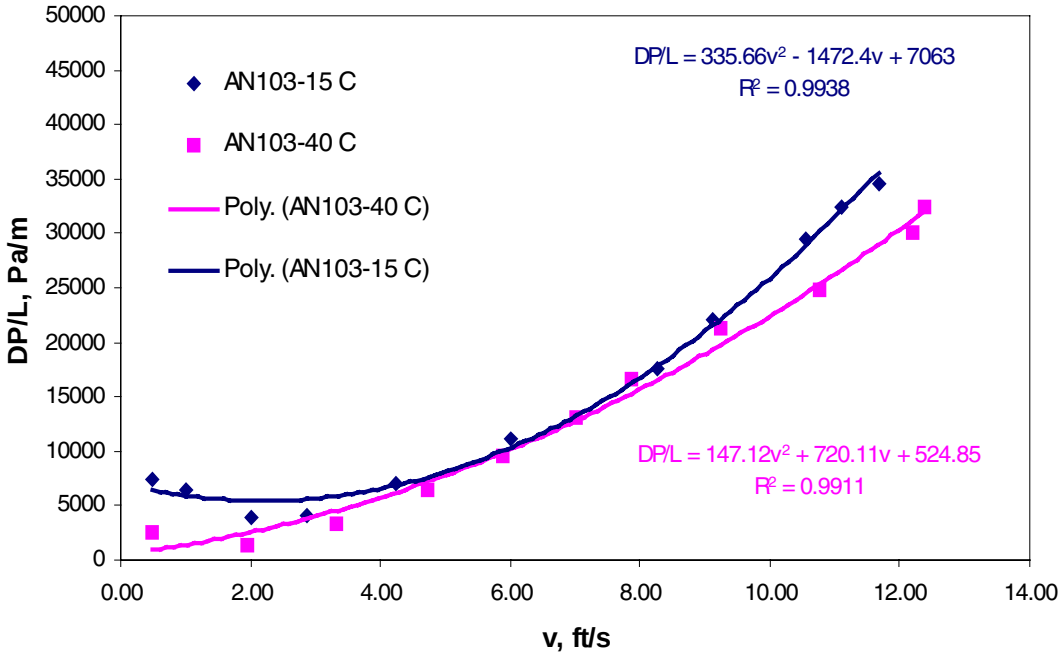

Fig. 9. Correlation models for AN-103 simulant pressure drop data.

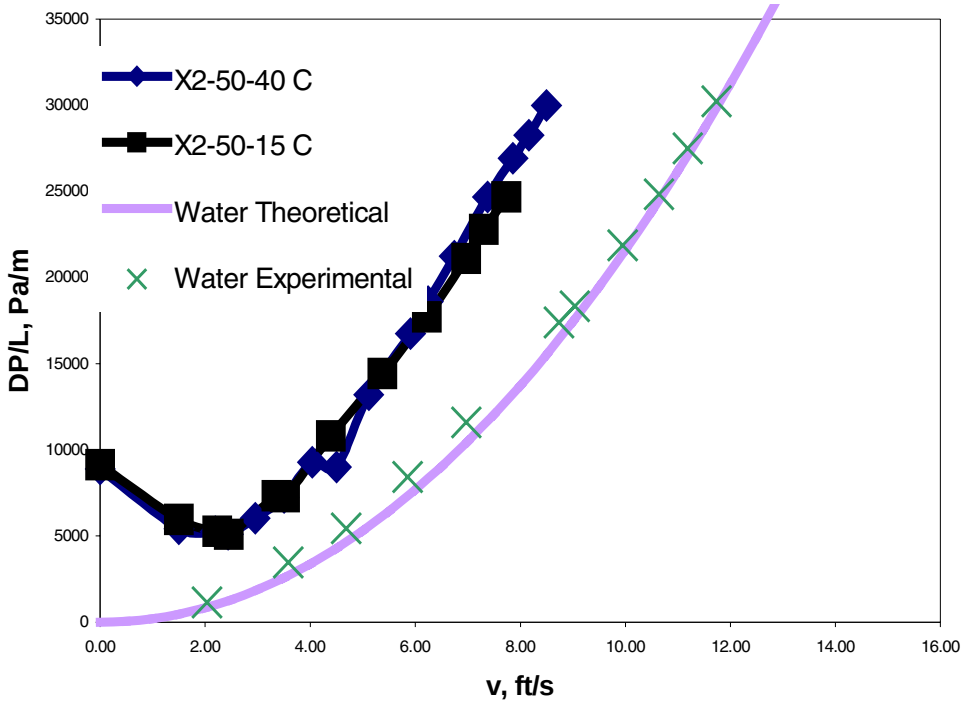

Fig. 10. Pressure drop versus flow velocity data for X2 simulant.

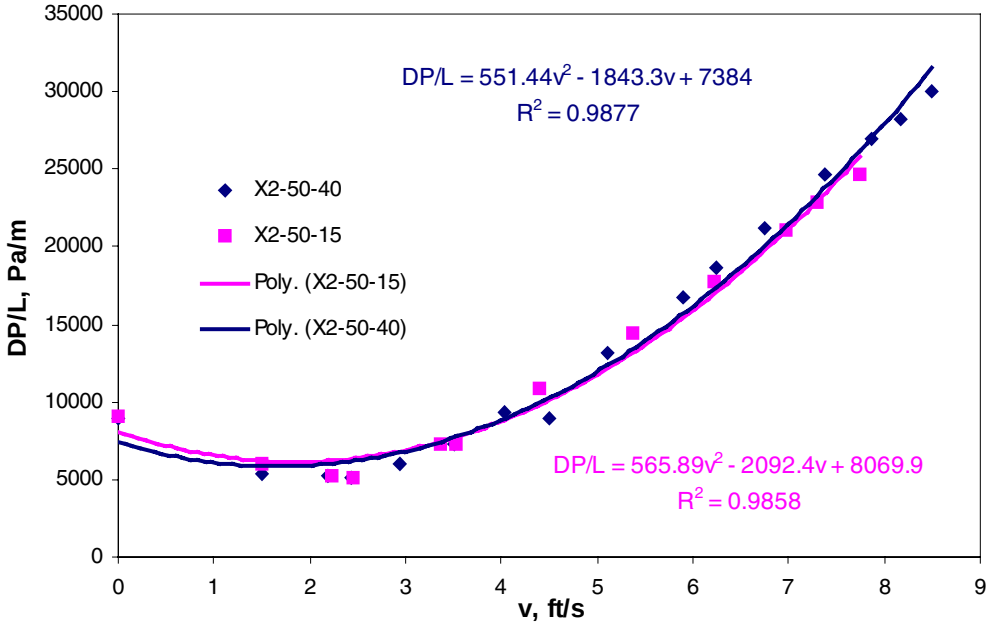

Fig. 11. Correlation models for X2 simulant pressure drop data.

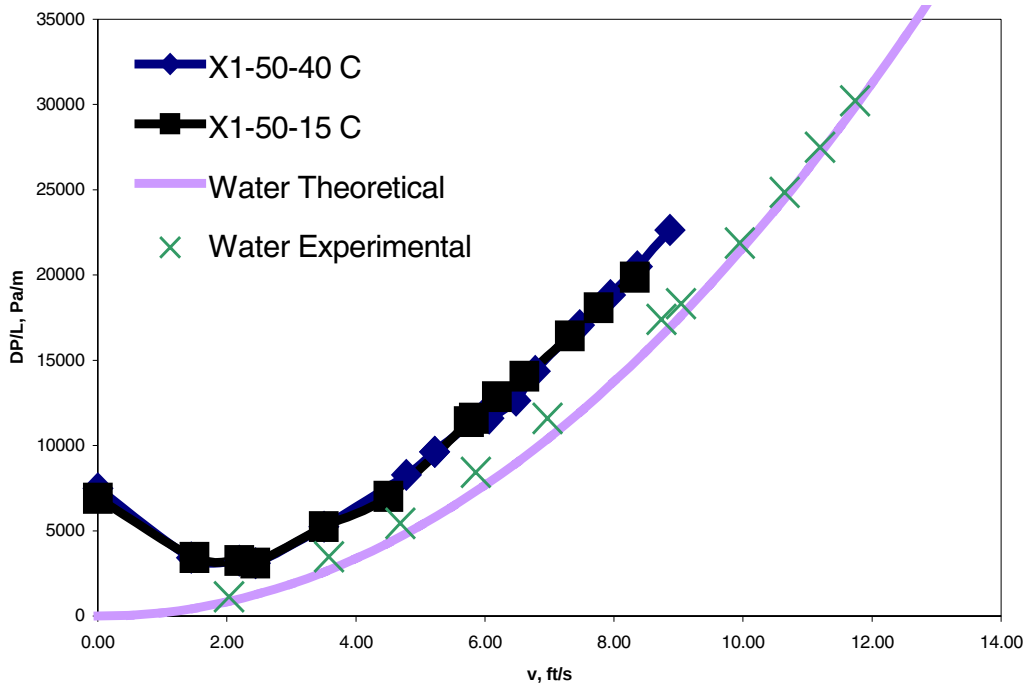

Fig. 12. Pressure drop versus flow velocity data for X1 simulant.

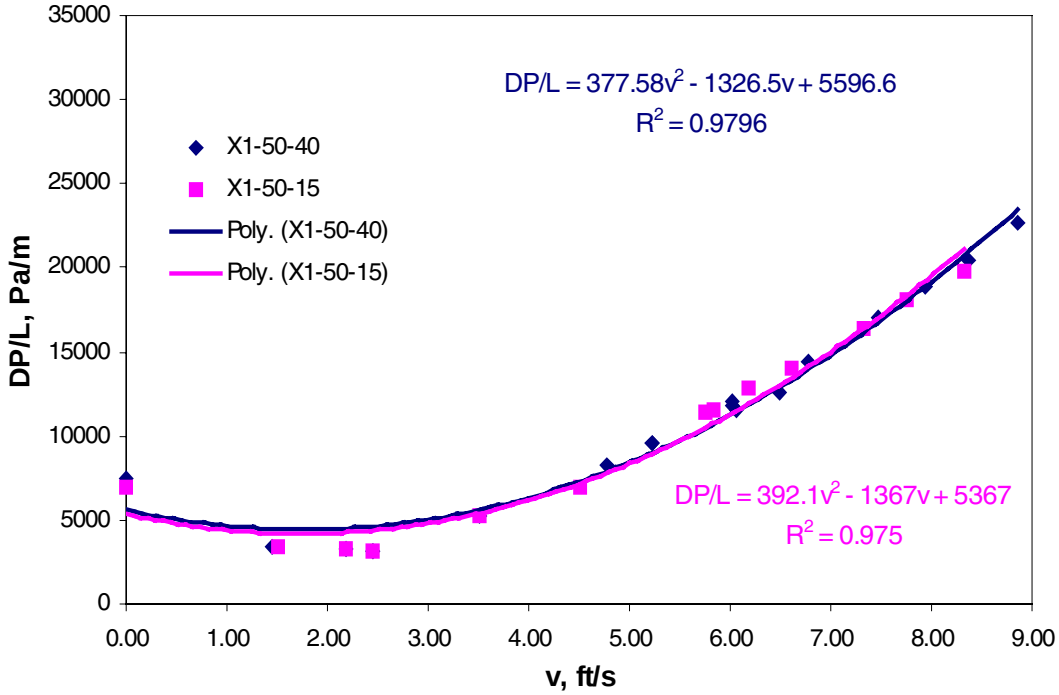

Fig. 13. Correlation models for X1 simulant pressure drop data.

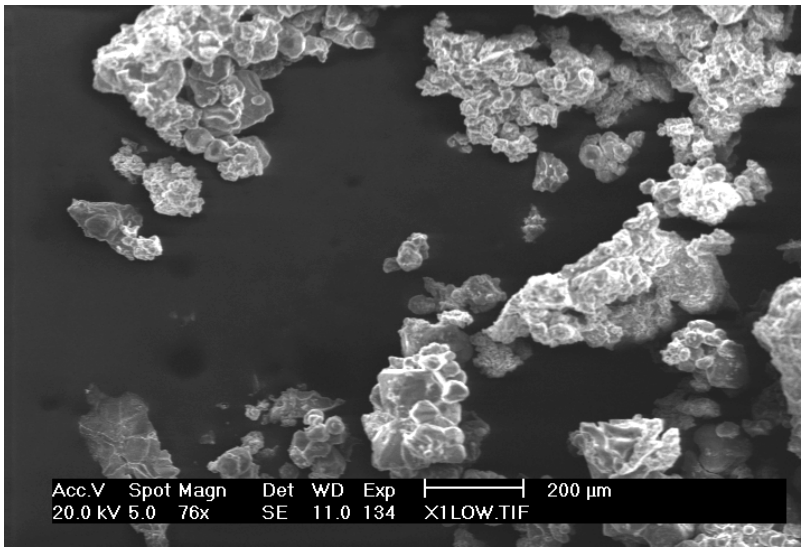

Fig. 14. X1 simulant after first plugging.

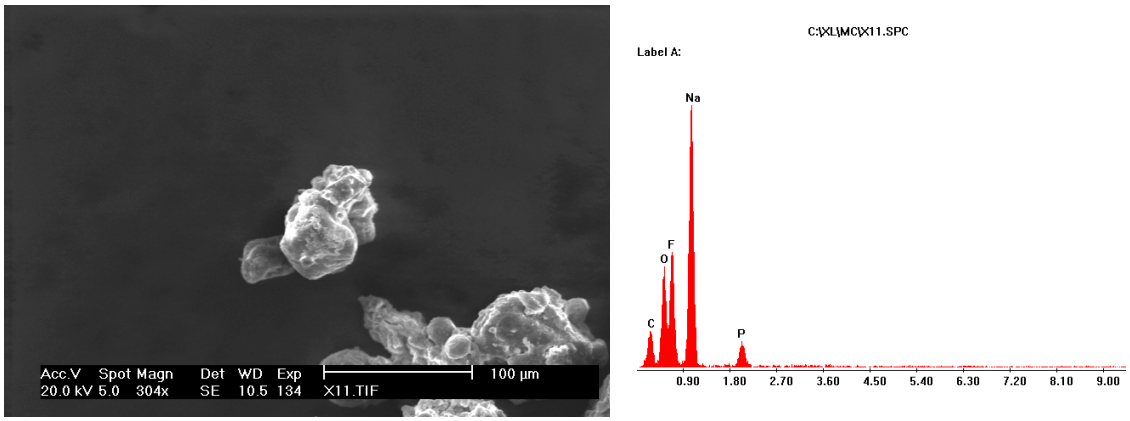

Fig. 15. Particle 1 of X1 simulant after first plugging.

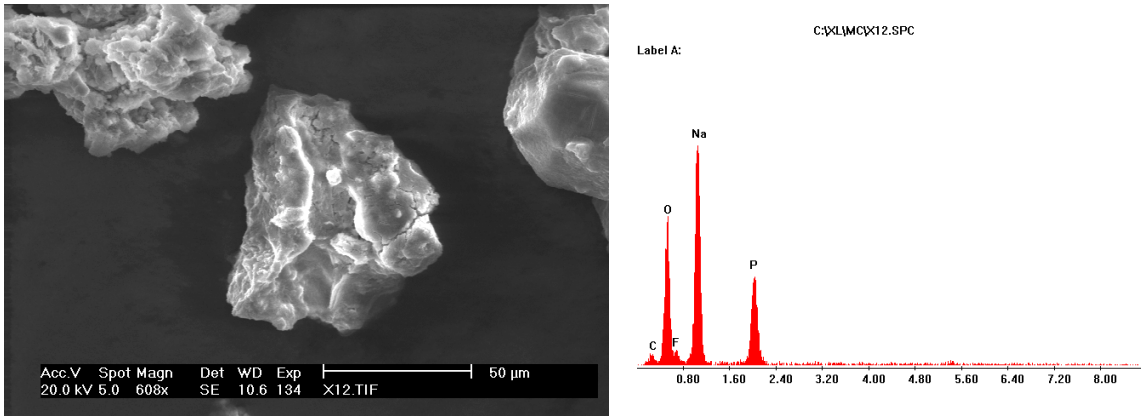

Fig. 16. Particle 2 of X1 simulant after first plugging.

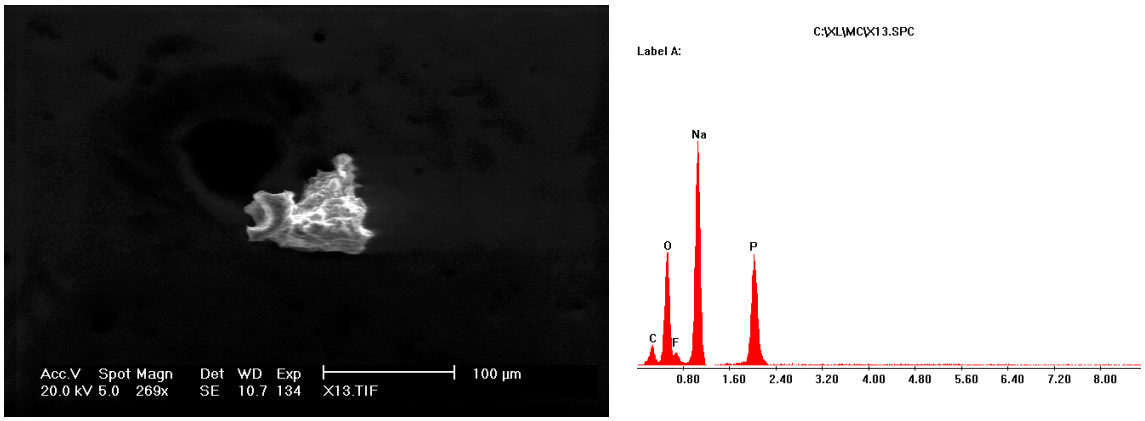

Fig. 17. Particle 3 of X1 simulant after first plugging.

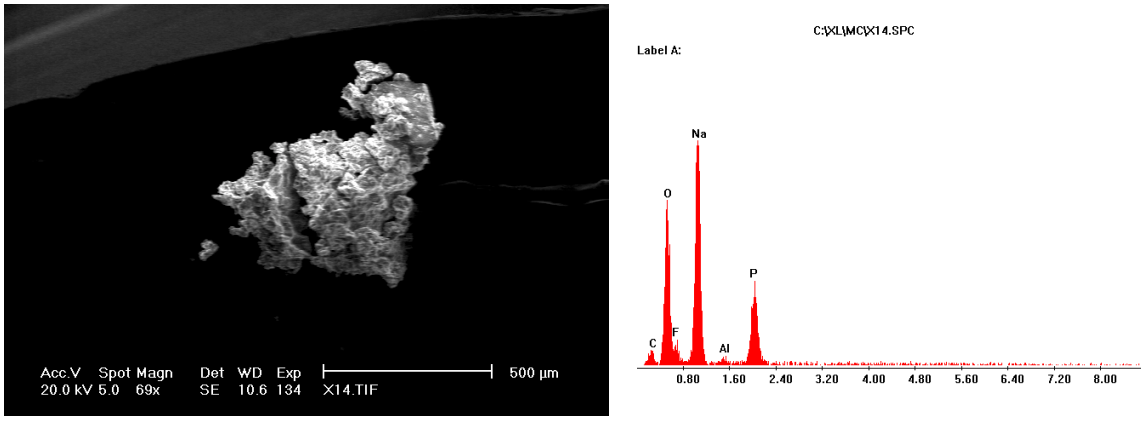

Fig. 18. Particle 4 of X1 simulant after first plugging.

Table 6. Compositional analysis of the X1 simulant after first plugging (% weight)

Element	Particle 1	Particle 2	Particle 3	Particle 4
C	15.20	7.24	12.39	7.17
O	20.32	36.26	32.97	36.48
Na	37.95	38.26	35.41	37.91
P	2.93	13.38	15.06	10.83
F	23.59	4.86	4.16	6.51
Al	—	—	—	1.10

X2 plug samples. SEM images for plug samples of simulant X2 are presented in Figs. 19 through 23. Table 7 shows the analysis of the X2 plug sample. The sample contains oxygen, sodium, carbon, and phosphorus.

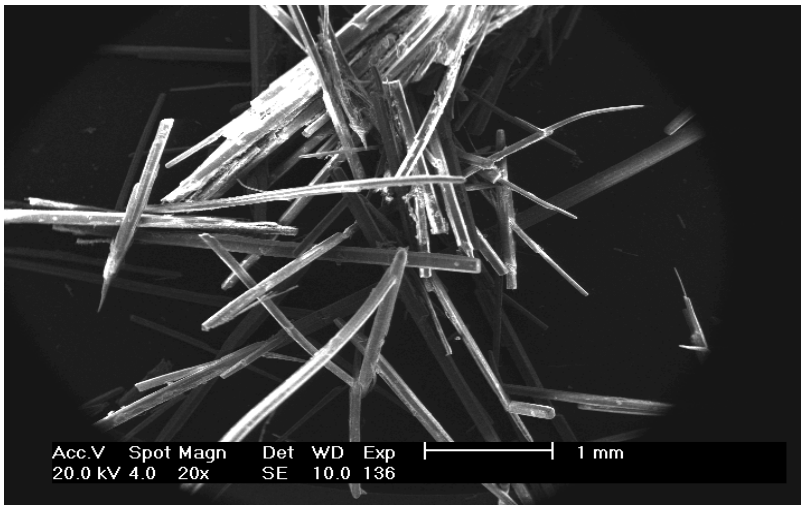

Fig. 19. Picture of the X2 plug sample.

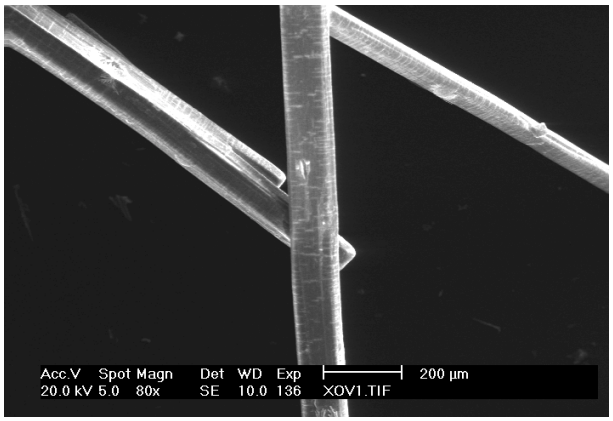

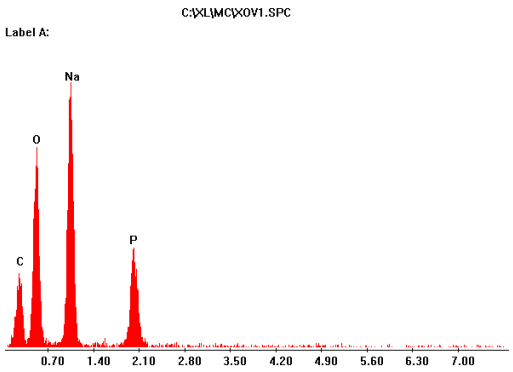

Fig. 20. Particle 1 of the X2 plug sample.

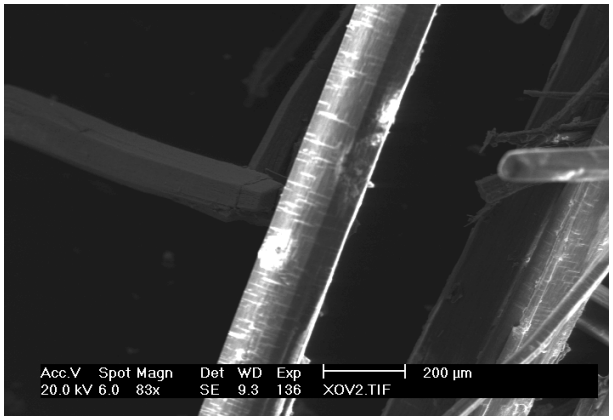

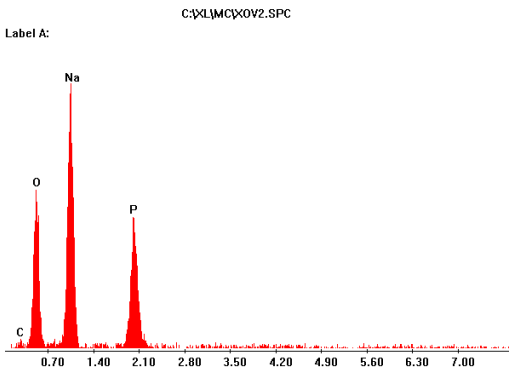

Fig. 21. Particle 2 of the X2 plug sample.

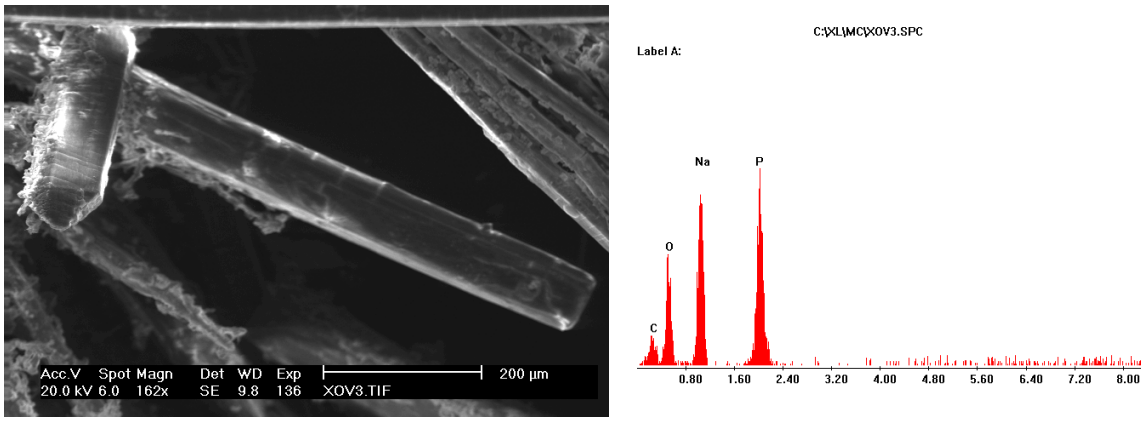

Fig. 22. Particle 3 of the X2 plug sample.

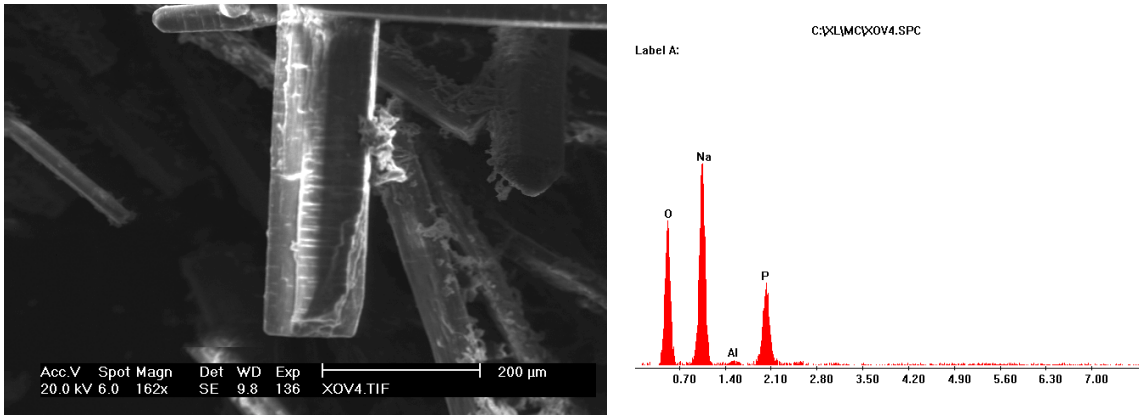

Fig. 23. Particle 4 of the X2 plug sample.

Table 7. Compositional analysis of the X2 plug sample (% weight)

Element	Particle 1	Particle 2	Particle 3	Particle 4
C	24.47	3.53	18.52	—
O	39.35	39.10	33.61	41.39
Na	27.84	39.63	27.12	42.80
Al	—	—	—	0.82
P	8.34	17.75	20.75	14.98

5.3 Pilot-Scale Study

5.3.1 Experimental

A pilot-scale unit was designed and constructed to model an actual transfer line at the site. The pilot-scale experimental setup was intended to test the plugging potential of Hanford simulants under flow conditions.

The design incorporated input from Hanford RPP engineers (O'Rourke 2000) as well as information gathered at the FY 2000 Saltcake Dissolution and Feed Stability Workshop, held at

the Hanford site in May 2000 (Hunt et al. 2000). Hanford users proposed that transfer from tank C-104 to the AY tank farm be modeled. The proposed design consists of a 4-in. supernatant transfer line from tank C-104 (C tank farm) to tanks AY-101 and AY-102 (AY tank farm). This transfer line, which has not yet been built at the site, includes a valve pit between the tanks. Figure 24 shows the geometric layout of this transfer line.

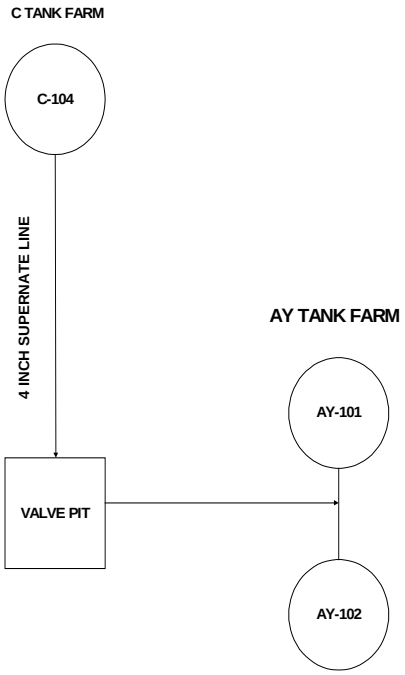

Fig. 24. Hanford waste transfer line geometry.

A typical valve pit includes vertical and horizontal pipe sections as well as 90° bends with no radius elbows (miter bends). There is plugging potential at the different bends present in the valve pit; therefore, these bends were included in the pilot-scale setup. In addition, there is an elevation of 2° between the tanks. Therefore, an incline section was also included. Transparent sections (bends) were included for plug monitoring.

Figure 25 shows a general layout of the pilot-scale setup. Figures 26 and 27 show the preliminary design for the simulation of a Hanford valve pit configuration. The unit shows four Hanford connectors (vertical and horizontal) as well as standard radius bends. These Hanford connectors were manufactured of transparent material (clear PVC) for plug monitoring.

Figures 28 and 29 show a comparison of a typical Hanford connector and its simulation with clear PVC. Note the 90° angle similarity in the elbows.

Figure 30 shows the valve pit configuration portion of the flow loop. The valve pit consists of transparent sections (PVC) of horizontal and vertical 90° miter bends to facilitate plugging visualization. The valve-pit section is immersed in a temperature-controlled bath.

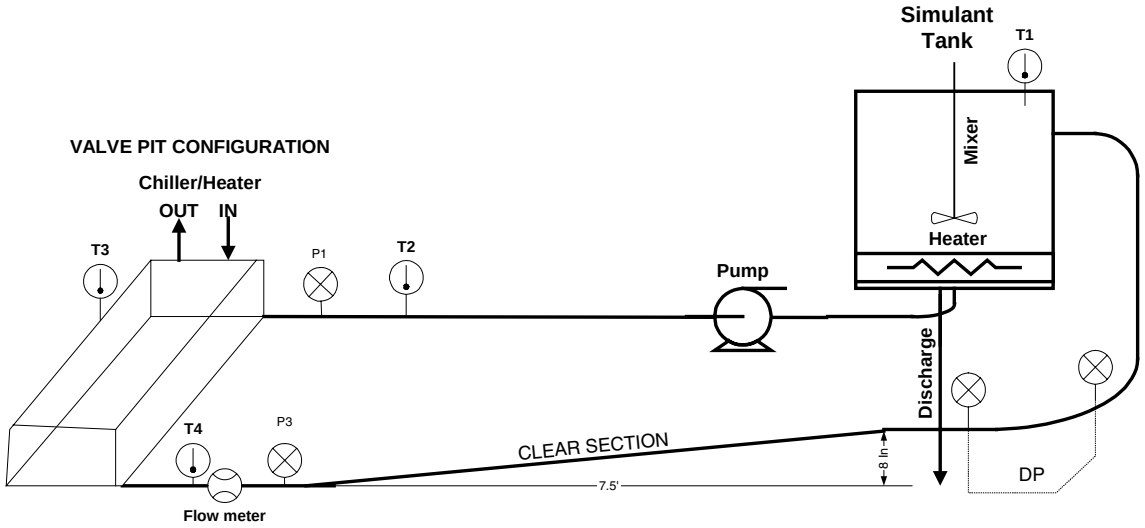

Fig. 25. Layout of the pilot-scale unit.

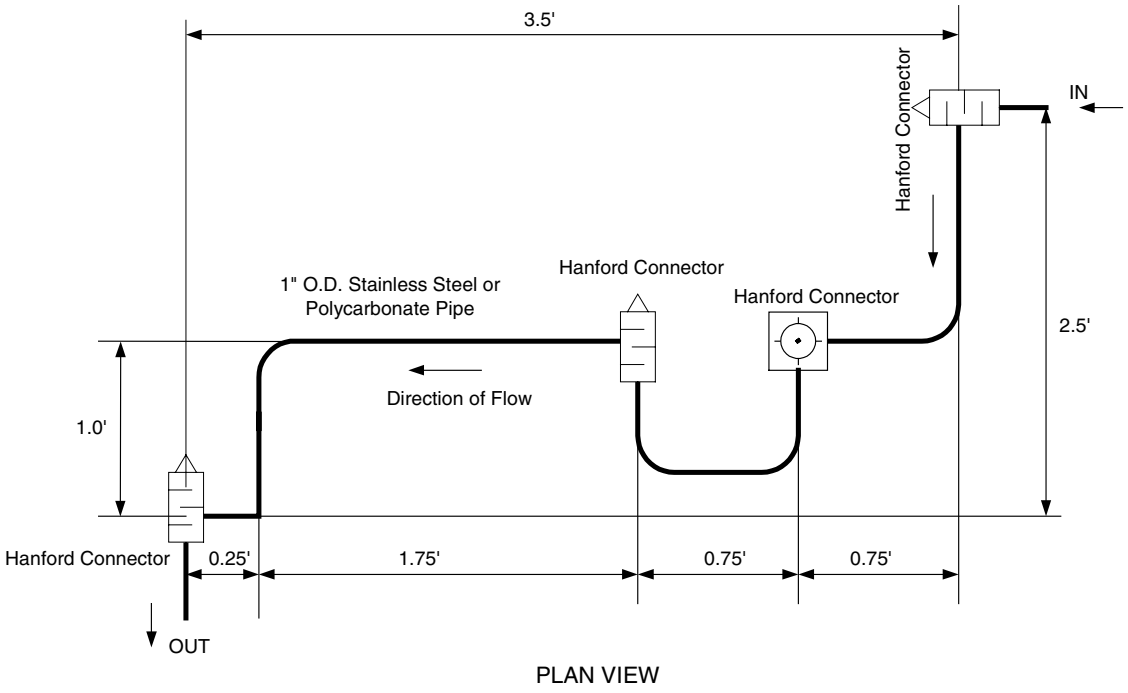

Fig. 26. Plan view of FIU-HCET valve pit configuration.

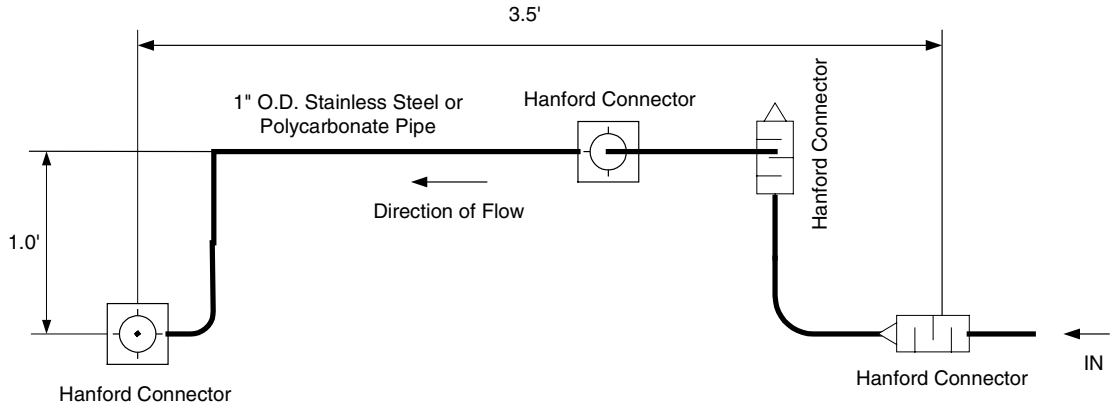

Fig. 27. Elevation profile of the FIU-HCET valve pit configuration.

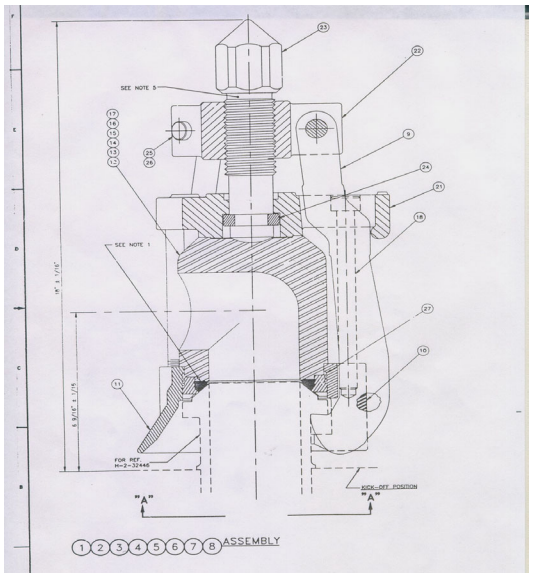

Fig. 28. Typical Hanford connector. (*Source:* Dwg no. H-2-32430, DOE Richland Operations Office, 1997.

Fig. 29. Hanford connector simulation.

Horizontal and vertical standard radius (5-in.) bends are present in the loop, as shown in Fig. 31. This section is located after a clear incline (2^{o}) pipe section and before the feed tank. The pressure differential across the horizontal bend is measured.

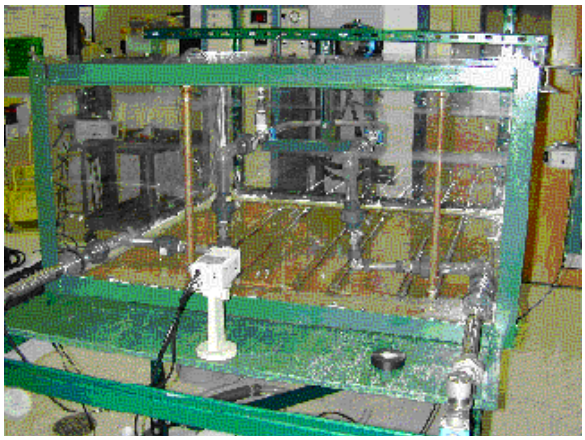

Fig. 30. Valve pit configuration.

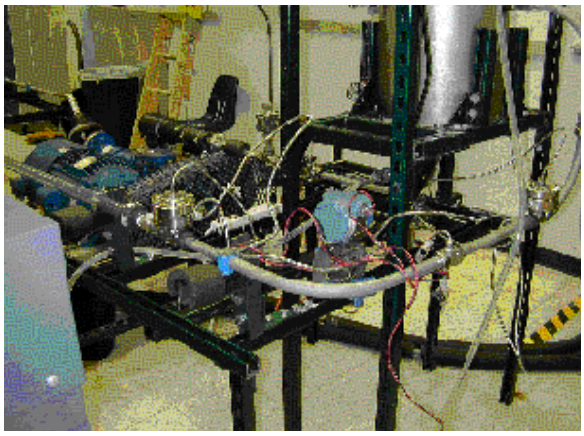

Fig. 31. Standard (5-in.) radius bend.

Simulants

Table 8 shows the chemical composition of the simulants tested. These simulants represent the actual radioactive waste present in the corresponding tanks at the Hanford site.

Table 8. Formulations and concentrations of the C-104 and AN-103 simulants

Compound	C-104		AN-103	
	Grams	Molality	Grams	Molality
$NaAlO_2$	367.73	4.486		1.982
Na_2CO_3	115.21	1.087		0692
$Al(NO_3)_3$	0	0		1.103
$Fe(NO_3)_3 \cdot 9H_2O$	153.80	0.381	0	0
NaCl	0	0		0.148
NaF	0	0		0.061
$NaNO_3$	0	0		2.016
Fe_2O_3	22.78	0.143	0	0
$Mn(NO_3)_2$	30.78	0.172	0	0
NaOH	81.52	2.038		6.744
$Na_2C_2O_4$	28.94	0.216	0	0
$Na_3PO_4 \cdot 12H_2O \cdot ¼NaOH$	28.48	0.073		0.031
$Na_2SiO_3 \cdot 5H_2O$	103.95	0.490		0.028
Na_2SO_4	8.95	0.063		0.045
ZrF_4	102.17	0.611	0	0
ZrO_2	42.51	0.345	0	0
H_2O	1086.60	60.316		49.113

Test Matrix

Table 9 shows the conditions at which the simulants were tested in the flow loop. The flow velocities of the experiments encompass the actual operation conditions at Hanford.

Table 9. Test matrix for pilot-scale study of AN-103 and C-104

Feed tank temperature (°C)	Tubing temperature (°C)	Flow velocity (ft/s)
50	15	1 Laminar flow
	40	
50	15	1.5 Transition flow
	40	
50	15	2 Transition flow
	40	
50	15	4 Turbulent flow
	40	
50	15	6 Turbulent flow
	40	
50	15	8 Turbulent flow
	40	
50	15	10 Turbulent flow
	40	

5.3.2 Results

This section includes experimental observations from the pilot-scale study for the AN-103 Hanford simulant, data pertaining to pressure drop versus flow velocity, and plug morphology as obtained via SEM analysis.

Table 10 shows the experimental observations from the pilot-scale study for the AN-103 Hanford simulant.

Pressure Drop Data

Several pressure differential measurements were monitored during the pilot-scale study across different sections of the loop. Table 11 provides the description of these measurements, and Fig. 32 shows the layout of the loop.

Table 10. AN-103 simulant pilot-scale tests experimental observations
(1.982 *M* $NaAlO_2$ + 1.103 *M* $Al(NO_3)_3 \cdot 9H_2O$ + 0.148 *M* NaCl + 0.692 *M* Na_2CO_3 + 0.061 *M* NaF + 2.016 *M* $NaNO_3$ + 6.744 *M* NaOH + 0.031 *M* Na_3PO_4 + 0.028 *M* $Na_2SiO_3 \cdot 5H_2O$ + 0.045 *M* Na_2SO_4 + 49.113M H_2O)

Feed tank temperature (°C)	Flow velocity (ft/s)	Comments	
		Temperature at test section (15°C)	Temperature at test section (40°C)
50	1.0 Laminar flow	• Moving bed observed. • Partial plugging. • Unplugging attained by increasing flow rate.	• No plugging. • Few solids observed.
50	1.5 Transition flow	• No plugging. • Solids formation.	• No plugging. • Few solids observed.
50	2.0 Transition flow	• No plugging. • Solids formation.	• No plugging. • Few solids observed.
50	4.0 Turbulent flow	• Normal flow conditions. • No solids observed.	• Normal flow conditions. • No solids observed.
50	6.0 Turbulent flow	• Normal flow conditions. • No solids observed.	• Normal flow conditions. • No solids observed.
50	8.0 Turbulent flow	• Normal flow conditions. • No solids observed.	• Normal flow conditions. • No solids observed.
50	10.0 Turbulent flow	• Normal flow conditions. • No solids observed.	• Normal flow conditions. • No solids observed.

Table 11. Differential pressure measurements

Name	Pressure differential location	Pressure differential across . . .
DP1	Valve pit configuration	One horizontal square bend
DP2	Valve pit configuration	Two vertical bends Upward flow direction
DP3	Valve pit configuration	Horizontal 5-in. radius 180° bend
DP4	Valve pit configuration	Two vertical bends Downward flow direction
DP5	Valve pit configuration	One horizontal square bend
DP6	Incline section after valve pit	7-ft incline section
DP7	Feed tank return	Horizontal 5-in. radius bend

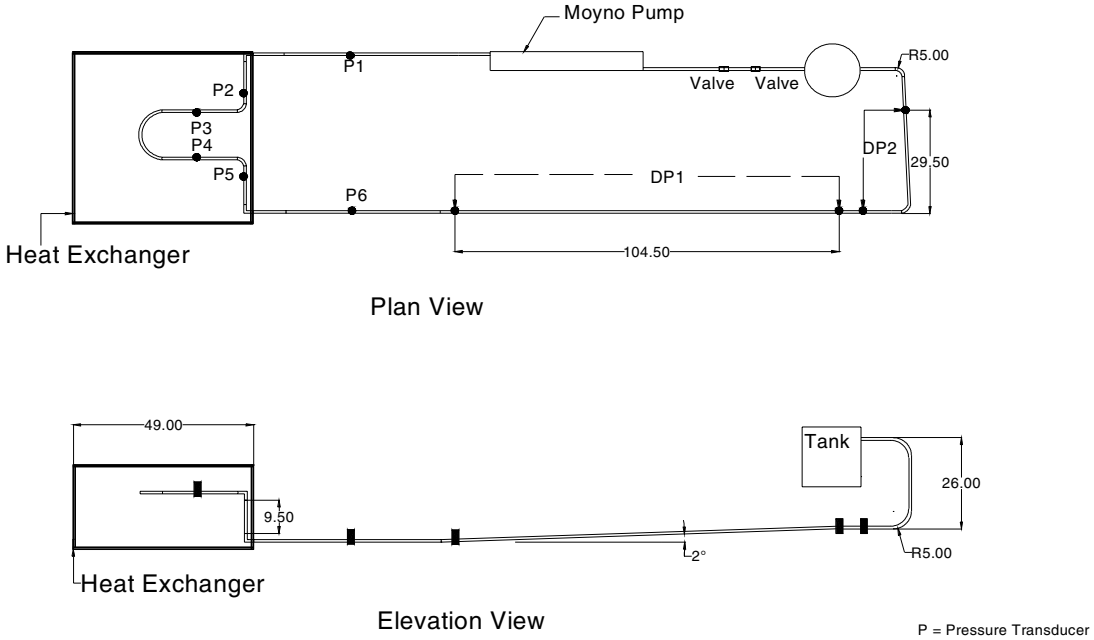

Fig. 32. Layout of the pilot-scale experimental flow loop.

Validation of the Pilot-Scale Loop

The validation and calibration of the pilot-scale loop was performed by running water tests through the system. The engineering Bernoulli equation for an incompressible fluid can be written as

$$\Delta P = (P_1 + \rho g z_1) - (P_2 + \rho g z_2) = K\rho\frac{V^2}{2} \quad , \tag{1}$$

where

ΔP is the differential pressure between points 1 and 2,
K is the ***velocity head loss coefficient***,
V is the reference velocity.

Based on Eq. (1), a plot of ΔP versus the square of the velocity (V^2) should be a straight line with a slope that is proportional to the ***velocity head loss coefficient*** and an intercept that is trivial (i.e., zero). A nonzero intercept is an indication of instrumentation bias. We have therefore used this approach to get estimates of the biases. The differential pressures are plotted against V^2 as shown in Fig. 33.

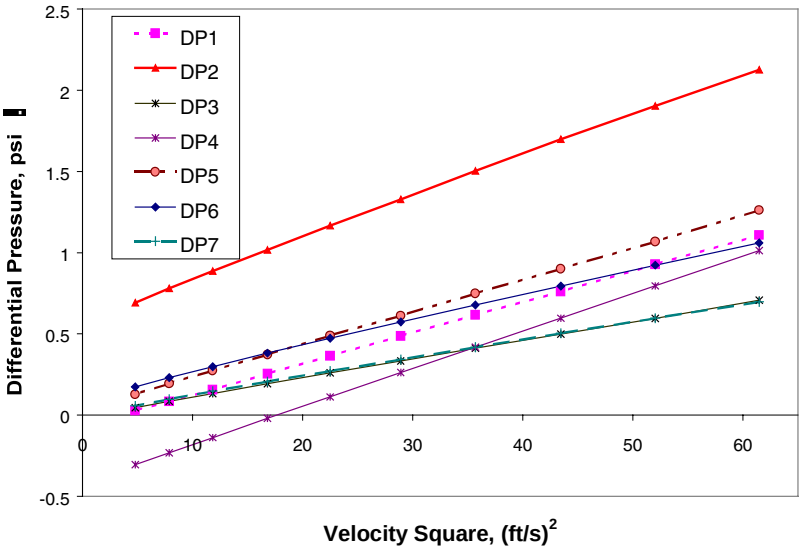

Fig. 33. Differential pressures DP1-DP7 for water tests.

The estimate of the bias can be obtained by performing a linear regression on the data to get an equation of the form

$$\Delta P = \mathbf{a} + \mathbf{b}V^2 \ , \qquad (2)$$

where **a** is the intercept and **b** is the slope. Thus, **a** gives us the bias.

As seen in Table 12, the extremely good agreement of the differential pressure data with the regression equations (R^2 is practically 1) verifies the form of the equation used. Also the values of the intercept can now be used to correct for the biases in the system instrumentation. The slope is proportional to the ***velocity head loss coefficient***, K. More specifically,

$$\text{Slope} = K\rho/2 \ . \qquad (3)$$

The velocity head loss depends on the length of the pipe, as well as the type and the number of valves and fittings in the pipeline between the points of interest. The major fittings in the valve-pit section in the pilot-scale loop are the 90° bends and the 180° 5-in. radius bend. In the case of DP6, the pressure drop is due to the losses in the inclined section, while the horizontal 5-in. radius bend accounts for DP7. The calculated values of K for the different sections of pilot-scale loop are shown in Table 13. The major fittings in the different sections of the loop are specified in Table 14.

Table 12. Regression summary for water tests

Differential (psi)	Intercept (a) (psi)	Slope (b) [(psi·s^2)/ft^2]	R^2
DP1	–0.067	0.0191	1.0000
DP2	0.587	0.0253	0.9995
DP3	–0.005	0.0116	0.9998
DP4	–0.414	0.0233	1.0000
DP5	0.037	0.0199	1.0000
DP6	0.113	0.0156	0.9993
DP7	0.012	0.0113	0.9994

Table 13. Calculation of K for different sections of the loop for water tests

Name	Slope (from regression) [(psi·s^2)/ft^2]	Slope (S.I. units) (kg/m^3)	K[a] = 2·Slope (S.I.) (ρ)
DP1	0.0191	1417.107	2.83
DP2	0.0253	1877.111	3.75
DP3	0.0116	860.6515	1.72
DP4	0.0233	1728.722	3.45
DP5	0.0199	1476.463	2.95
DP6	0.0156	1157.428	2.31
DP7	0.0113	838.3933	1.67

[a]Based on water density of 1000 kg/m^3.

Table 14. Fittings in the different sections of the loop

Name	Pressure differential across	Major valve or fitting	Number
DP1	One horizontal square bend	90° bend	1
DP2	Two vertical bends Upward flow direction	90° bend	2
DP3	Horizontal 5-in. radius 180°	180° 5-in. radius bend	1
DP4	Two vertical bends Downward flow direction	90° bend	2
DP5	One horizontal square bend	90° bend	1
DP6	Inclined pipe section	Pipe length	1
DP7	Horizontal bend	90° %-radius bend	1

Pilot-Scale Flow Loop Tests for AN-103

The pilot-scale flow loop tests were conducted according to the test matrix given in Table 15.

Table 15. Test matrix for AN-103 testing on pilot-scale unit

Test	Feed tank temperature (°C)	Valve-pit temperature (°C)	Flow rate (ft/s)[a]	
			Minimum	Maximum
1	50	40	2	8
2	50	15	2	8

[a]For the velocity ranges covered in the tests, there was no significant plugging.

Test 1: Valve-pit section maintained at 40°C. The differential pressure (ΔP) drop data are shown in Fig. 34 as a function of the flow velocity. The value of ΔP shows a quadratic dependence on velocity. The plot of ΔP versus V^2 (Fig. 35) is used to determine the slope, which is proportional to the velocity head loss coefficient, K, mentioned in Eq. (1). Calculations of K for different sections of the pilot-scale loop at 40°C are shown in Table 16.

Test 2: Valve-pit section maintained at 15°C. The differential pressure (ΔP) drop data are shown in Fig. 36 function of the velocity. The plot of ΔP versus V^2 (Fig. 37) is used to determine the slope, which is proportional to the velocity head loss coefficient, K, mentioned in Eq. (1). Calculations of K for different sections of the pilot-scale loop at 15°C are shown in Table 17.

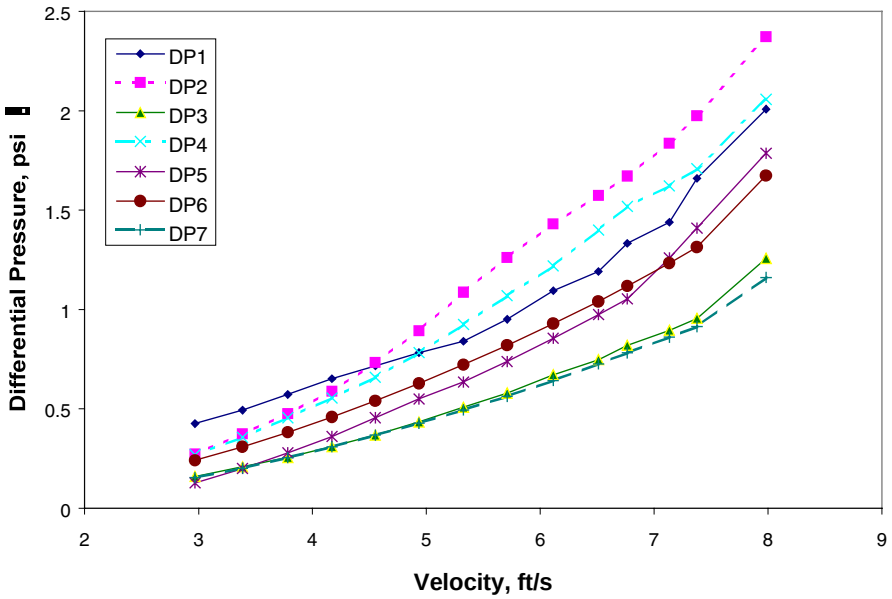

Fig. 34. Differential pressures DP1-DP7 versus velocity for test 1.

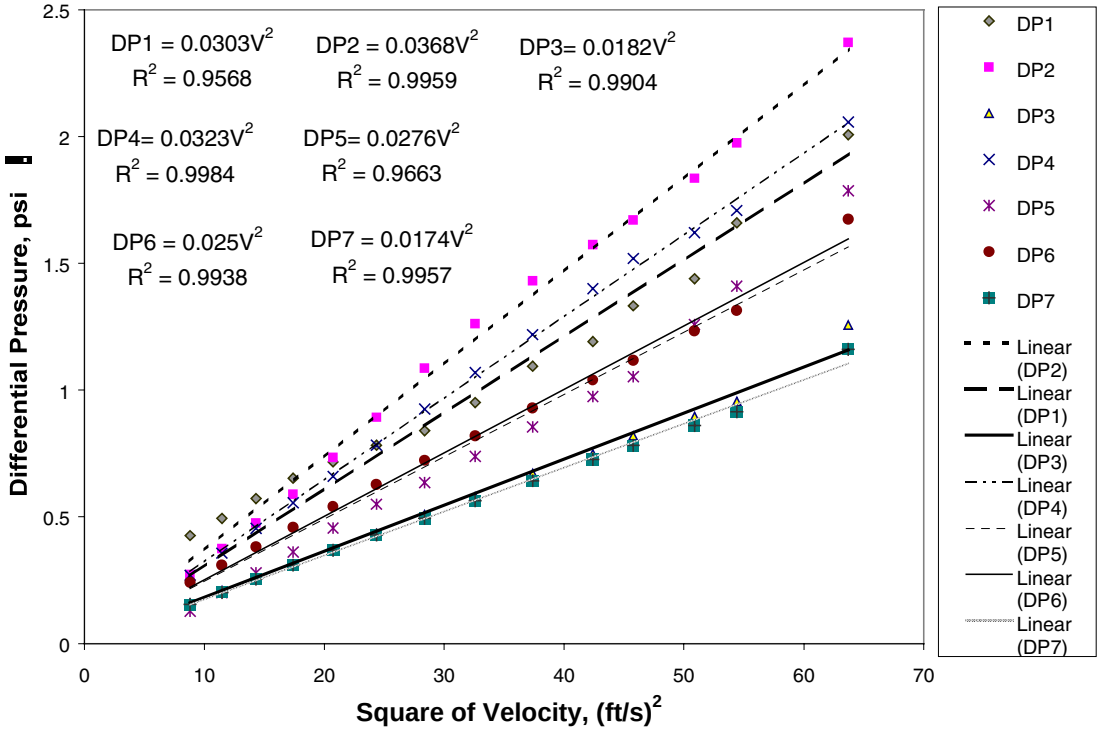

Fig. 35. Plot of the experimental and fitted differential pressures DP1-DP7 for test-section temperature of 40°C. The fitted equations are shown as well.

Table 16. Calculation of K for different sections of the pilot-scale loop at 40°C

Name	Slope [(psi·s^2)/ft^2]	Slope (S.I.) (kg/m^3)	K^a = 2·Slope (S.I) (ρ)
DP1	0.0303	2248.08	3.26
DP2	0.0368	2730.34	3.96
DP3	0.0182	1350.33	1.95
DP4	0.0323	2396.47	3.47
DP5	0.0276	1825.17	2.65
DP6	0.025	1854.8	2.69
DP7	0.0174	1290.98	1.87

[a]Based on AN-103 density of 1380 kg/m^3.

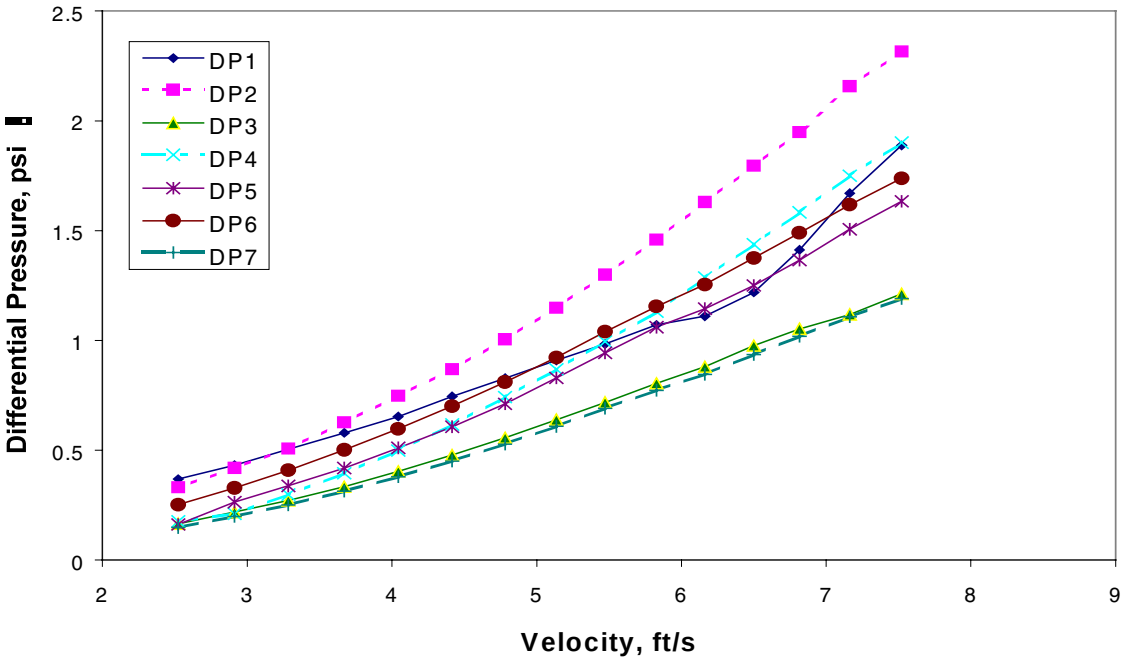

Fig. 36. Differential pressures DP1-DP7 versus velocity for test 2.

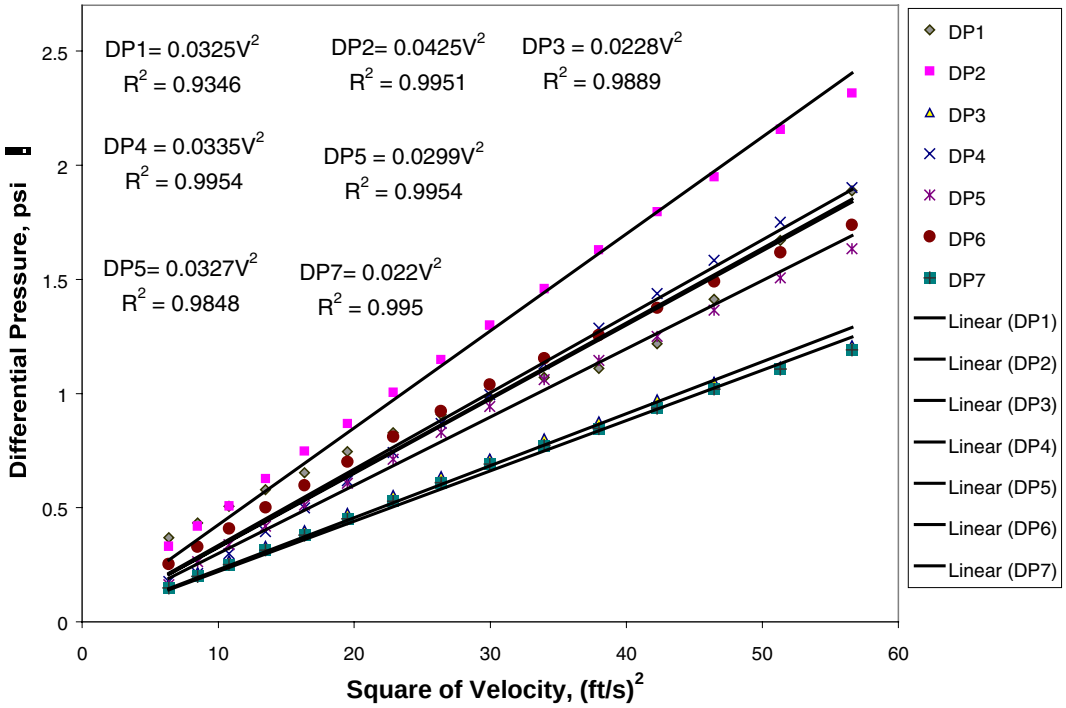

Fig. 37. Plot of the experimental and fitted differential pressures DP1-DP7 for test-section temperature of 15°C. The fitted equations are shown as well.

Table 17. Calculation of K for different sections of the pilot-scale loop at 15°C

Name	Slope [(psi·s^2)/ft^2]	Slope (S.I.) (kg/m^3)	K^a = 2·Slope (S.I.) (ρ)
DP1	0.0325	2411.308	3.49
DP2	0.0425	3153.249	4.57
DP3	0.0228	1691.625	2.45
DP4	0.0335	2485.502	3.60
DP5	0.0299	2218.403	3.22
DP6	0.0327	2426.147	3.52
DP7	0.022	1632.27	2.37

[a]Based on AN-103 density of 1380 kg/m^3

In Fig. 38, the K values for the AN-103 tests at different temperatures and water are compared. As expected, the velocity head loss is greater for AN-103 at all locations. The higher pressure losses can be attributed to the higher apparent viscosity of AN-103 in the loop when the test section is at 15°C. For the case of 40°C test-section temperature, the fluid inside the loop is at a higher temperature and hence has a lower viscosity.

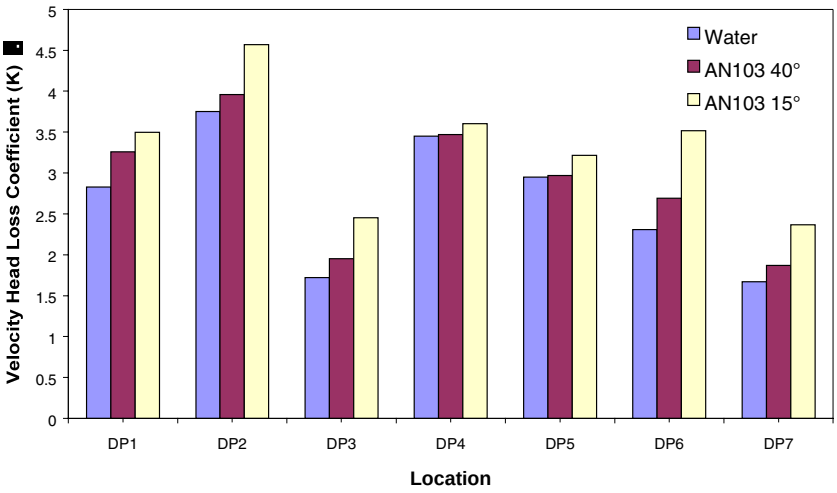

Fig. 38. Comparative plot of the K values for the various locations in the loop.

Plug Analysis

Samples obtained from the flow loop experiments were analyzed using SEM. Figure 39 shows a low-magnification picture of the AN-103-1 sample, and four of its particles are presented in Figs. 40–43.

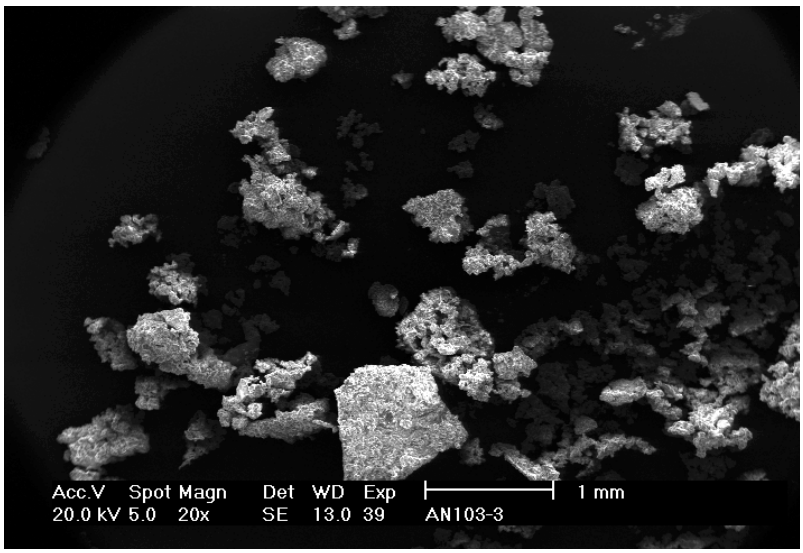

Fig. 39. Low-magnification image of the AN-103-3 sample, 20X.

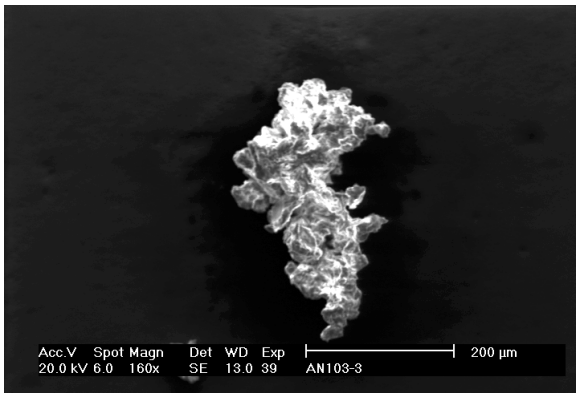

Fig. 40. Particle 1 of AN-103-3 sample, 160X.

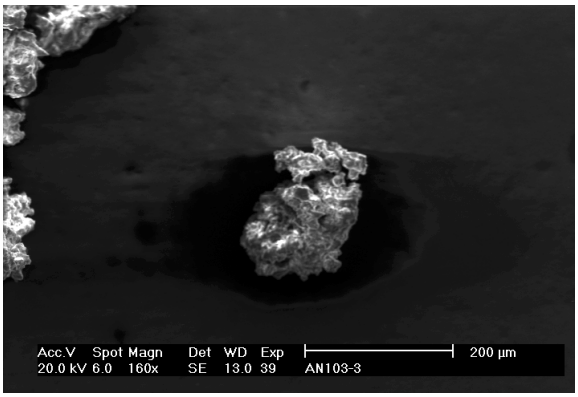

Fig. 41. Particle 2 of AN-103-3 sample, 160X.

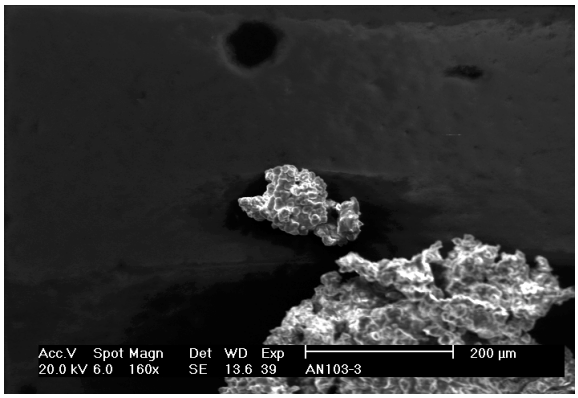

Fig. 32. Particle 3 of AN-103-3 sample, 160X.

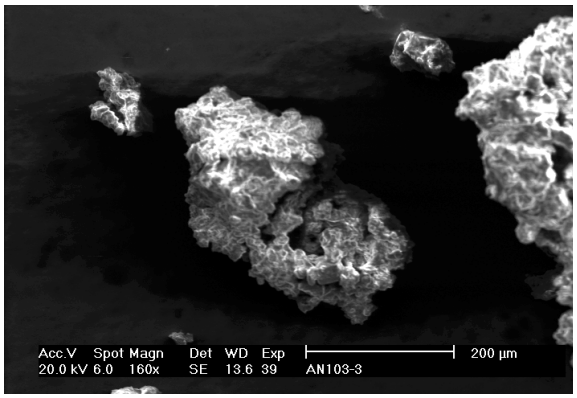

Fig. 43. Particle 4 of AN-103-3 sample, 160X.

Table 18 shows the compositional analysis of the AN-103-3 sample. Sodium, oxygen, aluminum, and silicon are the main components. Particle 1 contains phosphorus instead of silicon.

Table 18. Compositional analysis of AN-103-3 sample (% weight)

Element	Particle 1	Particle 2	Particle 3	Particle 4
O	47.01	47.86	43.98	46.31
Na	44.73	35.99	28.66	39.36
P	3.25	—	—	—
Al	5.01	12.43	19.48	12.04
Si	—	3.72	7.88	2.29

5.4 Simulant Rheology

Rheology measurements of the three simulants (X1, X2, and AN-103) were carried out by using a Haake RS75 RheoStress instrument. These measurements were done at different temperatures. A Bingham plastic model was observed in all cases. The Bingham model equation is

$$\tau = \tau_o + \gamma\eta \quad , \tag{4}$$

where τ = shear stress, τ_o = yield stress, γ = shear rate, and η = apparent viscosity. The yield stresses and viscosities decreased with temperature in all cases.

AN-103 Simulant

The shear stress–shear rate curves for AN-103 simulant at 15, 25, 30, 50, and 70°C are shown in Figs. 44–48.

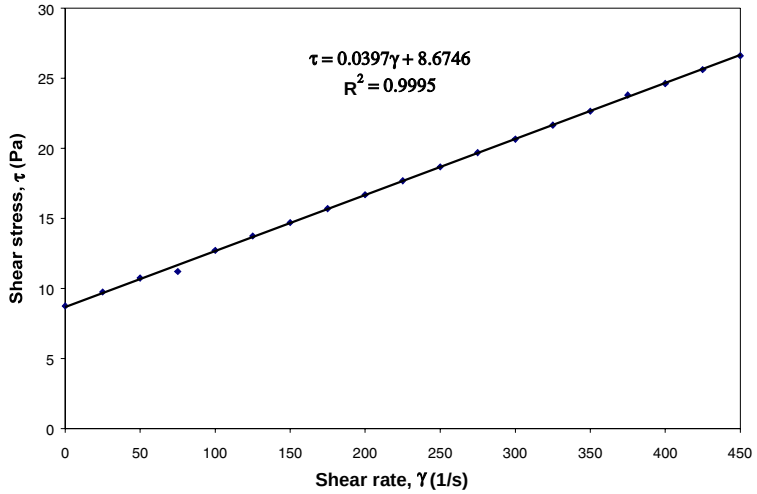

Fig. 44. Shear stress–shear rate curve for AN-103 simulant at 15°C.

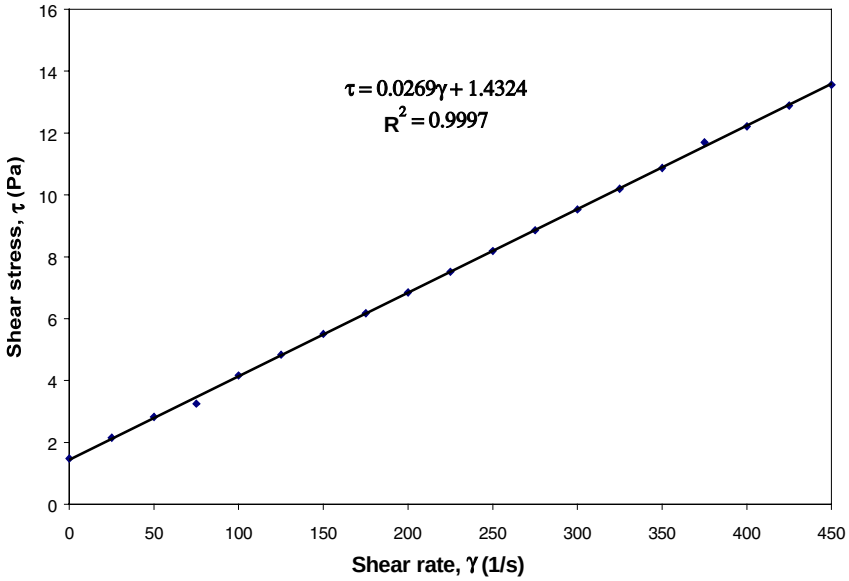

Fig. 45. Shear stress–shear rate curve for AN-103 simulant at 25°C.

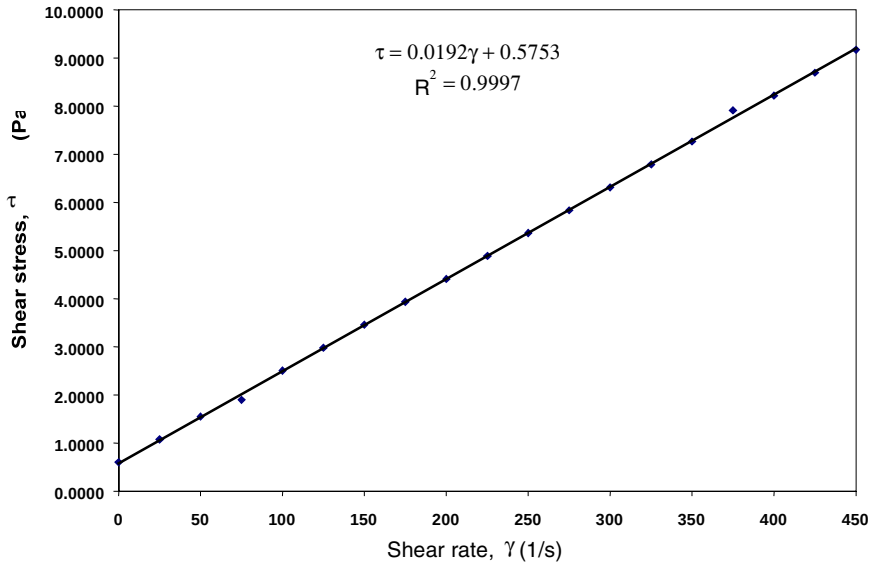

Fig. 46. Shear stress–shear rate curve for AN-103 simulant at 30°C.

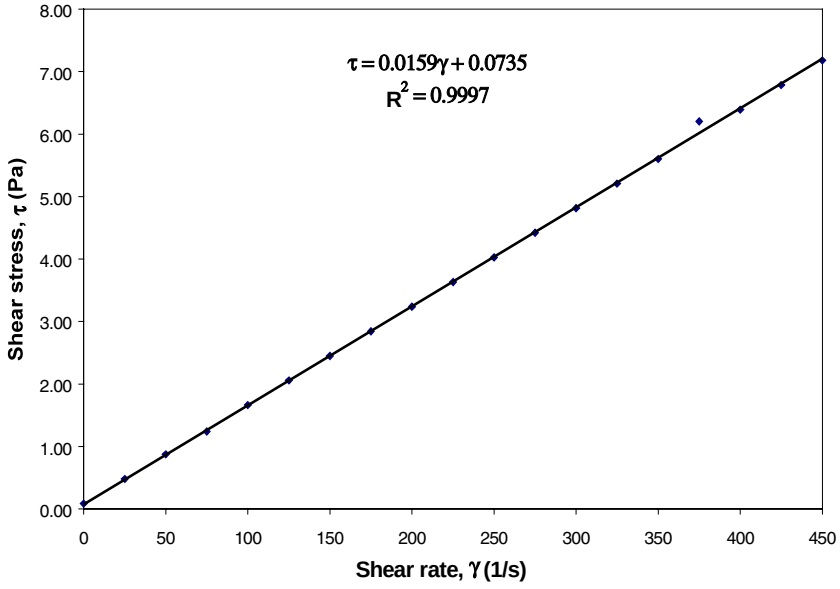

Fig. 47. Shear stress–shear rate curve for AN-103 simulant at 50°C.

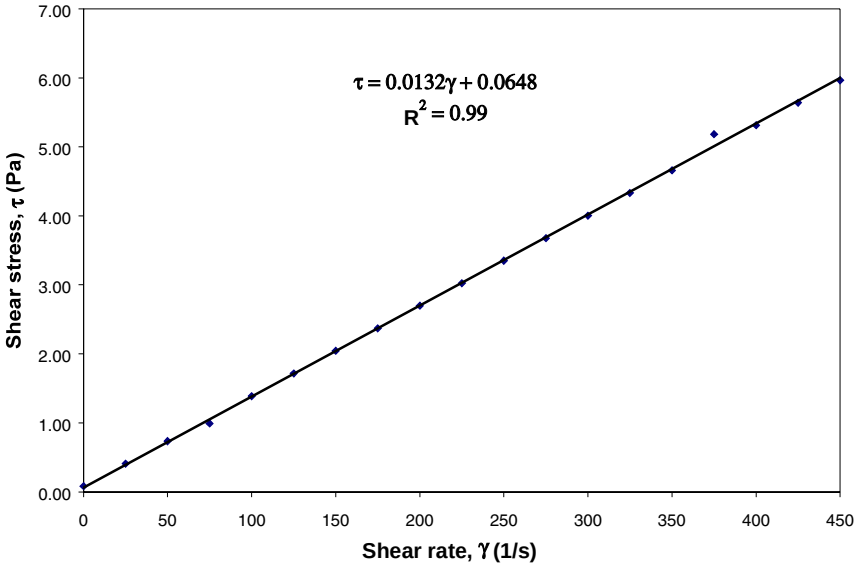

Fig. 48. Shear stress–shear rate curve for AN-103 simulant at 70°C.

The values calculated for apparent viscosity (η) and the yield stress (τ_0) for the AN-103 simulants for different temperatures are summarized in Table 19. Both η and τ_0 decrease with temperature (as shown in Figs. 49 and 50, respectively). The temperature dependence is given by the Eqs. (5) and (6):

$$\ln(\eta) = -0.7103 \ln(T) - 1.3682 \quad , \tag{5}$$

and

$$\ln(\tau_0) = -3.381 \ln(T) + 11.15 \quad . \tag{6}$$

Table 19. Apparent viscosity and yield stress values for AN-103 simulant

Temperature (°C)	Apparent viscosity [(N·s)/m^2]	Yield stress (Pa)
15	0.0397	8.6746
25	0.0269	1.4324
30	0.0192	0.5753
50	0.0159	0.0735
70	0.0132	0.0648

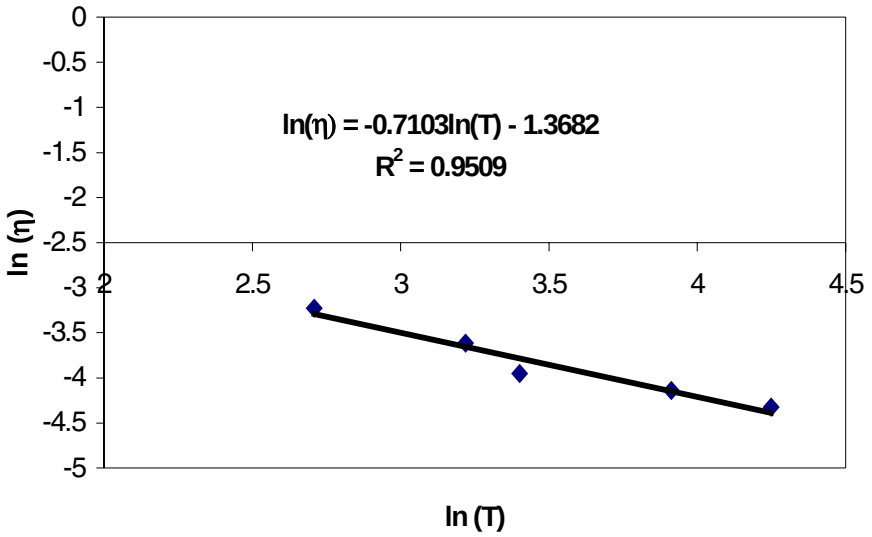

Fig. 49. Apparent viscosity dependence on temperature (AN-103 simulant).

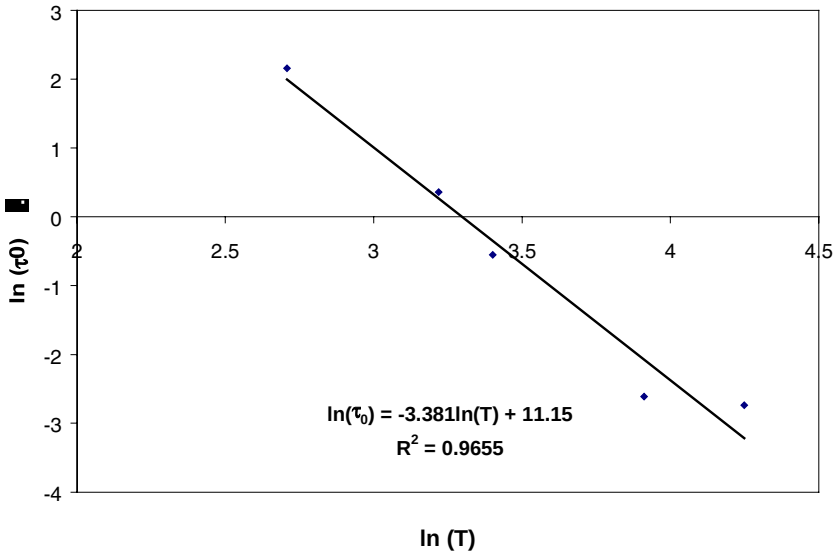

Fig. 50. Yield stress dependence on temperature (AN-103 simulant).

X1 Simulant

The shear stress–shear rate curves for X1 simulant at 15, 25, and 50°C are shown in Figs. 51–53, respectively.

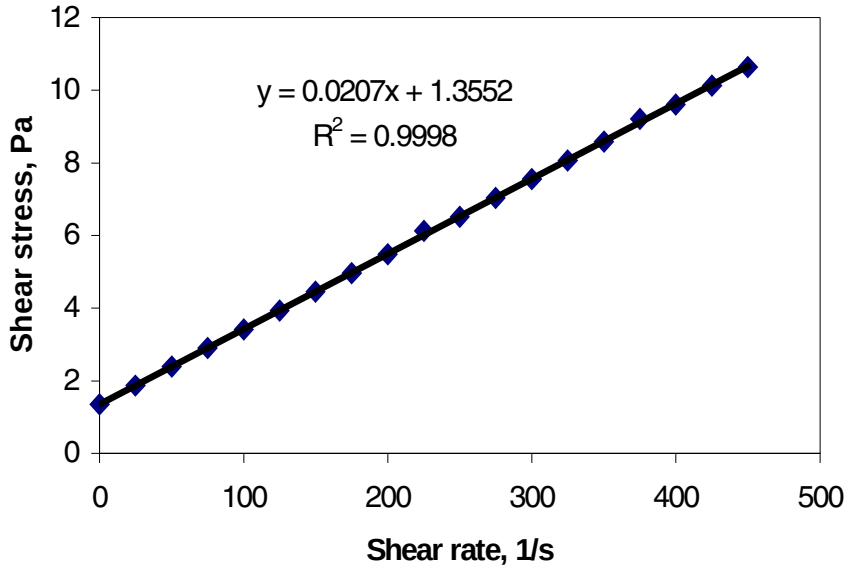

Fig. 51. Shear stress–shear rate curve for X1 simulant at 15°C.

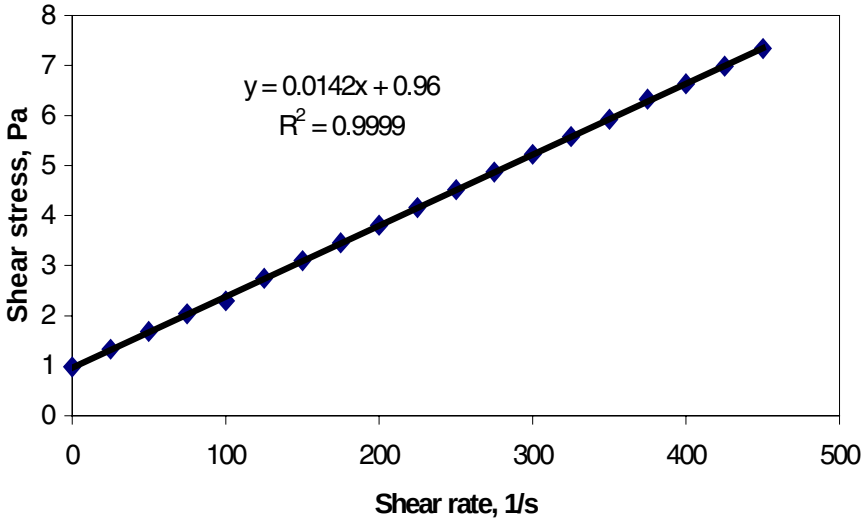

Fig. 52. Shear stress–shear rate curve for X1 simulant at 25°C.

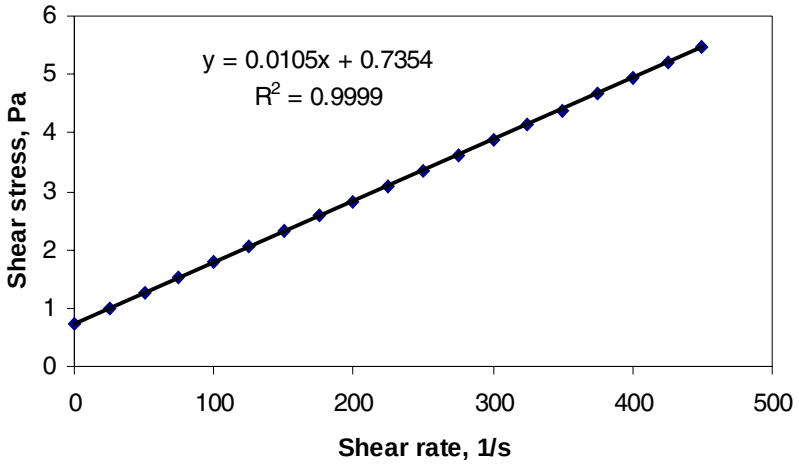

Fig. 53. Shear stress–shear rate curve for X1 simulant at 50°C.

The values calculated for apparent viscosity (η) and the yield stress (τ_0) for the X1 simulant for different temperatures are summarized in Table 20. Both η and τ_0 decrease with temperature, and the temperature dependence is given by the equations shown in Figs. 54 and 55, respectively.

Table 20. Apparent viscosity and yield stress values for X1 simulant

Temperature (°C)	Apparent viscosity [(N·s)/m^2]	Yield stress (Pa)
15	0.0207	1.3552
25	0.0142	0.96
50	0.0105	0.7354
70	0.0099	0.7105

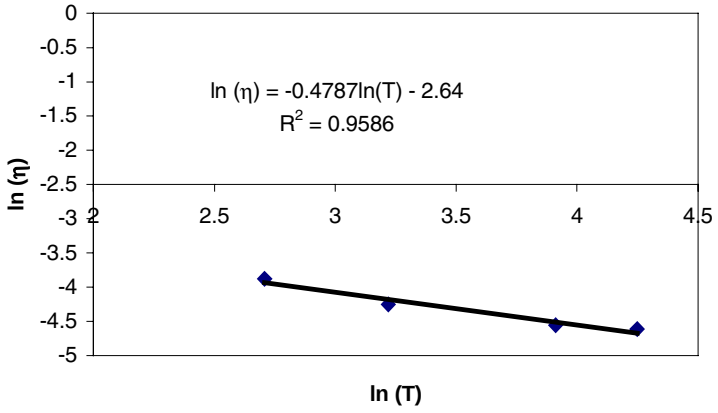

Fig. 54. Apparent viscosity dependence on temperature (X1 simulant).

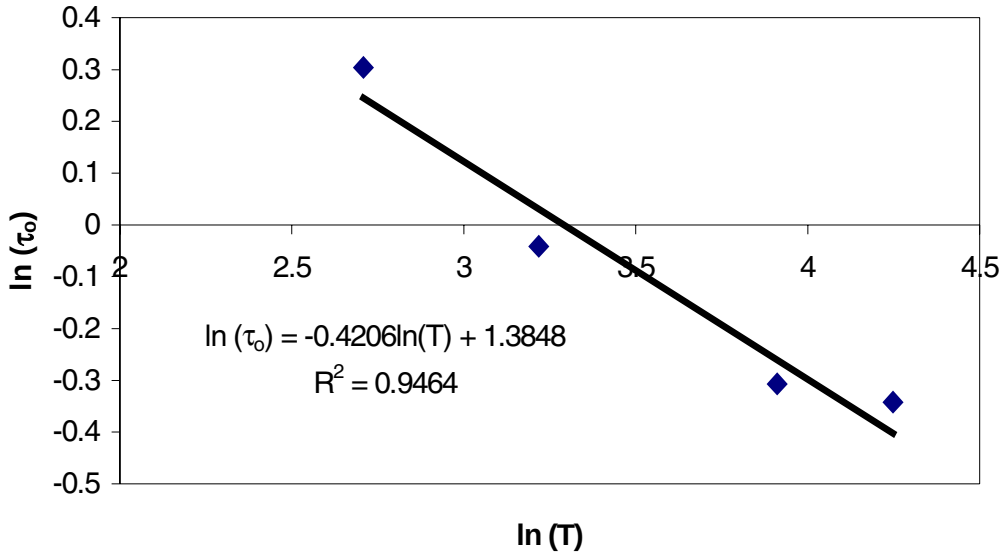

Fig. 55. Yield stress dependence on temperature (X1 simulant).

X2 Simulant

The shear stress–shear rate curves for X2 simulant at 15, 25, and 50°C are shown in Figs. 56–58, respectively.

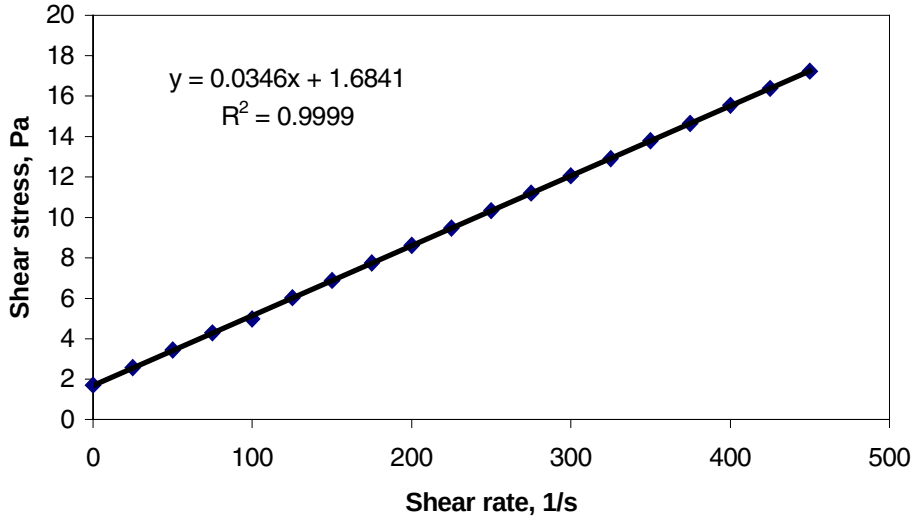

Fig. 56. Shear stress–shear rate curve for X2 simulant at 15°C.

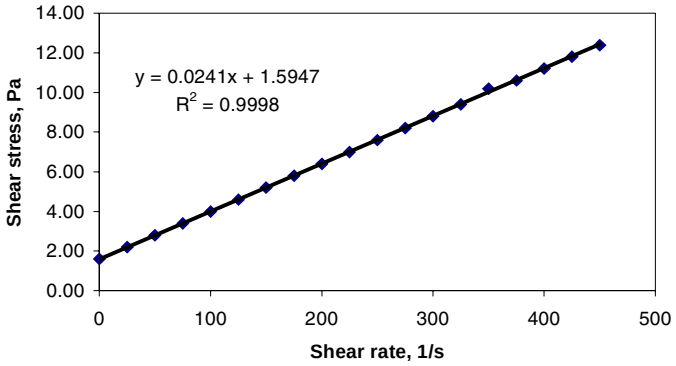

Fig. 57. Shear stress–shear rate curve for X2 simulant at 25°C.

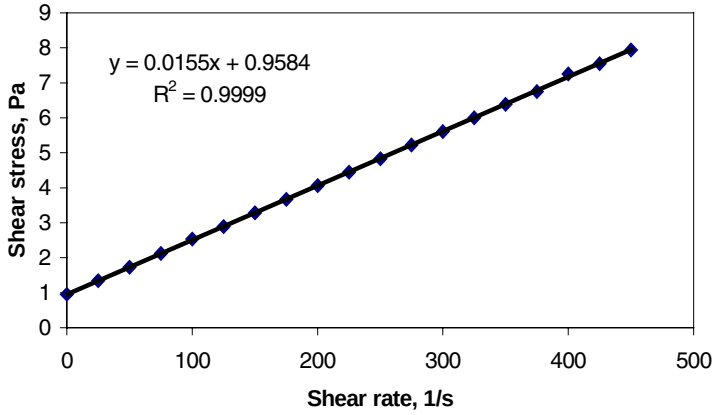

Fig. 58. Shear stress–shear rate curve for X2 simulant at 50°C.

The values calculated for apparent viscosity (η) and the yield stress (τ_0) for the X2 simulant for different temperatures are summarized in Table 21. Both η and τ_0 decrease with temperature, and the temperature dependence is given by the equations shown in Figs. 59 and 60, respectively.

Table 21. Apparent viscosity and yield stress values for X2 simulant

Temperature (°C)	Apparent Viscosity [(N·s)/m^2]	Yield stress (Pa)
15	0.0346	1.6841
25	0.0241	1.5947
50	0.0155	0.9584
70	0.0134	0.9232

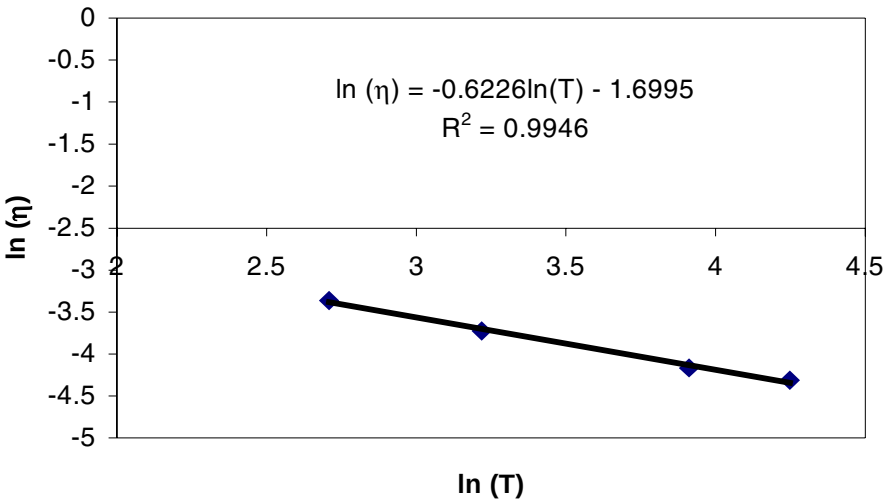

Fig. 59. Apparent viscosity dependence on temperature (X2 simulant).

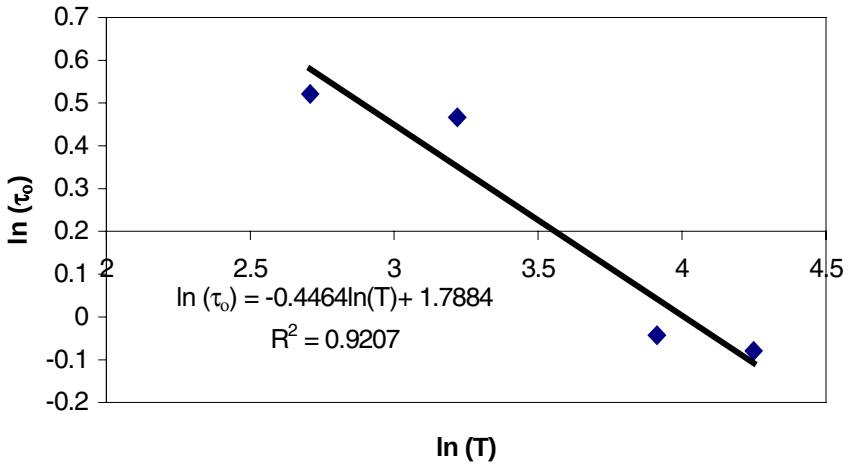

Fig. 60. Yield stress dependence on temperature (X2 simulant).

5.5 Conclusions

- The temperature of the simulant in the feed tank played an important role, as a considerable amount of solids precipitated when the temperature was just below 50°C. This problem was corrected by preparing the simulant at a higher temperature (70 to 80°C) prior to delivering it into the feed tank.
- Flow tests of the hydroxide-phosphate-fluoride systems (X1 and X2 simulants) demonstrated that most of the plugging occurred, with considerable solids formation, at low temperature (15 to 20°C) and at flow velocities lower than 3 ft/s. At higher temperature (40 to 50°C) and flow velocities higher than 3 ft/s, partial plugging was observed with few solids forming. No plugging was observed at flow velocities higher than 6 ft/s.
- Flow tests of the AN-103 Hanford simulant showed a plugging behavior similar to the X1 and X2 simulants.

- Both increasing the flow rate and heating the system resulted in unplugging of the AN-103 and X2 simulants. The X1 simulant plugs, however, could only be manually removed after stopping the pump.
- Rheology measurements of the three simulants tested (X1, X2, and AN-103) showed a Bingham plastic behavior. This means that in order for these fluids to commence flowing, a yield stress (τ_o) must be exceeded. Measurements performed at different temperatures (15, 25, 30, 50, and 70°C) indicated that both the yield stress and apparent viscosity of the simulants decreased as the temperature was increased.
- Figures 52 and 56 (shear stress–shear rate curves) show a variation of the Bingham plastic behavior between shear rates of 100 and 150 L/s. Further investigation is required to understand this phenomenon.
- SEM plug analyses showed needle-like phosphate crystals as well as aluminate, carbonate and fluoride particles in most samples. The sizes of these particles vary from 50 μm to 1 mm.

5.6 References

Hunt, R. D., C. P. McGinnis, C. F. Weber, T. D. Welch, and J. R. Jewett. 2000. *FY 2000 Saltcake Dissolution and Feed Stability Workshop*, ORNL/TM-2000/202, Oak Ridge National Laboratory, Oak Ridge, Tenn. (July).

López, R. D., and R. Srivastava. 1999a. *Solids Formation and Feed Stability During Waste Slurry Transfer Test Plan for FY 2000*, HCET-1999-T006-001-02, Rev. 4, Florida International University, Miami (November).

López, R. D., and R. Srivastava. 1999b. *Solids Formation and Feed Stability During Waste Slurry Transfer Project Technical Plan (PTP) for FY 2000*, HCET-2000-T006, Florida International University, Miami (September).

O'Rourke, J. F. 2000. *Results of Retrieval Studies with Wastes from Tank 241-C-104*, RPP-5798, Rev. 0A, CH2M Hill Hanford Group, Inc., Richland, Wash. (June).

6. DIAL/MSU PREVENTION OF SOLIDS FORMATION FY 2000 STATUS REPORT PART I: STUDIES ON SALT WELL PUMPING

J. S. Lindner, H. Al Habbash, and R. Toghiani
Diagnostic Instrumentation and Analysis Laboratory
Mississippi State University
205 Research Blvd.
Starkville, MS 39759

Abstract

Progress is reported on tasks specifically designed to evaluate, predict, and prevent solids formation associated with Hanford site operations.

The deposition of particles and the formation of plugs can result from low flow rates, line configurations with dead-flow zones, inadequate temperature controls, and changes that may occur based on these parameters and the chemical composition of the fluid. Salt well pumping operations have resulted in line plugs. This work is an experimental study of the influence of operating conditions and the waste chemistry on salt well solution line plugging. Results are presented for studies on salt well pumping.

A laboratory-scale salt well pumping apparatus was designed, constructed, and tested. Work focused on the use of a surrogate for Hanford tank 241-SX-104. Screening experiments were conducted in the laboratory, and Environmental Simulation Program (ESP) calculations were performed. Experiments in the test loop revealed plug formation from trisodium phosphate dodecahydrate. This material has been observed to form long, rod-like crystals and will hydrate 12 moles of water for each mole of trisodium phosphate formed. ESP calculations predict a solids loading of 0.68% by weight at the gelation temperature; even at this concentration, the rods form a sufficient number of secondary bonds to result in a 3-dimensional structure. The effects of pressures and temperatures on plug formation were observed.

The dependence on cooling rate could not be determined in initial experiments conducted at Reynolds number $R_{eD} = DV\rho/\mu = 223$ because the heat exchanger did not permit fine control of the surrogate temperature in the current configuration. Significant variations in the time needed to form a plug were found with an increase in R_{eD}. The average time needed to form a plug with the surrogate was 262 s at an R_{eD} of 223, 692 s at $R_{eD} = 319$, and 2656 s for an R_{eD} of 436. Rapid plug formation was found at low stream velocities, and a more gradual deposition was observed at the highest Reynolds number investigated. Plans for future experiments are described.

6.1 Introduction

For some time now, tank farm operators at Hanford have been implementing the interim stabilization program. In this process, commonly referred to as salt well pumping, the supernate and interstitial liquor in a given single-shell tank are pumped to a double shell tank and then routed to an evaporator. Benefits from this process include the minimization of leakage from aging tanks, thereby limiting migration of waste into the soil, and the temporary reduction of waste within the tank. Pumping of the supernate occurs through a screen with the aid of a jet pump. Recently, solids formation and plugging in transfer lines have been noted for wastes from tanks 241-SX-104, 241-U-103, and 241-BY-102 (Jewett 2000; Reynolds 2000). The primary solid responsible for the plugs from the first two tanks has been tentatively identified through experiments conducted on the waste liquid in the laboratory as $Na_3PO_4 \cdot 12H_2O$. The plug formed during salt well pumping of BY-102 was believed to arise from sodium carbonate (Reynolds 2000). In order to prevent future delays and associated cost overruns, workers have developed provisions for the addition of dilution water.

Other solids may participate in the plug formation process, depending on the solid-liquid equilibrium of the species contained in the waste stream. Aside from the laboratory screening experiments, little is known regarding the mechanisms of plug formation during salt well pumping. (The time needed for a plug to form can be determined from operations records, and the approximate location of the plug can be estimated from the transfer line configuration and flow rates.) However, prevention of inadvertent plugs may be possible based on a suitable engineering tool that will allow operators to tailor waste transfers.

Development of data on salt well pumping is the primary objective of this task. A test loop for obtaining data on supernate transfers does not currently exist. The work described in this report focuses on the development, construction, and testing of a salt well pumping apparatus. The information will support current operations at Hanford and will provide the data needed to support model development activities.

6.2 Results

6.2.1 Salt Well Pumping Flow Loop

The salt well pumping flow rates at Hanford range from 0.4 to 5 gal/min (Jewett 2000; Reynolds 2000). The supernate flows through nominal 3-in. mild steel pipe and can be diverted through junction boxes. Many portions of the transfer lines are heat-traced; however, the junction boxes that use either rigid or flexible insertion pipes (“jumpers”) may or may not be temperature-controlled. Changes in waste temperature will affect flow properties through changes in the solid-liquid equilibria. Development of a laboratory-scale test loop with 3-in. pipe and flow rates common to the actual operation was considered impractical. The initial configuration of the loop included a channel tube with double-pipe counterflow heat exchangers.

The design for the laboratory-scale test loop was scaled based on the Reynolds numbers commonly encountered in site salt well pumping operations. Flow of waste supernate with a density of 1424 kg/m^3 and absolute viscosity of 4.16 cP at a rate of 0.132 m^3/h (0.5 gal/min) through a 7.62×10^{-2} m (3-in.) pipe corresponds to a Reynolds number of 180. For the laboratory experiments, it was convenient to employ a 6.35×10^{-3} m (0.25-in.) ID stainless steel tube. The Environmental Simulation Program (ESP) calculated a density of 1460 kg/m^3 and an average

viscosity of 8 cP for the surrogate stream. The flow rate needed to match the flow conditions at the site was determined as 0.018 m^3/h (18 L/h).

The test loop supernate flow set the size of the holding tank and the initial volume of solution needed for a finite run without the provisions for diluting the stream or for recycle. The size of the heat exchangers was determined by considering the decrease in temperature necessary to produce a plug. Laboratory screening experiments indicated that the chosen surrogate was clear at 55°C and formed a gel at 40°C. Lower gel formation temperatures were observed with dilution of the sample. The heat exchangers were sized to provide a 25°C drop in surrogate stream temperature. They were sized by an energy balance and have a water jacket diameter of 2.54 cm and length of 45.37 cm.

Figure 1 shows the components of the system. The thermocouples, the stainless steel channel, the pressure transducers, and the surrogate/hot water flow meter were selected to minimize corrosion. Sampling ports were located along the flow loop as indicated in Fig. 1. The simulated waste composition was prepared in the inlet tank at an elevated temperature of 70°C and then cooled down to 55°C. The outer jacket of the heat exchanger was constructed from PVC pipe.

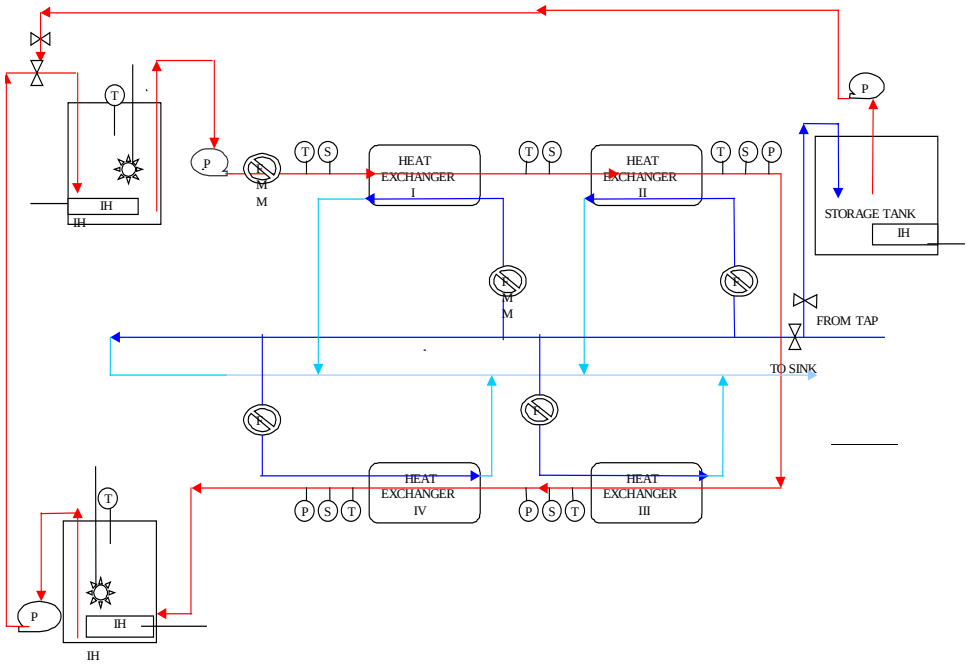

Fig. 1. Block diagram of the salt well pumping test loop.

A booster pump, not shown, was used to increase the delivery of water from the tap. Flow rates from 0.1 to 1.6 gal/min can be delivered to each exchanger. Shutting off three of the exchangers allowed a flow rate of as high as 3 gal/min through the remaining exchanger. Provisions for recycling the surrogate sample to the inlet tank before the solution enters the channel, in the case of a downstream plug, and at the end of the channel, in the event a plug did not form, were included in the design. The inlet stream recycling aided in continually mixing the tank contents.

In the event of plug formation, the sample line could be drained at the sample port and hot water added at the pump head in an attempt to unblock the channel. The locations of the sample ports were selected to permit future investigation of the effect of the amount of flush water. Thermocouples and pressure transducers were seated in wells and inserted into the flow cross section. Outputs from the sensors were interfaced to a Camile data acquisition and control system. At present all of the controls for the system are manual; provisions for automated control may be added in the future.

6.2.2 SX-104 Surrogate Screening

A surrogate recipe for SX-104 was developed by R. Hunt at Oak Ridge National Laboratory (ORNL) and was largely based upon previous studies of the tank supernate performed at Hanford (Herting 1998; Steen 1999a, 1999b). Anion concentrations are given in Table 1. Sodium was the cation in all cases. Samples 5 and 8 were developed in these laboratories following the initial evaluation of the ORNL surrogate.

Table 1. Tank 241-SX-104 supernate surrogate compositions

Anion	ORNL	Sample 5	Sample 8
Aluminate	1	1	1
Nitrate	7	7	7
Hydroxide	2	2	2
Phosphate	0.2	0.2	0.3
Carbonate	0.4	0.4	0.1

Previous work with the actual SX-104 supernate stream by Herting revealed that a gel, based on sodium phosphate dodecahydrate ($Na_3PO_4 \cdot 12H_2O \cdot 0.25NaOH$), formed when the liquid was cooled to 22°C (Herting 1998). Some dark gray solids were observed with the original SX-104 samples, which were removed by centrifugation prior to the cooling tests.

Different plug formation methods are clearly possible in transferring the different Hanford waste streams. For slurries, particle deposition and subsequent build-up are anticipated at velocities slower than the critical velocity. Plug formation in salt well pumping may occur in this manner, but it is also likely that gels could form, leading to a plug. The driving force for the latter mechanism is a reduction in stream temperature, leading to particle nucleation, subsequent growth, and eventual assembly of the 3-dimensional structure.

The ORNL surrogate (and samples 5 and 8) was prepared at a temperature of 70°C in the laboratory and then examined visually and with the polarized light microscope (PLM) as a function of temperature. On cooling to 40°C, the ORNL composition (“Rodney 2” in Fig. 2) formed a gel along with some loose solids, observable in the bottom of the glass tube. Changes were made to the original recipe (Table 1) in an attempt to reduce the amount of loose solids, thereby providing the potential for a plug based on gel formation only and allowing the elimination of the effects of loose particle deposition. Sample 5 provided some loose solids (presumably Na_2CO_3), whereas the formulation for sample 8 yielded gel only.

PLM images for the ORNL and Sample 8 surrogates are shown in Figs. 3 and 4. The long cylinders or rods observed in both images are crystals from $Na_3PO_4 \cdot 12H_2O \cdot 0.25NaOH$. The solids in Fig. 3 have been identified as gibsite ($AlOH_3$). The PLM results are consistent with the

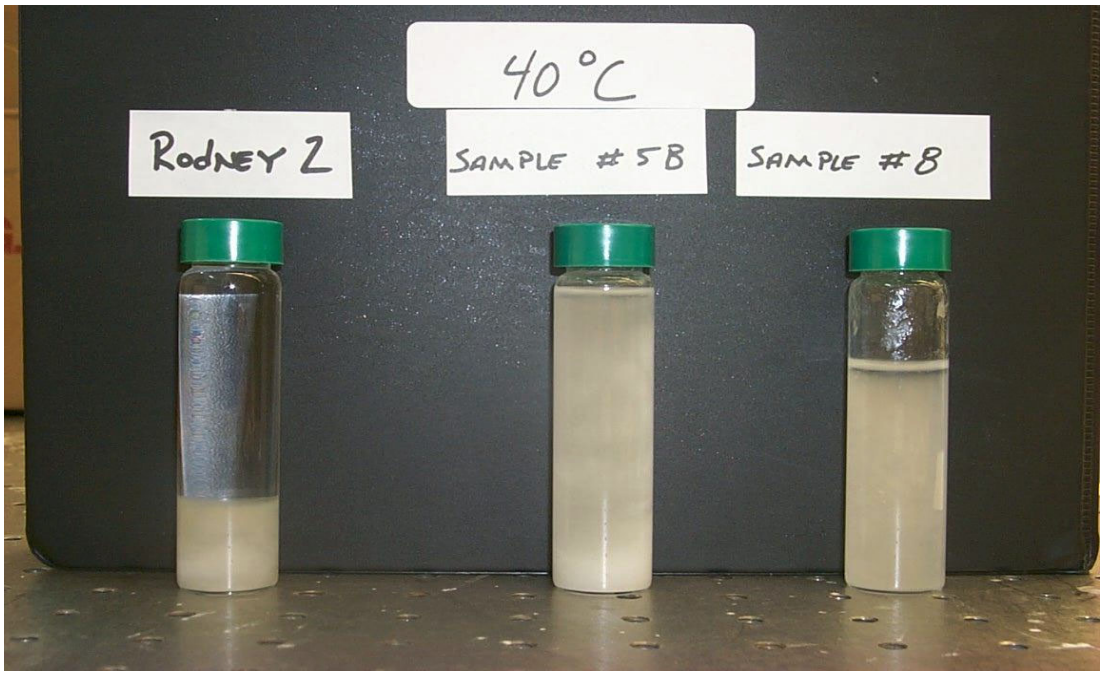

Fig. 2. Photograph of surrogate samples at 40°C. The "Rodney 2" sample is the ORNL composition.

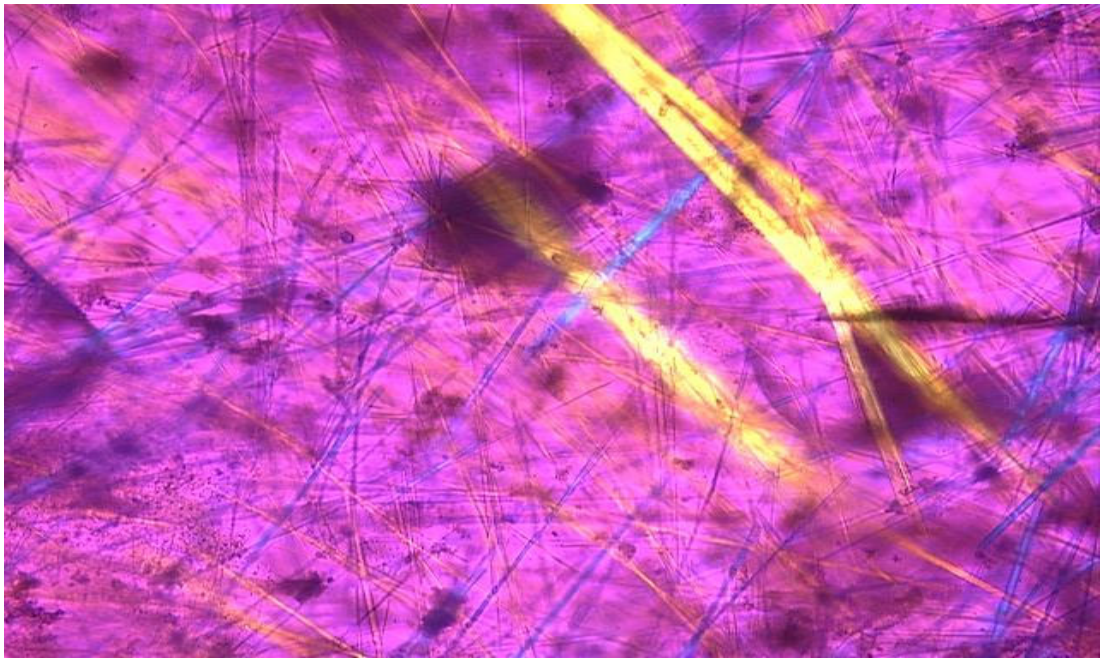

Fig. 3. Polarized light microscope image of the ORNL sample at 40°C.

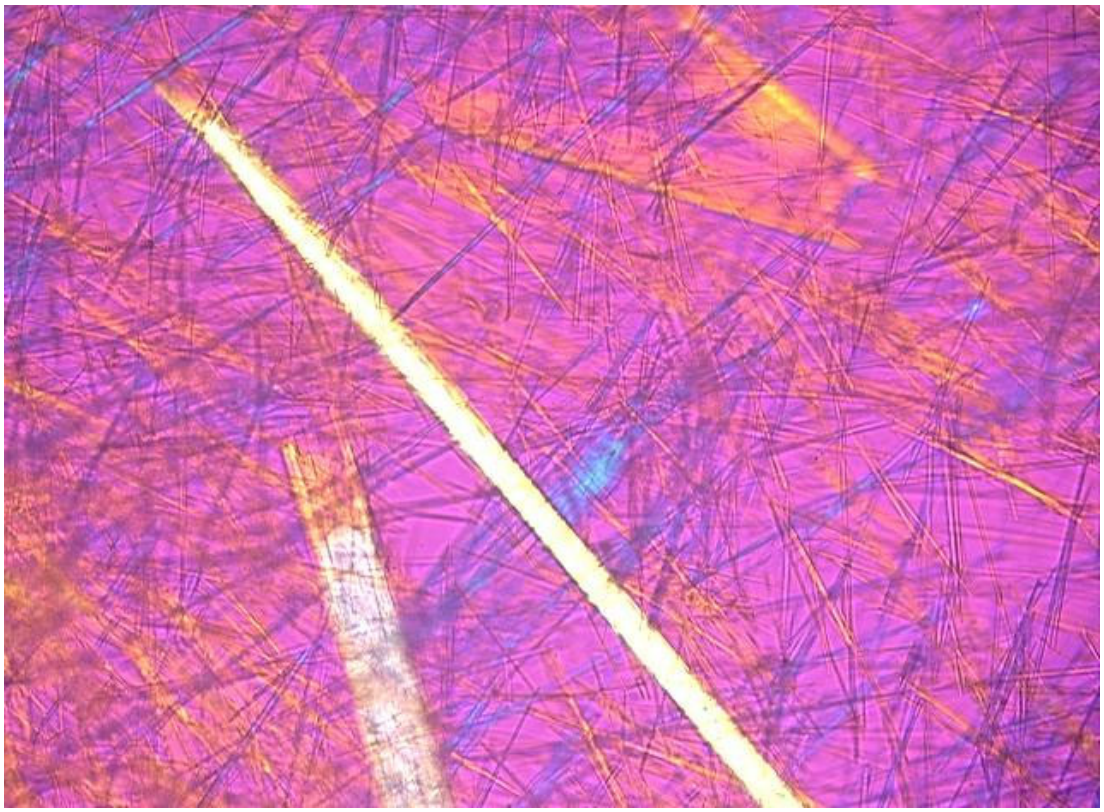

Fig. 4. Polarized light microscope image of the sample 8 surrogate.

solids fraction observed in the photograph in Fig. 2. The crystals in the PLM image for sample 8 at 25°C (not shown) consisted of the sodium phosphate dodecahydrate and sodium nitrate. The PLM images for sample 8 are similar to the images of the actual SX-104 supernate as reported by Herting (1998). The main difference between the waste stream supernate and sample 8 is that gel formation was observed for sample 8 consistently at 40 ± 1°C, whereas the actual waste stream liquid was found to form a network at 22°C. A higher phosphate loading is present in the surrogate sample.

Decreasing the temperature from 40 to 25°C resulted in gels of more rigidity. At 40°C, sample 8 contains a small amount of liquid on top of the gel (Fig. 2). At 25°C, the sample vial could be inverted and vigorously shaken without flow.

6.2.3 ESP Calculations Supporting the Laboratory Salt Well Pumping Experiments

The compositions in Table 1 provide a means to study plug formation during salt well pumping if only a gel forms or if a gel is formed along with various amounts of loose solids. ESP calculations (version 6.2) were carried out to provide additional information on surrogate chemistry and stream properties, such as enthalpies, solid-liquid partitioning, and liquid viscosities that are of interest in the actual pumping experiments. The chemistry model was constructed from the sodium species of Table 1. The Laboratory, TRONA, and public databases were employed. Initially, the ORNL and sample 8 surrogates were evaluated as a function of temperature. The sample 8 surrogate was then evaluated at different dilutions. These later

experiments were then compared with experimental observations. The solids distributions for the sample 8 surrogate at the different temperatures are listed in Table 2.

At temperatures above 41°C, the only solid predicted by ESP is sodium phosphate octahydrate. Attempts to observe the corresponding crystal with the PLM were unsuccessful. The particle size is apparently smaller than that dimension observable with the highest effective magnification of the microscope, 400×.

At an approximate temperature of 40°C, the octahydrate crystal is partitioned to the dodecahydrate that comprises 100% of the solids in the system at that temperature. Gibsite forms on cooling the composition to 35°C, and at lower temperatures, the model predicts the formation of $NaNO_3$(s). The model correctly identifies the crystals observed in the PLM images; however, the fact that the solids form an ordered network cannot be predicted by the code.

Totals for the sample 8 surrogate stream are given in Table 3. The calculated density at 50°C is above the criteria for waste transfers of 1.35 g/L (for liquids with less than 30% solids) and below the waste compatibility limit of 1.41 g/L (Reynolds 2000). The total stream density increases with decreasing temperature owing to the additional partitioning into the solid phase.

At the gel temperature of 40°C (Fig. 2), the model predicts the formation of ~9 g of solid sodium phosphate dodecahydrate per liter of solution.

The heat capacity is a critical value for determining the heat transfer characteristics of a given process. As part of the standard output from ESP, stream enthalpies and a total solution enthalpy are reported. The heat capacity is defined as the slope (dH/dT) of a plot of the enthalpy against absolute temperature. Data from ESP resulted in a heat capacity of about 3100 J/g·K. This value is compared with experimental results from the test loop in the following section.

6.2.4 ESP Simulations and Experimental Results for Dilution of SX-104 Surrogate Sample 8

Determination of the amount of dilution water needed to safely transfer salt well liquor will depend on the composition of the supernate and the solid-liquid partitioning at different temperatures. Water is used for both dilution and line flushing, and both operations result in an increase in waste volume. Based on evaluation of the conditions that led to the SX-104 plug, it appears that the operators were processing the liquid with no dilution water, stopped the transfer for a while, and on re-start developed a plug in an unheated jumper (Jewett 2000; Reynolds 2000). The plug was dissolved using hot water. Dilution water was subsequently injected at the pump head.

The technical basis for dilution and line flushing operations during salt well pumping is not well established; in fact, establishing the technical basis is the major benefit expected from this work. It has been noted that diluting the salt well liquor 1:1 has worked in preventing plugs (Reynolds 2000). Flushing is accomplished using 1 line volume of water and has occurred on different schedules. Nominally, the line is flushed whenever the jet pump is down for longer than 2 h. Flushing has been performed every week and is currently done every 21 d. The frequency of flushing, as well as the amount of dilution water added, will depend on the stream composition and the waste routing.

Table 2. Solids compositions and phase information for sample 8 SX-104 surrogate

	Sample information by temperature								
	15°C	20°C	25°C	30°C	35°C	40°C	42°C	43°C	50°C
Solids, g									
$Al(OH)_3$	31.37	25.77	19.16	11.42	3.51	0.00	0.00	0.00	0.00
$NaNO_3$	135.33	103.56	68.82	30.50	0.00	0.00	0.00	0.00	0.00
$NaPHOH \cdot 12H_2O$	84.69	80.45	72.67	58.92	37.15	9.35	0.00	0.00	0.00
$Na_3PO_4 \cdot 8H_2O$	0.00	0.00	0.00	0.00	0.00	0.00	9.26	1.25	0.00
Total wt, g	251.39	209.77	160.64	100.84	40.66	9.35	9.26	1.25	0.00
Volume, L	0.13	0.11	0.08	0.05	0.02	0.01	0.01	0.00	0.00
Density, g/L	2008.02	1975.56	1929.41	1846.82	1667.56	1619.96	1619.96	1619.96	0.00
% PO_4 solids/total	33.69	38.35	45.24	58.43	91.37	100.00	100.00	100.00	0.00

86

Table 3. Environmental Simulation Program predictions for sample 8 at different temperatures

	Sample information by temperature							
	15°C	20°C	25°C	30°C	40°C	42°C	43°C	50°C
Mass, g	1373.53	1373.53	1373.53	1373.53	1373.53	1373.53	1373.52	1373.53
Volume, L	0.96	0.96	0.97	0.97	0.99	0.99	0.99	1.00
Density, g/L	1437.78	1429.97	1420.86	1410.24	1388.26	1384.30	1383.35	1373.53
% Solids by wt	18.30	15.27	11.70	7.34	0.68	0.67	0.09	0.00
% Solids by vol	13.11	11.05	8.61	5.61	0.58	0.58	0.08	0.00
% Water by wt	49.22	49.39	49.70	50.26	52.26	52.32	52.59	52.64

87

The ESP model was used to calculate the effect of dilution water on the surrogate stream. These results correspond to dilutions of 25, 50, 75, and 100% by volume; details will be reported later. A 100-cc volume of the sample was made in the laboratory at elevated temperature (70°C and until clear) and then distributed to five different vials and subsequently diluted.

Gels were observed for the 1:0.25 and 1:0.5 dilutions at 30°C. On cooling to 25°C, a gel was observed for the 1:0.75 sample. A gel was not found for the sample diluted 1:1.

The samples were subsequently placed in the oven at 70°C overnight and then reexamined. Gibsite ($AlOH_3$) was observed to have formed on the bottoms of the test tubes. Upon cooling, only the baseline sample 8 composition without dilution formed a gel. This indicates that a re-partitioning of the samples occurred following the precipitation of the $AlOH_3$.

6.2.5 Viscosity of the Sample 8 Surrogate

The viscosity is a critical parameter in the transfer of fluids. The formula for the surrogate sample was sent to ORNL for analysis using ORNL's Brookfield instrument. The viscosity is plotted against shear rate for measurements at different temperatures in Fig. 5. Data points are shown for the measurement shear rate cycle. The data were initially obtained at low rates of shear; the speed of the rotor was then increased to a maximum, and then the shear was decreased to the original condition. Some hysteresis can be observed in the measurement cycles at the intermediate temperatures.

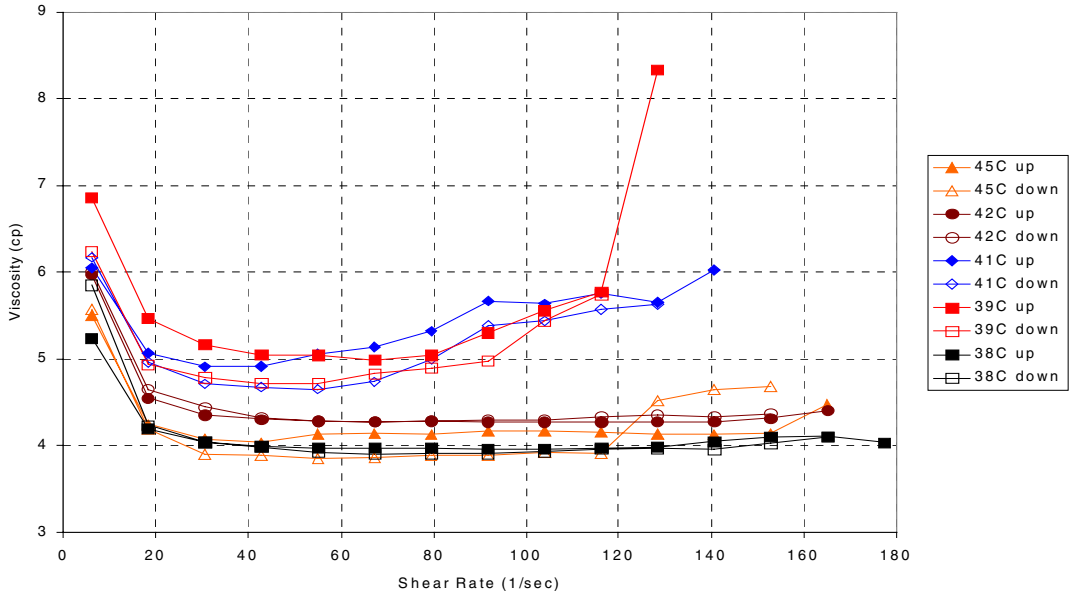

Fig. 5. Viscosity against shear rate traces for the sample 8 surrogate. The increase in viscosity at increasing shear rates is an example of shear thickening behavior.

The curves all show an increase in viscosity at the lower shear rates, indicative of non-Newtonian fluid flow. For the measurements at 45 and 42°C, the viscosity does not significantly depend on shear at rates greater than about 30 s^{-1}. As the temperature is decreased to 41 and then 39°C, the viscosity is seen to increase at shear rates above 50–70 s^{-1}. This behavior is consistent with shear

thickening and probably represents ordering of the $Na_3PO_4 \cdot 12H_2O$ rods. When the temperature decreases further to 38 and then 36°C (latter not shown), the viscosity again becomes independent of shear at rates greater than 30 s^{-1}. It is believed that the decrease is due to solids or gel formation below the rotor of the viscometer or on the walls of the sample holder. Partitioning of the fluid in this manner would lead to a decrease in the overall solution viscosity. Similar results were observed previously in the ORNL parametric viscosity study (Hunt et al. 2000).

The shear thickening behavior observed for the sample 8 surrogate implies that specific flow rates or Reynolds numbers may need to be avoided at certain waste stream temperatures.

6.2.6 Experiments on Plug Formation

Upgrades to the salt well pumping flow loop have been made during the course of this work. Initially, only three pressure transducers were installed. Following the beginning tests, it was noted that the optimal facility location where the plug should be generated was between heat exchanger 3 and heat exchanger 4. Upon plug formation, the pressures upstream of the blockage would be at maximum values; and downstream of this location, the pressures would tend to be at lower values.

In a typical experiment, 18 L of the sample 8 surrogate was prepared and held at 70°C until all of the solids had dissolved. The contents of the tank were then cooled to 50°C. Multiple experimental runs were performed with the initial composition. The sample channel was pre-heated with hot water from the water dilution tank to a temperature of about 60°C. The channel was then drained and the surrogate flow started at a desired rate. The liquid was allowed to flow in the channel and then to the receiving tank, where it was collected prior to transfer back to the holding tank. Temperatures were allowed to stabilize with no forced cooling. When the temperature at T4 reached 46°C, the water to the third heat exchanger (see Fig. 1) was started. Experiments were performed at a constant Reynolds number for different cooling rates. Additionally, plug formation tests were carried out at different Reynolds numbers with a constant flow of 1.2 gal/h to heat exchanger 3.

6.2.6.1 General Data Observations

Pressure and temperature traces for an experiment with a surrogate flow rate of 4.8 gal/h and an exchanger 3 cooling water flow of 0.1 gal/min are given in Fig. 6. The data shown are for the period after heat exchanger 3 was activated. Temperatures for all locations on the channel and for the holding tank are shown, along with the inlet cooling water temperature (TCW) and the exit temperature of the water from heat exchanger 3.

Small variations in the tank temperature and for thermocouples 1–4 arise from the cycling of the immersion heater in tank 1. Thermocouple 4 is located between heat exchanger 3 and heat exchanger 4; this position illustrates the change in temperature that is associated with plugging.

Of interest are the pressure increases that start around 13:54 and continue until they reach a maximum value that indicates a complete line blockage. The location of the pressure transducers (Fig. 1) confirms that the plug was established between heat exchanger 3 and heat exchanger 4. A reading was not observed on the flow meter following formation of the plug. The maximum pressure observed depends on the pump. The downstream pressure transducer shows a delayed increase because of the higher downstream temperature that reduced the rate of formation of the phosphate rods.

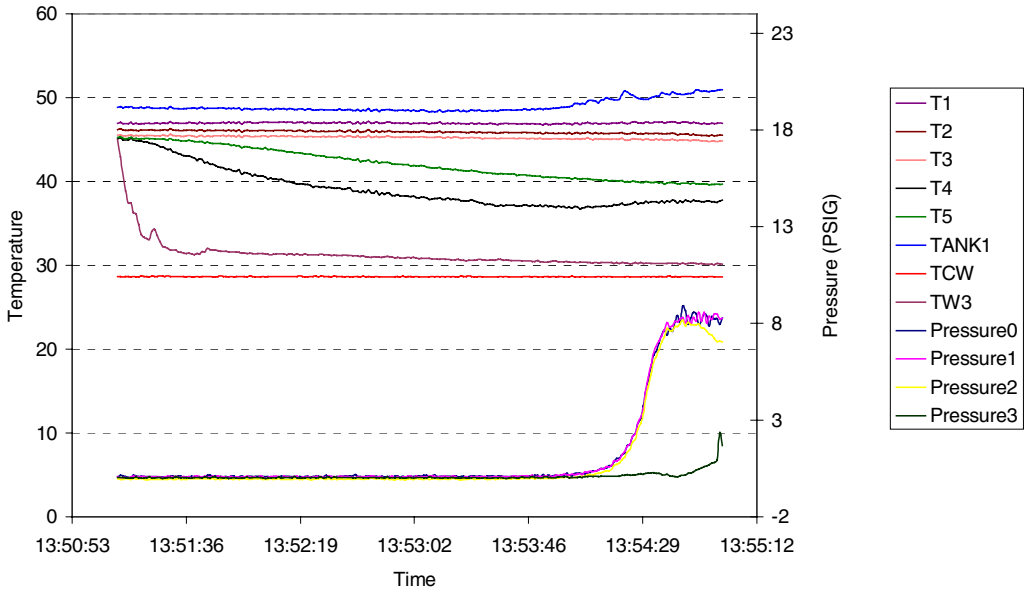

Fig. 6. Pressures and temperatures recorded for the experiment on 8/22/00. The surrogate flow rate was 3.5 gal/h, and the water to heat exchanger 3 was metered at 0.1 gal/min.

Based on the data in Fig. 6, the general properties of plug formation—such as time to plug, fluid temperatures after plug formation, temperature drops, and overall pressure increases—can be obtained. Heat exchanger thermocouples were only installed for the last two experiments. In this case, more information regarding the heat transfer properties of the flow can be obtained. A list of the experiments and the data and the averaged parameters are collected in Table 4.

Table 4. Characteristics of the initial experiments

Date	Surrogate flow (gal/h)	HEX 3 cooling water (gal/min)	Re	T4 rate of temp change (°C/s)	Time to plug (s)	Pressure at plug (psig)	T4 at plug (°C)	T5 at plug (°C)
8/11/00	3.5	0.10	223	0.044	294	9.0	38.3	38.4
8/18/00	3.5	0.10	223	0.051	222	8.3	37.6	39.7
8/23/00	3.5	0.10	223	0.063	288	8.5	43.1	41.0
8/10/00	3.5	0.66	223	0.073	268	8.9	38.8	39.7
7/21/00	3.5	1.20	223	0.153	264	8.0	38.8	39.4
8/14/00	3.5	1.20	223	0.055	248	8.6	40.6	40.1
8/17/00	3.5	1.20	223	0.048	250	8.6	39.4	39.8
7/21/00	5	1.20	319	0.087	692	7.7	43.5	42.5
7/24/00	6.8	1.20	436	0.073	2656	7.7	46.0	45.2

From Table 4, it appears that only minor variations in the measured experimental parameters were observed for the lowest-Reynolds-number experiments. At the lowest Reynolds number, the time required to plug was not correlated with the rate of temperature decrease for the range of decreases tested. Results for the time to plug at Re = 223 indicate that the plug was formed at a similar channel location for all the experiments conducted at this Re value, based on the constant inlet stream velocity and the pressure profiles. A main observation from the data is the increase in the time needed to form the plug at the higher surrogate flow rates.

The pressures at R_{eD} = 319 and 423 are somewhat reduced compared with the average values when all of the data are considered.

6.2.6.2 Comparison of Experimental Results for Different Reynolds Numbers

The following observations were made from the experiments with R_{eD} = 223, 319, and 436.

The pressure traces indicate that plug formation was more gradual at the higher Reynolds numbers. A delayed increase in pressure was observed at R_{eD} = 319, compared with the R_{eD} = 223 run, and an even more gradual pressure rise was found at the highest surrogate flow rate investigated.

6.3 Discussion

6.3.1 General Flow Characteristics, Heat Capacity and Dimensionless Numbers

The Reynolds number, $R_{eD} = DV\rho/\mu$, begins at a known value and approaches zero upon completion of the plug. The density, velocity, and viscosity change as the plug is forming. The density of the surrogate waste was calculated from ESP as 1.39 kg/L at 40°C. The density of solid trisodium phosphate (TSP) is 1.62 kg/L. Assuming that the plug is solid TSP, the stream density would only increase by about 17%. The total solid loading upon gel formation is only 0.68% by weight, so the change in the density is not significant.

If the flow remains laminar and constant, the change in pressure can be expressed as

$$\Delta P = (32\mu V)/d^2 \quad (1)$$

where *d* is the inner diameter of the channel. The experimental data show that for some period of time, the pressure is below that observed after complete channel blockage, indicating some flow. This time may be related to an induction period where the rods are starting to form but are not of sufficient size or number to form the gel. During this time, the changes in *V*, μ, and d are not sufficient to increase the pressure above the baseline value.

At plug formation, the pressure is at a maximum, and the channel diameter available for transport of the surrogate stream becomes 0. During plug formation, the pressure increases. Surrogate metered into the channel remained at a constant flow rate until just before reaching the limiting pressure. The local viscosity is considered to be the same as that measured at the plug temperature; thus, $\Delta P \propto K/d^2$, where *K* is a constant.

The time needed to form the plug depends on the Reynolds number; and based on the equation in the preceding sentence, the governing parameter is the fluid velocity. Although additional data are needed, it appears that increasing the velocity will reduce the time available for interaction of

the rods with one another. Intramolecular interactions are necessary to assemble the three-dimensional gel structure; the gel is not formed from covalent bonds.

As the stream velocity increases, the contact time between the rods may decrease owing to additional transport forces on the rods. In essence, the additional molecular velocity at the higher flow rates reduces the number of "sticky collisions." This explanation would amount to a preferential orientation of the rods at higher velocities.

The results obtained thus far imply that, from a practical standpoint, transport of salt well liquor under constant cooling conditions will be more successful at higher flow rates.

Little discussion has been focused on the thermal effect associated with the experiments. It is quite clear that the extent of cooling of the fluid will determine the number of TSP rods formed, and this, in turn, will set the gel formation point. The heat capacity of the sample 8 surrogate was determined using the flow loop. The specific heat was determined based on heat balance as ~3400 J/(kg·K). This result is within 9% of that value [3100 J/(kg·K)] obtained from the ethalpies calculated using ESP

At low Reynolds numbers, the plugging process is extremely rapid. Formation of the plug does not follow a traditional sedimentation pattern. Rapid growth of the TSP crystals has been observed (Francis et al. 2000). Laser diffraction experiments, conducted at AEA Technology, were unable to follow the kinetics of the process. Additional experiments are needed to further understand the plug formation process and translate the pertinent variables into working expressions.

6.3.2 Future Work

The work reported in this chapter has been conducted over an 8-month period. Aspects of the research relating to line flushing and the amount of dilution water required to safely transport the surrogate waste (or other waste of a similar composition) have not yet been performed; however, the experiment reported for the highest-Reynolds-number flow provides an initial condition with which line flushing can be evaluated. With regard to the dilution experiments, it is expected that plug formation will proceed at a much slower rate; in that case, the other dimensionless numbers may become more accessible. Nucleation and growth kinetics of the rods are expected to be more tractable at the diluted conditions. In regard to the observations, additional data are needed on the viscosity at both low and high shear rates.

Correlation of the experimental results with operations process data is also needed. It is believed that the pressures recorded during salt well operations provide the best means of comparison. Discussions with engineers at the site are in progress (Lamphere 2000).

Experiments on an additional surrogate from Hanford tank 241-U-103 are scheduled. TSP was also thought to be responsible for the plugging of the transfer line during salt well pumping from this tank. We plan to use the surrogate composition as received. Thus, the higher-density phase is expected to partition into some loose solids along with the gel. A transition from gel formation to sedimentation is expected; and, in that case, the standard framework describing particle deposition can be evaluated.

6.4 Conclusions

A laboratory-scale flow loop based on the conditions at the site was designed, constructed, and calibrated with water. Flow experiments were conducted on a surrogate derived from the supernate of tank 241-SX-104. Previous experience at the site indicated the propensity of the SX-104 surrogate to form a gel based on sodium triphosphate dodecahydrate. The surrogate was characterized for gel formation at different temperatures, and PLM measurements indicated the rod-like crystals. ESP calculations were used to determine the solid–liquid equilibria and heat capacity. Researchers at ORNL performed initial viscosity measurements, and the results indicated that the fluid was shear-thickening.

Transport experiments in the flow loop revealed that the gelation of the surrogate and subsequent plug formation was a complex process that depended primarily on the velocity. The results obtained to date indicate that—while plugs have been formed at all flow rates examined—the higher the velocity, the longer the time needed to form the plug. Based on the observed pressure profiles, two different plug formation mechanisms have been observed. The lower Reynolds numbers experiments result in the rapid assembly of the plug. At the highest velocity evaluated, the gel assembly process is somewhat different in terms of deposit formation and eventual assembly. The time necessary for the plug at the lowest Reynolds number was within 10% for all runs, indicating the plug formed in approximately the same channel location. The heat capacity from ESP was found to agree to within 9% of the measured heat capacity.

Interpretation of the data is in progress using dimensionless numbers. Initial observations indicate that many of the fundamental parameters that describe the flow may exhibit changes in the vicinity of the gel formation temperature. Further laboratory experiments are needed to delineate the variation of the viscosity with shear and temperature and to understand the nucleation and growth processes associated with TSP. Work aimed at evaluating the amounts of water necessary to ensure safe transfer and provide the basis for line flushing frequency is in progress.

6.5 References

Francis, A., et al. 2000. *Progress Report on Precipitation Studies of Hanford Tank Simulant*, AEAT/R/NS/0164, AEA Technology, Harwell, UK, June.

Herting, D. L., 1998. *Tank 241-SX-104 Dilution Testing, Interim Report*, Internal Memo 8C510-PC98-024, Numatec Hanford Corporation, Richland, Wash.

Hunt, R. D., T. A. Dillow, J. R. Parrott, J. C. Schryver, C. F. Weber, and T. D. Welch 2000. *Waste Preparation and Transport Chemistry: Results of FY 2000 Studies*, ORNL/TM-2000/298, Oak Ridge National Laboratory.

Jewett. J. R. 2000. Personal communication from J. R. Jewett of Numatec Hanford Corporation to T. D. Welch of ORNL and J. S. Lindner of Mississippi State University, “Tank Farm Information for TFA Workers” and ”Saltwell Pumping from Tank SX-104,” Numatec Hanford Corporation, Richland Wash., January 24.

Lamphere, J. E., 2000. Personal communication to J. S. Lindner of Mississippi State University, August.

Reynolds, D. A., 2000. “Status of Waste Transfers, Criteria, and Plans,” Presented at the Third Saltcake Dissolution and Feed Stability Workshop, Richland Wash., May 16, 2000.

Steen, F. H., 1999. *Ammonia Analysis Results for the Final Report for Tank 241-SX-104*,Memo, WMH-9852843, Numatec Hanford Corporation, Richland, WA (1999).

Steen, F. H., "Analysis Results for the Final Report for Tank 241-SX-104," Memorandum WMH-9856353, Numatec Hanford Corporation, Richland, Wash.

7. DIAL/MSU PREVENTION OF SOLIDS FORMATION FY 2000 STATUS REPORT PART II: MODELING OF SLURRY TRANSPORT AND SALT WELL PUMPING

J. S. Lindner, H. Al Habbash, and R. Toghiani
Diagnostic Instrumentation and Analysis Laboratory
Mississippi State University
205 Research Blvd.
Starkville, MS 39759

Abstract

Specifics of the modeling approach and the development phases of the engineering tool that will help prevent plug formation incidents during the salt well pumping and slurry transfer operations at Hanford are outlined. The efforts are mainly aimed at producing a model that will accurately predict, if, where, and when a plug will form during a transfer process, while taking into account the dynamic behavior of the transfer process and reflecting the impact of the waste chemistry. Efficiency and ease of use to the operators and applicability to the operations at Hanford are considered top priorities.

The modeling approach, based on building the model using separate modules that represent a specific physical or chemical process, has started. A general computational fluid dynamics system that will represent the transport module was acquired. Initial test simulations were performed for simple but relevant transport processes. Other tests addressing module sensitivity to grid distribution, initial and boundary conditions, and initial velocity distribution at the entrance are in progress.

Simulations for the Florida International University slurry C experiments, which demonstrate the process of settling of a simple suspension, produced good agreement with the reported results. The simulations suggested that flow rates with entrance velocities of larger than 1.0 m/s will produce a moving bed flow. The higher the flow rates, the less likely a significant amount of particles will deposit and eventually lead to the formation of a plug. To prevent the establishment of stationary bed flow, a pumping flow rate must be used that produces velocities higher than the settling velocity for the largest particle available to transport. This will ensure at least a minimum level of moving bed flow.

Incorporation of more elaborate formulation and additional modules into the overall model is in process. This will include capabilities that will account for the complex characteristics of the waste. Modifications will include the effects of the change of solids concentration on the viscosity of the flow, phase transition, particle nucleation and growth, and chemical reaction capabilities.

7.1 Introduction

U.S. Department of Energy (DOE) waste pretreatment and retrieval activities at Hanford have suffered from several delays in their transport operations because of plugging in transfer lines (Reynolds 2000). These activities include two distinct types (from a fluid mechanics point of view) of transport processes. The first involves the movement of supernates [salt well (SW) pumping and concentrated evaporator brines]. This type of flow is initially characterized by negligible or low solids concentrations. The second process involves the transfer of waste slurries (ST) in which solids are present at moderate to high concentrations, mostly at less than 20% by volume. Pipeline plugging in both operations results from the unintentional formation or deposition of solids during transport.

The main aim in this work is the development of an engineering tool that will accurately and efficiently predict particle deposition and plug formation while taking into account the dynamic behavior of the waste transport processes and, in so doing, reflect the impact of the waste chemistry. Once validated using data from companion work on laboratory and pilot-scale flow loops, the package will be tested at Hanford, upgraded if needed, and eventually transferred to site operations to help the operators minimize possible delays due to plug formation in transfer lines.

The physical processes that must be taken into account to model particle deposition and plug formation in both the SW pumping and pipeline ST processes are similar. They include fluid transport properties, heat transfer, chemical reactions, phase change, particle growth, agglomeration and particle settling, and adherence dynamics. Despite these general similarities, the mathematical formulations needed to accurately represent the transport of multi-phase fluid flow differ (Crowe et al. 1998). At low solids concentrations, the usual practice is to use an Eulerian/Lagrangian formulation (Crowe et al. 1998). In this case, the Eulerian framework is used to account for the continuous (carrier) phase, and the Lagrangian formalism is used to represent the dispersed/dilute phase as particles start forming in the flow. On the other hand, in simulations involving solids present at high volume fractions, usually more than 5% by volume, an Eulerian/Eulerian formulation is considered for both phases (Crowe et al. 1998). This practice is due to the presence of a high concentration of solids in the flow and to the inefficiency of the Lagrangian formulation in accounting for particle/particle interactions and the two-way transfer of mass, momentum, and energy between phases—in particular, how the dynamics of the dispersed phase influence the dynamics of the carrier phase.

In what follows, the specific desired characteristics for the engineering tool, the modeling approach based on these requirements, and a description of the overall model are given. Results are then presented describing the initial efforts in assembling the model and evaluating the performance of the main transport module. Simulations were conducted based on a Westinghouse Savannah River Company (WSRC) surrogate composition previously evaluated in the slurry flow test loop at Florida International University (FIU) (Ebadian 1999). Details of the calculations and a comparison with the experimental results are given. Ongoing model development activities are then described.

7.2 Engineering Tool Objectives, Requirements, and Approach

Prior to and shortly after this work was begun, a number of objectives for the engineering tool were identified. These stem largely from the need at the site for the safe and efficient transfer of wastes. Delays in meeting scheduled deliveries can, depending on contractor requirements and interagency agreements, result in fines or actions imposed on DOE (Reynolds 2000). Currently,

only one cross-site transfer line is available to move waste from the 200 West to 200 East area (Reynolds 2000). Plugging the transfer line would severely impact vitrification operations and further delay the remediation of the waste.

7.2.1 Model Objectives

The requirements for the engineering tool were derived directly from the objectives; from these, it became possible to develop the modeling approach. Section 7.2.2 describes these analyses, the model configuration, and the data requirements. The engineering tool must meet these goals:

- Be capable of predicting the formation of a plug in a transfer line for both ST and SW operations
- Allow the determination of the location of a plug and the approximate time needed to form the plug
- Predict the values of variables that are measurable by the tank farm operators, such as flow rates, pressures, temperatures and species concentrations
- Be practical in terms of operator expertise to set up and run the model for a specific site transfer
- Be modular to optimize and minimize computational times

7.2.2 Model Requirements

As a starting point (without taking into account possible simplifications and/or the use of experimental data and correlations), the following physical processes and properties may have to be accounted for to predict the fluid transport process, sedimentation, and plug formation accurately:

1. Number of species present in the flow field
2. Concentration of each species
3. Fluid properties, (flow rate, pressure, density, viscosity, etc.)
4. Conservation of mass of all species
5. Conservation of momentum for all phases, between phases, and of all species
6. Conservation of energy and heat transfer in the flow field and between species
7. Chemical reactions between species and the formation of solids (all types of reactions should be accounted for until more simplifications are possible)
8. Solid particle size, shape, and density
9. Solid particle population balance and growth kinetics
10. Phase equilibria
11. Effects of chemical reactions and phase changes on the flow properties
12. Particle sedimentation, agglomeration, and adherence behavior

These elements are to be incorporated and assembled in the overall model(s) by means of separate modules (in terms of the set of mathematical equations solved). Each module will be responsible for calculating and/or correlating a specific process in the flow field. All of the modules will be assembled in an integrated package.

7.2.3 Modeling Approach

The process by which the model is going to predict plug formation in a transfer pipe will require the solution of several highly complicated partial differential equations that describe the physical

processes occurring during the transport (Tannehill 1997). This solution is carried over the entire flow field as a function of position or space (x,y,z) and time. The solution process starts by discretizing the governing partial differential equations of mass, momentum, and energy for one or multiple phases (Eulerian or Lagrangian) over a finely spaced grid that spans the entire flow field. This grid is necessary to accurately define (in a discrete form) the geometry of the flow field and to apply the physical boundary and initial conditions. As the solution proceeds over the flow field (in space and time), the model will also require a means by which the results from the solution are accurately interpreted and understood.

The subjects of grid generation (pre-processing) and results interpretation (post-processing) require a great deal of special expertise and time-consuming development that adds considerably to the model complexity. In addition, the development of a thoroughly tested and verified computational fluid dynamics (CFD) code is known to consume long periods of time and require highly specialized expertise. For those reasons, the modeling approach in this work is based on using a simple but general-purpose CFD system, thereby taking advantage of established capabilities. The work will then proceed with the addition of the required modules and assessment of parameter significance. This approach is believed to allow for a reduction in development time.

A flowchart for the proposed model is shown in Fig. 1. The equations that are pertinent to the function of some of the modules (described in the following paragraphs) have not been formalized yet owing to possible modifications.

Input module. The main role of the input module is to provide a means by which the flow field geometry (pumping distance, junctions, valves, etc.) is defined, the necessary grid for the solution is generated, and the physical boundary and initial conditions are applied. The initial and boundary conditions consist of the already known properties regarding the waste composition and the waste transfer process. The data on waste composition may consist of a subset of the chemistry of the waste or a more detailed description. The data on the waste transfer process comprise temperatures, pump pressures, flow rates, and geometrical data.

Chemistry module. The accurate prediction of the types and amounts of solids that could form in the SW and the total solids concentration in the ST for the given pumping process is essential for determining if a plug could form. Determination of the solids partitioning requires accurate calculations and well-tested and well-verified data. Accurate data are especially important for the waste streams under consideration here. The solids prediction module can be bypassed; replaced by available correlations/curve fits of experimental data; or calculated by, for example, the Environmental Simulation Program (ESP). Output from this module consists of the densities of the solids, the viscosity of the supernate, heat capacity, thermal conductivity, solids speciation and loading, and other critical supernate species that may participate in future particle formation.

Particle growth/nucleation module. The shape of the particles and the associated size will have a direct effect on plug formation. The particle shape, size, and mass impact the transport dynamics, which have a direct connection to the critical particle velocity and deposition behavior. Additionally, under certain conditions, the particle loading may increase or decrease depending on the temperature, solid-liquid equilibria, and kinetics. This effect will also have a direct impact on the bulk viscosity of the fluids.

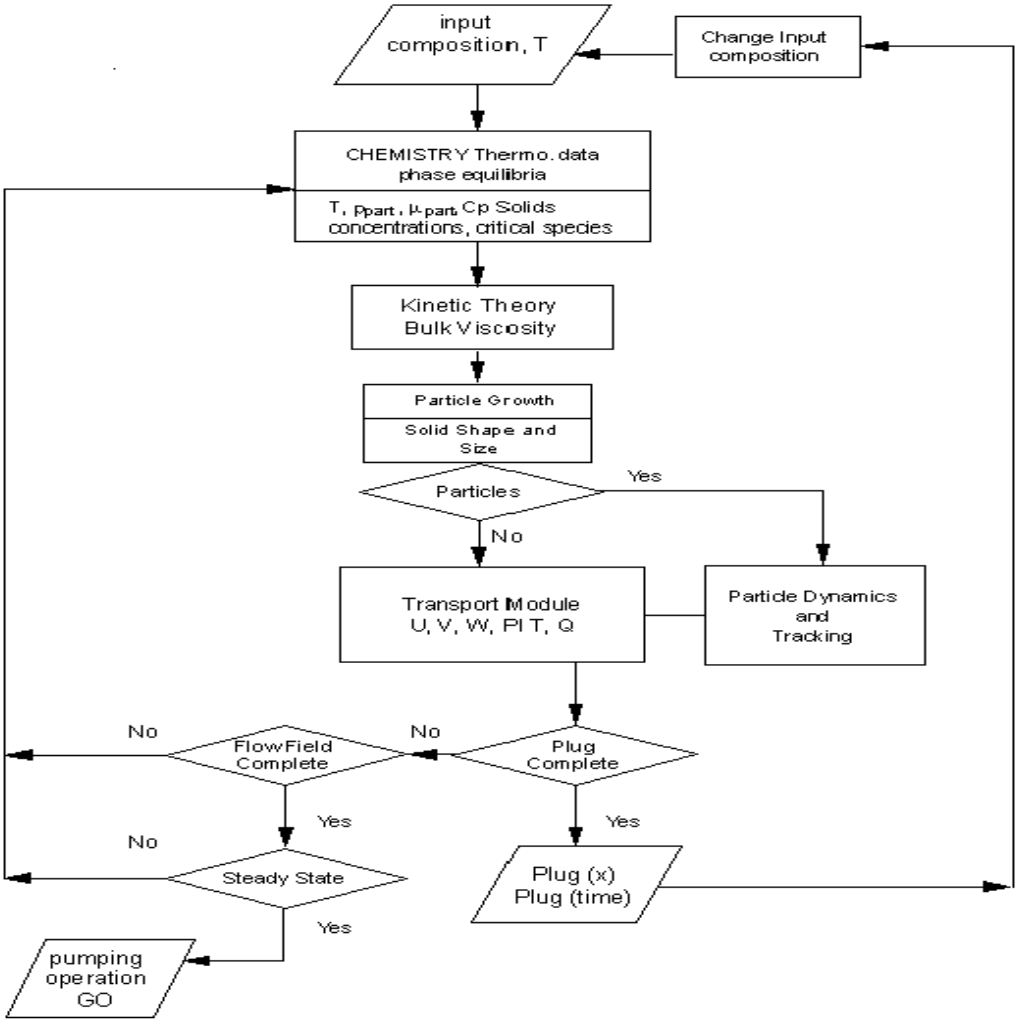

Fig. 1. Model flow chart.

Bulk viscosity. Two distinct coefficients of viscosity are needed to describe the laminar flow of a two- or multi-phase fluid. Of these coefficients, the shear viscosity μ is the more familiar. It describes the resistance of the fluid to changes of shape. The bulk viscosity describes the irreversible resistance, over and above the reversible resistance given by the isotropic bulk modulus, to changes of volume. The effects of bulk viscosity can be ignored for dilute monatomic gases and for simple incompressible fluids. As the solids concentration in the fluid increases, the bulk viscosity starts to have a direct effect on particle transport and must be calculated as a function of flow properties and particle formation. This module could be replaced by experimental correlations (as they become available) that can be used as an input to the module containing the equations that govern the fluid flow.

Transport module. This module provides calculation of the pertinent quantities relating to plug formation and process operation. It can be divided into two sub-modules, as shown in the lower half of Fig. 1.

In Fig. 1, in the sub-module labeled “transport module,” the contiuum/Eulerian partial differential equations governing the fluid transport process are solved. These equations consist of a set of mass, momentum, and energy (and turbulence, when needed) conservation equations for each phase available in the case of flows with high solid content. Or only one set of mass, momentum, and energy equations is necessary for the continuous phase in the case of flows with zero or low solids content. The transport sub-module will also calculate particle population balance, deposition velocity, and settling or adherence position (if any) in the flow field as the simulation develops. This module is the largest and most involved and consists of many subprograms that perform specific functions.

The sub-module to the right, labeled “particle dynamics and tracking,” can be used in two different ways. It provides for the description of particle dynamics, their interaction, and the resulting effects on the continuous phase for those situations where particle loadings are low. In addition, for both ST and SW, it provides a mechanism to dynamically track the solid particles in the flow field as they grow and/or agglomerate and ultimately, under adverse conditions, form a plug. The particle growth kinetics and tracking modules are essential for modeling the low-solids supernate pumping operations and are believed to be computationally very intensive even for a two-dimensional simulation.

The modules are executed in the sequence presented in the figure. Calculations are performed iteratively over the whole flow field as a function of time with recourse to the fundamental solid-liquid equilibrium (SLE) of the system. The results from the transport model are evaluated after each time step to determine if, where, and when a plug will form along the transfer line. If a plug has not been formed but is suspected, the program proceeds to the next time step until additional development is observed. The user can then change (if necessary) the initial pumping parameters (e.g., add water or increase the flow rate) and restart the simulation. If the flow field has been completely evaluated and a plug has still not been observed, then the composition of the waste and the engineering parameters are consistent with safe transfer.

Advantages of the proposed approach are the modularity (some calculations can be bypassed if not needed) and the capability to initially develop correlations from laboratory experiments that can transfer results directly to the main transport module.

Effort will be devoted to the simplification and/or elimination, when possible, of some of the modeling parameters (dimensions, chemical processes, kinetics, etc.) based on the results gained from the accompanying experimental effort(s) and experience, as they become available. Those findings should give a clearer view and greater insight as to which of the modeling parameters play a major role and must be completely accounted for, and which ones can be simplified, correlated, or even ignored.

Description of the physical processes inherent in particle deposition and eventual plug formation is thought to require a considerable amount of information. As noted in the flowchart and the previous discussion, a large portion of this data will be specific to the experiments scheduled as part of the overall Prevention of Solids Formation Program. These parallel efforts are being performed at Oak Ridge National Laboratory (ORNL), AEA Technology, FIU, and the Diagnostic Instrumentation and Analysis Laboratory/Mississippi State University (DIAL/MSU). The model development philosophy is based on a multi-phase approach and will initially focus on surrogates from Hanford tanks 241-AN-103 for ST and 241-SX-104 for SW pumping.

Workers at FIU are performing ST and plug formation experiments in a pilot-scale closed-loop system. The FIU studies can provide data needed to develop and validate the model, especially the main transport module for the ST process. This information will include

Module/Model Inputs
- Slurry composition data, solids loading, slurry density, supernate viscosity
- Particle size/shape/growth characteristics
- Bulk viscosity of the slurry
- Geometry information on pipe diameter, length, temperature, and heat tracing
- characteristics
- Pressures, pressure drops, and flow rates as a function of time
- Thermal characteristics of the process (temperatures, thermal conductivities, heat capacities)
- Fluid/particle velocities

Module/Model Comparisons
- Time needed to form a plug under specific operating conditions
- Characteristics of the plug (e.g., location, solids composition)

Additional information will be available from AEA Technology on particle size, growth, agglomeration, and disruption studies for the AN-103 surrogate. These results could be used to replace the particle growth module. As part of this work, DIAL/MSU will perform solid-liquid equilibrium calculations on the surrogate. These will provide the data necessary to initiate model development activities for the main transport module. The data can then be compared with the AEA and FIU results on the solids formed and the pertinent volume fractions.

Workers at ORNL are performing viscosity experiments for the SW process and developing viscosity correlations using a neural-network model for the prediction of bulk viscosity and rheology. The neural network results will not be available for incorporation into the viscosity module during FY 2000. The waste feed stability subtask at ORNL is also developing submodels that can be used in our rigorous simulations and is developing simplified macroscopic balance models of waste transport.

As another part of the overall Prevention of Solids Formation Task, work was initiated on the development of a laboratory-scale test loop for SW pumping. The validation data for the development of a SW model will come largely from this system. Data requirements are the same as those for the ST model, except that solids will not initially be present in the SW liquor. Runs have been conducted with SX-104 simulant and are planned for U-103. Parallel activities at ORNL and AEA will focus on the SX-104 surrogate.

The viscosity studies on the SX-104 surrogate from ORNL and the particle size/nucleation experiments from AEA will be employed. MSU/DIAL will perform SLE calculations for both the model and test loop development. The data will be transformed into correlations to streamline and allow concentration on the main transport module.

7.3 Results

Prior to the development of the current modeling approach, a preliminary study was developed to determine what other multiphase slurry transport models were available. Helix Technologies offers the Delta Q program that allows the calculation of the critical settling velocity for slurries with various particle size distributions (Delta Q Pipe Network Analysis Program, Helix

Technologies Pty. Ltd., P.O. Box 610, Morley, WA 6943, Perth, Australia). Initial calculations based on particle information indirectly obtained from ESP and studies conducted previously at FIU indicated that the critical settling velocity could be calculated to within 5%. This code, however, falls short in addressing all of the current model requirements in that the formation of a plug does not consider the potential reacting nature of the flow, heat transfer is not formally considered, and the model is only one-dimensional.

Other software has been noted, specifically the work of Pacific Northwest National Laboratory with the TEMPEST code (Onishi 1998, 1999; Lyczkowski 1994). TEMPEST is a powerful analysis tool and is capable of performing simulations in two and three coordinate dimensions with accounting for mass, momentum, and heat transfer for incompressible flow. It is available in N- and T-versions. The T-version has more capabilities and is not available to the public. The main drawback related to the current work is that TEMPEST lacks built-in (to our knowledge) capabilities for particle tracing, particle growth kinetics, particle/particle interaction, and changes in bulk viscosity due to solids formation that are necessary for the SW model. Additionally, the available N-version of the code is restricted to Cartesian or cylindrical coordinates and lacks pre-/post-processing capabilities.

These studies, compared with the modeling requirements, resulted in the proposed model depicted in the flowchart of Fig. 1.

7.3.1 Commercial CFD Code Selection and Procurement

A number of commercial CFD packages that are capable of simulating complex transport processes are available: FLUENT 4.5 and 5.0 from FLUENT, Inc.; CFD2000 from SIMUNET Corp.; PHOENICS 3.3 from Concentration, Heat and Momentum (CHAM) Ltd.; CFX 4 and 5 from AEA Technology; FLOW 3-D from Flow Science, Inc.; and STAR-CD from Computational Dynamics, Ltd. (among others). These codes are well tested, validated, and documented. Most of these companies integrate pre-processing and post-processing programs into their packages without the need for other programs to produce complete simulation and prediction results. None of these codes, however, contains all of the physics for the proposed model.

After a careful and thorough search and comparison of the available CFD software with our requirements, a decision was made to obtain the PHOENICS 3.3 package from CHAM. The code's strongest attraction for the current modeling effort is that most of the flow-solver part of the program is available in an open-source code format so that it can be modified, optimized, and tailored or completely changed. The code has been used to study single-, two-, and multi-phase flows with Eulerian/Eulerian and Eulerian/Lagrangian descriptions for the two- and multi-phase materials; and several different turbulence models are available. Simulations are obtainable for most types of flows on simple and complex geometries in Cartesian, cylindrical, and curvilinear body-fitted coordinates. From an end-user perspective, the code can be run using a graphical user interface (Virtual Reality Editor) by choosing from a preprogrammed collection of simulation cases tailored to the specific tank farm operation needs. This option will not require more than being familiar with inputting some numbers concerning the pumping operation in progress, such as dimensions, compositions, concentrations, and flow rates.

7.3.2 Preliminary Code Testing

The PHOENICS code version 3.3.0 arrived at DIAL/MSU around the end of April 2000. It was installed on the available PC system, which had a Pentium-II-class microprocessor. Standard tests were then performed involving (1) geometry definition, coordinate system, and grid generation

for simple shapes; (2) solver setup: flow model, associated physics, initial and boundary conditions definition, and solution execution; and (3) results manipulation, visualization, analysis, and verification.

The software simulation setup process (for simple flow with simple physics) was systematic with easy-to-follow steps and with limited guidance from the software. Because of time and effort constraints, only a few of the relevant code capabilities have been examined.

7.3.3 Early Model Development, Simulations, and Results

The proposed model as shown in Fig. 1 contains several modules. The best approach to ensure its proper function and validity is to build and test each module separately, if possible, as it evolves. PHOENICS will mainly represent the transport and probably the particle dynamics modules. As customary with any new predictive software tool, it was deemed necessary to perform a series of simulations on two- or multi-phase flows that start with simple but relevant physics and gradually increase in complexity. The results are then compared with available data.

In a related effort, researchers at FIU experimented with Savannah River Site (SRS) slurry C simulant that consisted of a carrier fluid with solid particles of two sizes (Table 1) (Ebadian 1999).

Table 1. Characteristics of SRS slurry C simulant used by FIU

	Density (kg/m^3)	Viscosity (cP)	Diameter (μm)	Concentration (% volume)
Carrier fluid	1005	0.913		92.4
Particle 1	3147		45	2.9
Particle 2	3147		220	4.7

The FIU experiments were related to ST and particle settling velocity. The settling of particles is believed to play a major part in plug formation, especially in the presence of large particles at low flow rates. The results from the FIU experiments amounted to an excellent way to test the model.

The PHOENICS code offers the choice of simulating multiphase flow using Eulerian/Lagrangian or Eulerian/Eulerian formulations. As noted in Table 1, the solids are present in the FIU experiments at a volume fraction of 7.6%. At this loading, the more efficient Eulerian/Eulerian method is to be used. Two sets (for liquid and solids) of conservation low partial differential equations must be solved, for mass, momentum, and energy, with the lows governing the exchange between the phases. The presence of turbulence will also require the solution of some additional equations, depending on the method used to model it. This large number of equations makes the number of unknowns to be solved for at each grid point or cell extremely large and lengthy even for the most powerful computers.

An alternative offered by PHOENICS is the drift flux method (CHAM n.d.). This is an Eulerian model that postulates that there exists one continuous medium in which there are various dispersed phase components, up to 99 components in PHOENICS (CHAM n.d.). The mixture of the continuous and dispersed phases behaves as a single fluid with properties that are referred to as the mixture properties. In this formulation, only one set of differential equations is solved to give the mixture-mean velocity at each point and time. Then separate sets of equations are solved,

one for each phase, which govern its relative velocities, i.e., their differences from the mean. The later equations are algebraic ones, which are derived from the original conservation equations by neglect of the second-order terms. This entails that the relative velocities are computed by reference only to the local pressure gradients, body forces, and inter-phase friction. The volume fractions occupied by each phase, at each point and time, are calculated at the same time. This method is referred to in PHOENICS as the algebraic slip method. This method is useful for simulating sedimentation and other multiphase processes, for example, the separation of oil, gas, and water in a centrifuge (CHAM n.d.). This formulation was used in simulating the FIU slurry C experiment that demonstrates the process of particle settling of a simple suspension.

The geometry chosen for the FIU experiment simulations was a straight pipe with a length of 12.9 m and a diameter of 0.0275 m. This simple geometry was used to obtain reasonably approximate simulations quickly to test the code. More realistic geometries are being developed. After experimenting with various grid distributions along the pipeline, a computational grid composed of 60000 cells was used, 600 cells in the axial direction with 100 (10×10) cells across the radial direction, all evenly distributed.

A parametric study was performed to investigate particle settling and sedimentation along the transfer pipe as a function of velocity. Simulations with entrance velocities ranging from 0.5 to 2.5 m/s were obtained, and they included the effects of turbulence. Since the flow for all cases is in the turbulent regime, the k-ε model (an eddy-viscosity model that adds two conservation equations, one for the turbulence kinetic energy k, and one for the dissipation rate ε) with wall functions was used with a 5% intensity at the entrance. The average simulation run time (CPU) was approximately 12 h with continuous graphical convergence display. Deactivation of the graphical display will decrease the CPU time required. Calculations were performed on a work station with dual 866-Mhz Pentium III Xeon processors that was acquired in late July 2000. Run times on a 400-Mhz Pentium II were prohibitive. Table 2 shows the entrance velocities for the cases to be presented in the coming few pages.

Table 2. Entrance flow velocity for simulation cases

Case number	Case 1	Case 2	Case 3	Case 4	Case 5
Flow velocity (m/s)	0.5	0.8	1.1	1.2	2.5

The 220-μm and 45-μm particle concentrations for the cases in Table 2 are presented in Figs. 2 and 3. The concentrations in the figures are enlarged 50 times in the radial direction, and they scale from 0.0 to 1.0. The concentrations show, as expected, that the larger, heavier particles tend to settle fast on the bottom of the pipe, especially at low flow velocities.

The simulations showed that flow velocities of lower than 1.0 m/s will create a stationary bed flow that eventually causes a plug to form. Most of the sedimentation structure was composed of the 220-μm particles, as expected. The presence of particles will have a dampening effect on turbulence through gravity/density gradients interactions (CHAM n.d.). The change of geometry (flow terrain)—i.e., bends, elbows, and junctions—can also create adverse effects on the flow.

For velocities of greater than 1.0 m/s, the fluid establishes a moving bed regime where the particles move along the bottom of the transfer pipe. At still higher flow velocities, the particles move much faster and stratify through the fluid layers (e.g., the 45-μm particle moving at 2.5 m/s

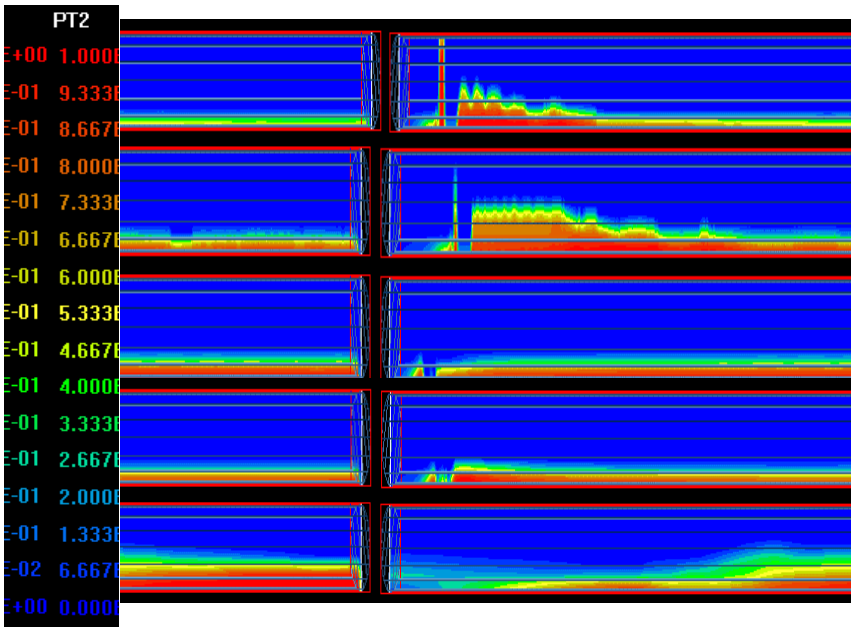

Fig. 2. A 220- (or 400-) μm particle concentration along the transfer pipe center line as a function of flow velocity at the entrance, U = 0.5, 0.8, 1.1, 1.2 and 2.5m/s.

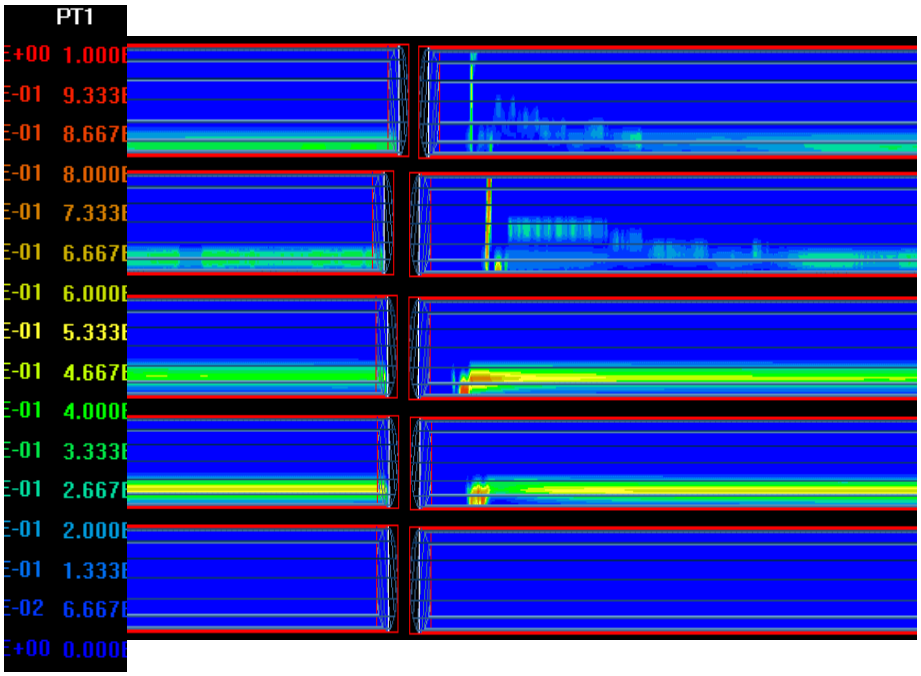

Fig. 3. A 45-μm particle concentration along the transfer pipe center line as a function of flow velocity at the entrance, U = 0.5, 0.8, 1.1, 1.2 and 2.5 m/s.

shown in Fig. 3). Velocities high enough to prevent settling must be used to prevent stationary bed flow and the possible formation of plugs in the transfer line.

The researchers at FIU reported that stationary bed flow regime was established at velocities less than or equal to 0.85 m/s for the slurry C experiment (Ebadian 1999). They did not give any details regarding plugging structure or specify any plug location. The model prediction of 1.0 m/s minimum flow velocity exhibits a good agreement with the experimental results and even better agreement with the Delta Q (Helix Delta Q Pipe Network Analysis Program) prediction of 0.95 m/s, bearing in mind that the differences could be in the range of experimental uncertainty and error. Other factors could contribute to small differences, such as the need for higher grid resolution or an entrance velocity distribution other than uniform. All of these factors will be addressed as the model development continues.

7.4 Conclusions

Work was initiated on the development of an engineering tool that will help to prevent plug formation during SW pumping and ST operations at Hanford. The efforts are aimed at producing a model that will accurately predict, if, where, and when a plug will form during a transfer process, while taking into account the dynamic behavior of the transfer process and reflecting the impact of the waste chemistry. Efficiency and ease of use to the operators and applicability to the operations at Hanford are top priorities.

The modeling approach, based on building the model using separate modules that represent a specific physical process, has started. A general CFD system that will represent the transport module part was acquired. Initial tests using simple transport processes were performed on the transport module. Other tests addressing module sensitivity to grid distribution, initial and boundary conditions, and initial velocity distribution at the entrance are in progress.

Simulations representing the transport process in the FIU slurry C experiments produced good agreement with the reported results. The simulations suggested that flow rates with velocities larger than 1.0 m/s will produce a moving bed flow. The higher the flow rates, the less likely a significant amount of particles will deposit and eventually lead to the formation of a plug. This leads to the following preliminary conclusions based on the simulation results; in the absence of significant heat transfer and chemical reactions, simulations based on the more efficient and less computationally demanding drift flux formulation for multiphase flow will produce acceptable predictions for the ST process.

To prevent the establishment of stationary bed flow that leads to plug formation in the pipe, a pumping flow rate must be used that produces velocities higher than the settling velocity for the largest particle available to transport. Such a rate will ensure a minimum of moving bed flow.

Incorporation of more elaborate formulation and additional modules into the overall model is in process. Capabilities that will account for the complex characteristics of the waste will be included. Modifications will include the effects of the change of solids concentration on the viscosity of the flow, phase transition, particle nucleation and growth, and chemical reaction capabilities.

7.5 References

CHAM (Concentration, Heat and Momentum) n.d. "Multi-phase Flow Simulation in PHOENICS," *PHOENICS Encyclopaedia*, PHOENICS On-Line Information System, Concentration, Heat and Momentum Limited, Bakery House, Wimbledon Village, London SW19 5Au, UK, http://www.cham.co.uk/phoenics/d_polis/polis.htm.

Crowe, C., M. Sommerfeld, and Y. Tsuji 1998. *Multiphase Flows with Droplets and Particles,* CRC Press, Boca Raton, Fla.

Ebadian, M., C. Lin, and J. L. Xu 1999. *Plugging and Unplugging of Waste Transfer Pipelines, Preliminary Data and Results,* FY 1998 Year end Report, Florida International University, Center for Engineering and Applied Sciences, Miami, Fla., January.

Lyczkowski, R., J. Bouillard, J. Ding, S.-L. Chang, S. Lottes, and S. Burge 1994. "State-of-The-Art Review of Computational Fluid Dynamics Modeling for Fluid-Solids Systems," invited paper submitted to the International Symposium on Parallel Computing in Multiphase Flow Systems, American Society of Mechanical Engineers, Chicago, Ill., November 6–11, 1994.

Onishi, Y., and D. Trent 1998. *TEMPEST Code Modifications and Testing for Erosion-Resisting Sludge Simulations*, prepared for the U.S. Department of Energy, Pacific Northwest National Laboratory, Richland, Wash., January.

Onishi, Y., and K. Rechnagle 1999. *Simulation of Hanford Tank 241-C-106 Waste Release into Tank 241-Y-102,* prepared for the U.S. Department of Energy, Pacific Northwest National Laboratory, Richland, Wash., May.

Reynolds, D. A. 2000. "Status of Waste Transfers, Criteria, and Plans," presented at the Third Saltcake Dissolution and Feed Stability Workshop, Richland Wash., May 16, 2000.

Tannehill, J., D. Anderson, and R. Pletcher 1997. *Computational Fluid Dynamics and Heat Transfer,* Taylor & Francis, Bristol, Penn.

INTERNAL DISTRIBUTION

1. J. M. Begovich
2. V. F. de Almeida
3. D. W. Depaoli
4. R. D. Hunt
5. J. N. Herndon
6. R. T. Jubin
7. B. E. Lewis
8. C. P. McGinnis
9. D. A. Palmer
10. S. M. Robinson
11. C. Tsouris
12. J. S. Watson
13. C. F. Weber
14–19. T. D. Welch
20. ORNL Laboratory Records–RC

EXTERNAL DISTRIBUTION

21. H. Alhabbash, Diagnostic Instrumentation and Analysis Laboratory, 205 Research Boulevard, Starkville, MS 39759-9734
22. D. Baide, CH2M Hill Hanford Group, P.O. Box 1500, MSIN S7-90, Richland, WA 99352
23. B. Barton, CH2M Hill Hanford Group, P.O. Box 1500, MSIN R-11, Richland, WA 99352
24. J. Bell, 137 Bowsprit Lane, Kingston, TN 37763
25. B. Brendel, CH2M Hill Hanford Group, P.O. Box 1500, MSIN S7-90, Richland, WA 99352
26. J. Bryant, Pacific Northwest National Laboratory, P.O. Box 999, MSIN K7-94, Richland, WA 99352
27. W. Callaway, Cogema Engineering Corporation, P.O. Box 1000, MSIN T6-07, Richland, WA 99352
28. J. Cammann, CH2M Hill Hanford Group, P.O. Box 1500, MSIN T4-08, Richland, WA 99352
29. B. Carteret, Pacific Northwest National Laboratory, P.O. Box 999, MSIN K9-91, Richland, WA 99352
30. A. B. Carlson, Numatec Hanford Corporation, P.O. Box 1300, MSIN R3-73, Richland, WA 99352
31. A. F. Choho, Numatec Hanford Corporation, , P.O. Box 1300, MSIN H6-22, Richland, WA 99352
32. D. Crass, Numatec Hanford Corporation, P.O. Box 1300, MSIN S7-90, Richland, WA 99352
33. J. Cruz, Department of Energy, Office of River Protection, P.O. Box 550, MSIN H6-60, Richland, WA 99352
34. R. Edwards, Westinghouse Savannah River Company, Building 704-3N, Aiken, SC 29808
35. F. F. Erion, Pacific Northwest National Laboratory, P.O. Box 999, MSIN K7-15, Richland, WA 99352
36. S. Estey, CH2M Hill Hanford Group, P.O. Box 1500, MSIN R2-11, Richland, WA 99352
37. A. Felmy, Pacific Northwest National Laboratory, P.O. Box 999, MSIN K8-96, Richland, WA 99352
38. K. Gasper, CH2M Hill Hanford Group, P.O. Box 1500, MSIN L4-07, Richland, WA 99352
39. P. Gauglitz, Pacific Northwest National Laboratory, P.O. Box 999, MSIN K6-28, Richland, WA 99352
40. D. Geniesse, Cogema Engineering Corporation, 2425 Stevens Drive, Richland, WA 99352
41. P. Gibbons, Numatec Hanford Corporation, P.O. Box 1300, MSIN K9-91, Richland, WA 99352
42. R. Gilchrist, Pacific Northwest National Laboratory, P.O. Box 999, MSIN K9-91, Richland, WA 99352
43. J. Henshaw, AEA Technology, B220 Harwell, Didcot, Oxfordshire, UK, OX11 0QJ
44. D. Herting, Fluor Hanford, P.O. Box 1000, MSIN T6-07, Richland, WA 99352
45. J. Honeyman, CH2M Hill Hanford Group, P.O. Box 1500, MSIN H6-18, Richland, WA 99352
46. J. Huckaby, Pacific Northwest National Laboratory, P.O. Box 999, MSIN K7-15, Richland, WA 99352
47. J. Jewett, Numatec Hanford Company, P.O. Box 1300, MSIN R3-73, Richland, WA 99352

48. G. Josephson, Pacific Northwest National Laboratory, P.O. Box 999, MSIN K6-69, Richland, WA 99352
49. L. J. Julyk, CH2M Hill Hanford Group, P.O. Box, 1500, MSIN R3-83, Richland, WA 99352
50. N. W. Kirch, CH2M Hill Hanford Group, P.O. Box, 1500, MSIN R3-73, Richland, WA 99352
51. R. Kirkbride, Numatec Hanford Company, P.O. Box 1300, MSIN R3-73, Richland, WA 99352
52. W. L. Kuhn, Pacific Northwest National Laboratory, P.O. Box 999, MSIN K7-15, Richland, WA 99352
53. J. Lindner, Diagnostic Instrumentation and Analysis Laboratory, 205 Research Boulevard, Starkville, MS 39759-9734
54. R. López, Florida International University, 10555 West Flagler St., CEAS 2100, Miami, FL 33174
55. R. Luyendijk, Waste Policy Institute, 2000 Craft Drive, Suite 1000, Blacksburg, VA 24060
56. G. MacLean, Fluor Federal Services, P.O. Box 1050, MSIN G3-10, Richland, WA 99352
57. B. Mauss, Department of Energy, Office of River Protection, P.O. Box 550, MSIN H6-60, Richland, WA 99352
58. P. Meyer, Pacific Northwest National Laboratory, P.O. Box 999, MSIN K7-15, Richland, WA 99352
59. J. Morin, Westinghouse Savannah River Co., 703-H Bldg./Rm. 119 Aiken, SC 29808
60. J. Noble-Dial, U.S. Department of Energy, Oak Ridge Operations Office, 55 Jefferson, Oak Ridge, TN 37831
61. Y. Onishi, Pacific Northwest National Laboratory, P.O. Box 999, MSIN K7-15, Richland, WA 99352
62. R. Orme, Numatec Hanford Company, P.O. Box 1300, MSIN R3-73, Richland, WA 99352
63. J. Pike, Westinghouse Savannah River Co., Building 704-196N, Aiken, SC 29808
64. J. Plodinec, Diagnostic Instrumentation and Analysis Laboratory, 205 Research Boulevard, Starkville, MS 39759-9734
65. M. Poirier, Westinghouse Savannah River Company, Building 773-42A, Aiken, SC 29808
66. D. Reynolds, CH2MHill Hanford Group, Inc., MSIN: R2-11, 2440 Stevens Center, P.O. Box 1500, Richland, WA 99352-1505
67. J. Roecker, 17123 North Brookside Lane, Colbert, WA 99005
68. W. Schulz, W2S Company, 12704 Sandia Ridge Place, NE, Albuquerque, NM 87111
69. R. Srivastava, Florida International University, 10555 West Flagler Street, CEAS 2100, Miami, FL 33174
70. Tanks Focus Area Headquarters Program Lead, c/o Kurt Gerdes, DOE Office of Science and Technology, 19901 Germantown Road, 1154 Cloverleaf Building, Germantown, MD 20874-1290
71. Tanks Focus Area Program Manager, c/o T. P. Pietrok, U.S. Department of Energy, Richland Operations Office, P.O. Box 550, MSIN K8-50, Richland, WA 99352
72. Tanks Focus Area Technical Team, c/o B. J. Williams, Pacific Northwest National Laboratory, P.O. Box 999, MSIN K9-69, Richland, WA 99352
73. L. Tavlarides, Syracuse University, Dept. of Chemical Engineering & Materials Science, 334 Hinds Hall, Syracuse, NY 13244-1190
74. J. Thompson, Department of Energy, Office of River Protection, P.O. Box 550, MSIN H6-60, Richland, WA 99352
75. M. Thompson, Westinghouse Savannah River Company, Savannah River, Technology Center Building, 773-A, C140 Aiken, SC 29802
76. R. Thompson, CH2M Hill Hanford Group, P.O. Box 1500, MSIN T4-08, Richland, WA 99352
77. R. Toghiani, Mississippi State University, School of Chemical Engineering, P.O. Box 9595, MS State, MS 39762
78. G. Vandegrift, Argonne National Laboratory, Building 205, 9700 South Cass Avenue, Argonne, IL 60439
79. D. T. Vladimirof, CH2M Hill Hanford Group, P.O. Box 1500, MSIN S7-20, Richland, WA 99352
80. F. Washburn, Westinghouse Savannah River Company, Building 704-196N, Aiken, SC 29808
81. T. Weber, 6622 West Victoria Avenue, Kennewick, WA 99336
82. J. Westsik Jr., Pacific Northwest National Laboratory, P.O. Box 999, MSIN K9-91, Richland, WA 99352